MINUTES OF THE MEETING
STEERING COMMITTEE (SC)

Meeting Noº 65

Thursday, March 14, 2024

1:30 PM to 4:30 AM

Videoconference on TEAMS

Present:	Félix Boulanger	EMRWB representative Nation Government
	Daniel Brosseau	Hydro-Québec
	Marc Dunn	Niskamoon Corporation
	Luc Duquette	Hydro-Québec
	Jean-Philippe Gilbert	Hydro-Québec
	Louie Kanatewat	Cree Nation of Chisasibi
	John Lameboy	Cree Nation of Chisasibi
	Mélanie Leblanc	Niskamoon Corporation
	Geraldine Mark	Cree Nation of Wemindji
	Johanna Ménélas	Hydro-Québec
	Ernest Moses	Cree Nation of Waskaganish
	Robbie Tapiatic	Cree Nation of Chisasibi
Guest:	Simon Bélanger	University of Quebec at Rimouski
	Mimie Neacappo	Niskamoon Corporation
	Mary O'Connor	University of British Columbia
	Cassandra Weapenicappo	Cree Nation of Eastmain
Absent:	James Bobbish	Cree Nation of Chisasibi
	Carine Durocher	Hydro-Québec
	Josée Lefebvre	Canadian Wildlife Service
	Marie-Eve Lemieux	Hydro-Québec
	Gregory Mayappo	Cree Nation of Eastmain
	Graeme Morin	Cree Nation Government
	Roderick Pachano	Cree Nation of Chisasibi
	Ernie Rabbitskin	Niskamoon Corporation

MEETING CHAIR AND SECRETARY

Luc Duquette chaired the meeting, and Johanna Ménélas acted as the meeting secretary.

PROPOSED AGENDA

1. Approval of the Agenda
2. Presentation of Final report for Eelgrass Team Final Report
3. Presentation on the opportunity to develop satellite-based monitoring of Eeyou Istchee
4. Approval of the minutes from the previous meetings
    a. January 30, 2023 – Noº 55
    b. February 13, 2023 – Noº 56
    c. March 8, 2023 – Noº 57
5. Miscellaneous
6. Summary and Next Steps
7. Next Meeting

---

1. Approval of the Agenda

The Chair reviewed the agenda, and no additional points were proposed. Thus, the agenda was approved as presented.

The Chair offered a warm welcome to Mimie Neacappo (**Ms. Neacappo**), acknowledging that it was her first meeting with the Committee and mentioning that she is working for Niskamoon.

2. Presentation of Final report for Eelgrass Team Final Report

Mary O'Connor (**Mrs. O'Connor**) delivered a presentation titled "Eelgrass Team Final Report," based on the document Eelgrass Team Final Report and a copy of the presentation and document is appended to these minutes for reference. She expressed gratitude for the opportunity to participate in the project, emphasizing the transformative impact it had on the team's professional and personal lives. The presentation highlighted the collaborative nature of the project and the valuable feedback received from the Committee.

The objectives outlined in the 2019 project proposal focused on assessing current eelgrass distribution and condition, comparing historical data to assess change, and evaluating the roles of environmental factors in eelgrass health and change. The presentation provided an overview of the team's activities, including fieldwork, experiments, and community consultations.

Mrs. O'Connor shared insights from the team's research, discussing changes observed in eelgrass distribution and condition over the course of the project. The presentation also addressed experiments conducted to investigate the impact of environmental factors on eelgrass health, such as light and nutrients.

During the presentation, John Lameboy (**Mr. Lameboy**) inquired about the condition of specific sites, noting variations observed over time. Mrs. O'Connor provided detailed responses, highlighting changes in eelgrass density and shoot length and addressing questions about the stability of eelgrass ecosystems.

Marc Dunn (**Mr. Dunn**) reflected on the project's evolution and emphasized the importance of aligning scientific research with community priorities. He commended the efforts of the team in fostering collaboration and integrating traditional knowledge with scientific findings. Mr. Dunn expressed support for accepting the final report, acknowledging the ongoing need for further investigation.

Mrs. O'Connor thanked the Committee for their support and reiterated the team's commitment to data sharing and accessibility.

Mr. Dunn continued the discussion by underscoring the importance of the eelgrass component within the broader study. He detailed the initial challenges faced and expressed gratitude for the subsequent realignment of the project's direction. Acknowledging the pivotal role played by the new team, he praised their efforts in fostering community alliances and bridging the gap between traditional knowledge and scientific research.

Jean-Philippe Gilbert (**Mr. Gilbert**) echoed Mr. Dunn's sentiments, commending the improvements made by the new team and highlighting the significance of accurate data. He also inquired about the nutrient levels in sediment, sparking a discussion about potential restoration opportunities in phase two.

Mr. Lameboy shared his perspective on the integration of traditional knowledge with Western science, emphasizing the importance of continued collaboration. He also expressed curiosity about the potential regrowth of eelgrass and observed fluctuations in its presence over the years.

Louie Kanatewat (**Mr. Kanatewat**) raised concerns about the cyclical disappearance of eelgrass and its impact on local ecosystems. Mrs. O'Connor acknowledged these concerns, affirming the complexity of the issue and emphasizing the need for further research in phase two.

Ernest Moses (**Mr. Moses**) reflected on the project's accomplishments and underscored the ongoing need for comprehensive understanding and collaboration. He praised the team's efforts and expressed confidence in their ability to address unanswered questions in the future.

Mr. Lameboy inquired about monitoring salinity levels in conjunction with eelgrass growth, prompting Mrs. O'Connor to discuss the integration of various teams' efforts in phase two.

With no further questions or comments, the Chair concluded the discussion, thanking Mrs. O'Connor for her presentation and expressing interest in hearing personal reflections on the project's impact in the future.

The presentation concluded with a recommendation to accept the final report.

3. Presentation on the opportunity to develop satellite-based monitoring of Eeyou Istchee

Simon Bélanger (**Mr. Bélanger**) delivered a presentation titled "A satellite-based monitoring system and services for Eeyou Istchee coastal habitats," and a copy of the presentation is appended to these minutes for reference.

During the presentation, the Chair raised questions about the involvement of the Cree Nation Government (**CNG**) and the specific objectives of the project. Mr. Bélanger then elaborated on the project, explaining its origins and objectives. He discussed the idea's beginning years ago, its proposal to the Canadian Space Agency, and the subsequent selection for Phase One of the project. The goal is to refine the concept presented during Phase One and potentially proceed to Phase Two. The project aims to establish a satellite-based monitoring system and services tailored to the needs of stakeholders in the coastal habitats of Eeyou Istchee. To achieve this, consultations with Cree stakeholders are ongoing to assess needs and perspectives and explore opportunities for collaboration between satellite monitoring and community-based monitoring efforts.

The presentation showcased various applications of satellite data, including sea surface temperature, water quality assessment, bathymetry estimation, shoreline detection, eelgrass mapping, and forest fire monitoring. Mr. Bélanger emphasized the importance of combining satellite data with field measurements to enhance interpretation accuracy. He also discussed the accessibility of satellite data, data processing, and the envisioned user-friendly platform for accessing and utilizing the generated information.

The consultation process with Cree stakeholders was highlighted, aiming to assess their needs and perspectives regarding environmental assessment and monitoring in the region. The goal was to integrate satellite monitoring with community-based monitoring, aligning with the objectives of the Comprehensive Coastal Habitat Research Project.

Mr. Bélanger discussed various applications of satellite data, including sea surface temperature, water quality, bathymetry estimation, shoreline detection, eelgrass mapping, wetlands mapping, and forest fire monitoring. He addressed concerns about the resolution of satellite imagery and explained the need for collaboration between remote sensing and field measurements.

During the presentation, Daniel Brosseau (**Mr. Brosseau**) shared pictures of Eastmain, contributing to discussions about turbidity in the area. There were also discussions about skepticism regarding remote sensing data and the importance of combining it with field measurements for accurate interpretation.

Questions were raised about the involvement of the CNG in the project and the project's objectives. Mr. Bélanger clarified that the project aimed to develop a system for processing and disseminating satellite data, providing a user-friendly platform for accessing information. The ultimate goal was to support monitoring efforts in the region, complementing existing initiatives by organizations like the CNG.

Mélanie Leblanc (**Mrs. Leblanc**) provided examples of how the project could enhance existing platforms like the Cree Trapper Association's app by integrating additional information such as sea ice mapping. The project was seen as complementary to the work of the CNG's GIS department, providing valuable data for climate change and environmental assessments.

With no further questions or comments, the Chair concluded the discussion, expressing gratitude to Mr. Bélanger for his presentation. The Chair encouraged Mr. Bélanger to reach out to Hydro-Quebec's GIS team for further collaboration. He suggested that Mr. Bélanger could discuss potential contributions to the project and explore mutual benefits. The Chair indicated that either Mr. Brosseau or Mr. Gilbert could facilitate this connection and arrange the necessary discussions.

4. Approval of the minutes from the previous meetings

Since the Chair was the secretary in those past meetings, he initiated the review and approval of the minutes from the following meetings:

- January 30, 2023 – Noº 55
- February 13, 2023 – Noº 56
- March 8, 2023 – Noº 57

There was a brief discussion regarding the composition of the Committee and the agreement about the quorum. Mrs. Leblanc provided clarification on the quorum requirement, indicating that it consisted of two local and one regional member minimum to convene a meeting.

Robbie Tapiatic (**Mr. Tapiatic**) suggested waiting for the members who were present at the respective meetings to review the minutes. The Secretary noted the absence of several members, including Mr. Dunn and Mrs. Durocher, and proposed postponing the approval until they could participate. The Chair concurred, suggesting involving retired members like Réal Courcelles to ensure comprehensive review and participation.

Amidst considerations for future meetings, Mr. Kanatewat raised a concern about his absence being recorded incorrectly in the minutes, prompting the Chair to acknowledge the error and commit to correcting it.

Decision: The Committee agreed to postpone the approval of the minutes until all relevant members could participate, ensuring accuracy and fairness in the review process.

5. Miscellaneous

- **Presentation of the platform DiliTrust**

The Secretary introduced a platform called DiliTrust and proceeded to present it as a tool for facilitating document sharing within the Committee, enhancing accessibility. Describing the platform's features, she aimed to make document access more seamless for all members.

Following Mr. Tapiatic's expressed reticence and difficulties adapting to new technology, the Secretary offered to arrange a one-on-one meeting with him to ensure he becomes familiar with the platform.

Decision: The Committee approved the usage of DiliTrust.

6. **Summary and Next Steps**
   - Mrs. O'Connor's presentation was approved with minimal comments, as was Mr. Belanger's presentation.
   - Approval of the minutes was deferred due to the absence of key members, necessitating a separate meeting dedicated solely to reviewing and approving pending minutes.
   - The Committee confirmed the approval of the platform DiliTrust, and the Secretary offered to arrange a one-on-one meeting with Mr. Tapiatic if needed to help him get comfortable with the platform.
   - Mrs. Leblanc mentioned that the next team to present their final report is Zou Zou Kuzyk's team, ideally by the end of April, after which meetings will focus on addressing the backlog of minutes.

7. **Next Meeting**

Following the exchange on the availability of each, it was agreed that the next meeting will be held on Tuesday, April 9, 2024, from 1:30 PM to 4:30 PM, via Teams.

ADJOURNMENT OF THE MEETING

Considering that all items on the agenda were addressed, the meeting is adjourned at 3:36 PM.

The meeting secretary,

Johanna Ménélas

Coastal Habitat Comprehensive Project

Eelgrass Team Final Report

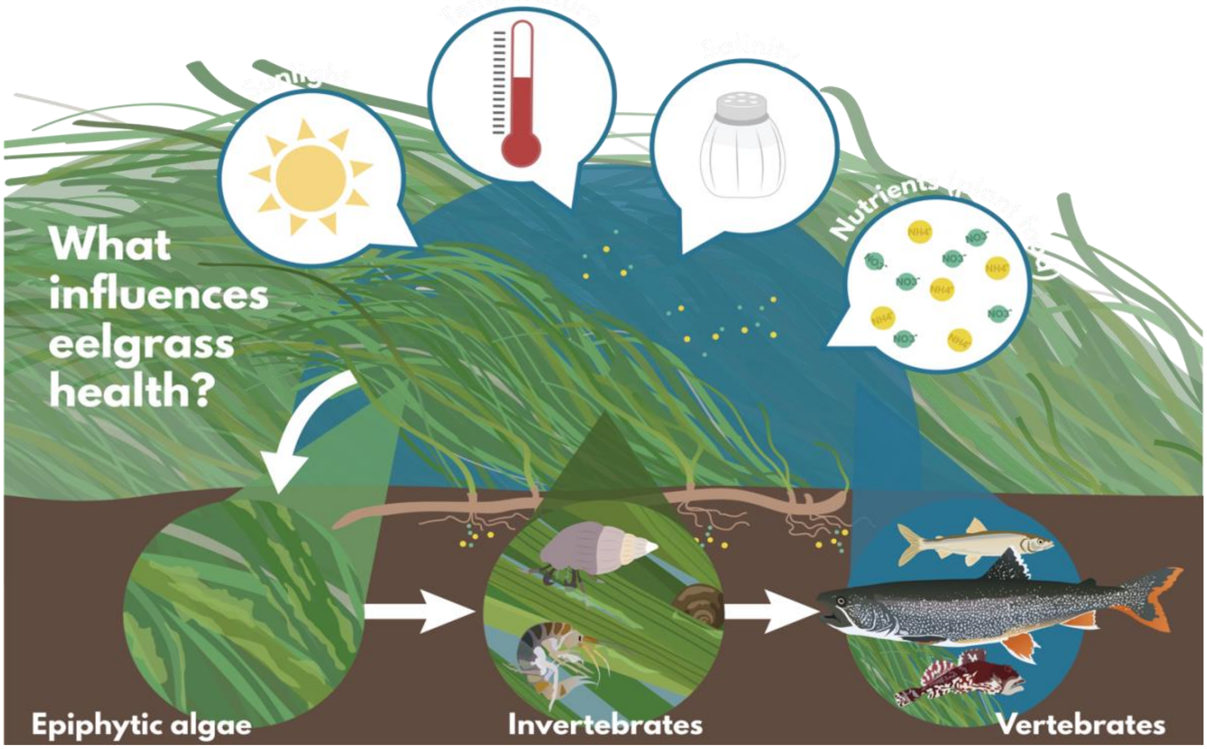

Illustration credit: Align Illustration

July 21, 2023

Mélanie-L. Leblanc, Mary O'Connor (Principal Investigator, PI), Fanny Noisette (co-PI), Brigitte Leblon (co-PI), Kaleigh Davis, Kevin Clyne, Armand LaRocque, Abraham Olatunji, and Murray Humphries (co-PI)

Table of Contents

List of Figures

List of Tables

Acknowledgements

We would like to express our gratitude to the steering committee for their feedback and suggestions on the eelgrass team's research throughout the years. We would like to thank Niskamoon's Local Officers (Ernest Moses, Gregory Mayappo, Geraldine Mark, and Ernie Rabbitskin) and Norman Cheezo for their help during fieldwork and for organizing meetings and workshops with land users. We would like to thank the land users of Waskaganish, Eastmain, Wemindji, and Chisasibi for allowing the research to be carried out on their traditional hunting lands, as well as for logistical support offered to the research team in the form of guides, boat drivers, and helpers. Most importantly, we want to thank the Crees for contributing essential knowledge about their lands and ecological processes as part of the research effort.

INTRODUCTION

The Coastal Habitat Comprehensive Research Project (CHCRP) is a large-scale research project led by Niskamoon Corporation that spans the whole eastern coast of James Bay and involves all four Cree coastal communities. The program was established as a result of an agreement reached in August 2016 between the Cree Nation Government, Niskamoon Corporation, and Hydro-Québec to better understand the overall decline of eelgrass (*Zostera marina*) beds along the eastern James Bay coast. Eelgrass decline has coincided with wider changes, most notably changes in the distribution and abundance of migrating waterfowl. To properly grasp the magnitude of these changes, a comprehensive research program was required to relate the various factors of this complex system.

The CHCRP was governed by the following central research questions: 1) What are the main factors affecting the current growth of eelgrass along the eastern coast of James Bay? and 2) What is the impact of the current state of eelgrass meadows on waterfowl presence along the coast of James Bay and, subsequently, Cree hunting activities? Working collaboratively with Cree land users in all four coastal communities, the eelgrass team of the CHCRP aimed to characterize the different factors likely influencing the distribution, growth, and productivity of eelgrass using samples collected in activities in 2019, 2020, and 2021. These observations, in conjunction with freely available satellite imagery and a current general understanding of eelgrass decline and recovery dynamics, was used to assess the current distribution and condition of eelgrass meadows.

In section 1 of this final report, we summarized the early findings about eelgrass beds and shoots characteristics and probable factors affecting eelgrass growth and conditions based on data collected between 2019 and 2021, with **a focus on information not yet published in the peer-reviewed literature.** In section 2, we presented a thorough description of the fieldwork undertaken in 2019, 2020, and 2021, as well as a complete list of type samples collected, and variables measured. In section 3, we provide detailed information on how the different coastal maps were generated. We have listed the peer-reviewed research papers that are published or in preparation. In section 4, we described the outreach activities organized and planned by the eelgrass team. Finally, the eelgrass team will prepare a separate document that will provide information about the raw data compiled and outreach documents (posters and presentations), where the information (raw data and outreach documents) is stored and where it can be accessed if stored in data repository.

SECTION 1 WHAT WE KNOW ABOUT EELGRASS

In section 1 of this final report, we summarized the early findings about eelgrass beds and shoots characteristics and probable factors affecting eelgrass growth and conditions based on data collected between 2019 and 2021, with *a focus on information not yet published in the peer-reviewed literature.*

Seagrasses are marine flowering plants that form some of the most productive ecosystems in the world and play a critical role in coastal environments (Orth et al. 2006). Seagrass meadows are used as shelter for countless species of invertebrates (Valentine et al. 2006), essential nursery areas for fish (Warren et al. 2010), and food for vertebrate grazers such as waterfowl (Kollars et al. 2018). Seagrass meadows also provide essential ecosystem services, including nutrient cycling (Duarte et al. 1990), sediment stabilization (Fonseca et al. 1983), and carbon sequestration and storing (Duarte et al. 2005). Seagrasses are also among the most threatened ecosystems as a result of anthropogenic activities leading to decrease of coastal water quality (Waycott et al. 2009), although declines in northern regions are less reported (Krause-Jensen et al. 2020). The predominant seagrass species in Canada is *Zostera marina* L. (eelgrass), considered as an Ecologically Significant Species by DFO (DFO 2009).

Environmental changes associated with climate, changes in hydrology and geomorphology, and water quality, can all change the growing environment for eelgrass and its competitors. Some changes can enhance growth if light, temperature, and nutrient conditions remain favorable. However, if light levels are reduced or salinity, temperature or water chemistry becomes intolerable to seagrasses, seagrass may no longer be able to grow well, or grow at all. Signs of stress or reduced growth in remaining meadows may be detected using analyses of seagrass morphology, reproductive features, recent productivity, and physiological conditions (Roca et al. 2016).

Healthy eelgrass meadows provide habitat and food for a wide range of algae and invertebrates, as well as fish and birds. Indicators of health in eelgrass meadows include eelgrass shoot size (length and aboveground biomass) and density (length), indicators of recent productivity in rhizomes (length of internodes) and blade structure (sheath) that indicates new tissue throughout the growing season, signals of flowering (number of reproductive shoots) and spread into disturbed areas, and physiological condition (pigments, nitrogen and carbon contents) (Duffy 2006, Ruesink et al. 2015; Figure 1). Healthy eelgrass meadows are also characterized by diverse epiphytic algae in moderate to low standing stock, as well as an assembly of invertebrate grazers, fish, and invertebrate predators, and even wading birds and waterfowl (Duffy 2006; Leblanc et al. 2023a, 2023b).

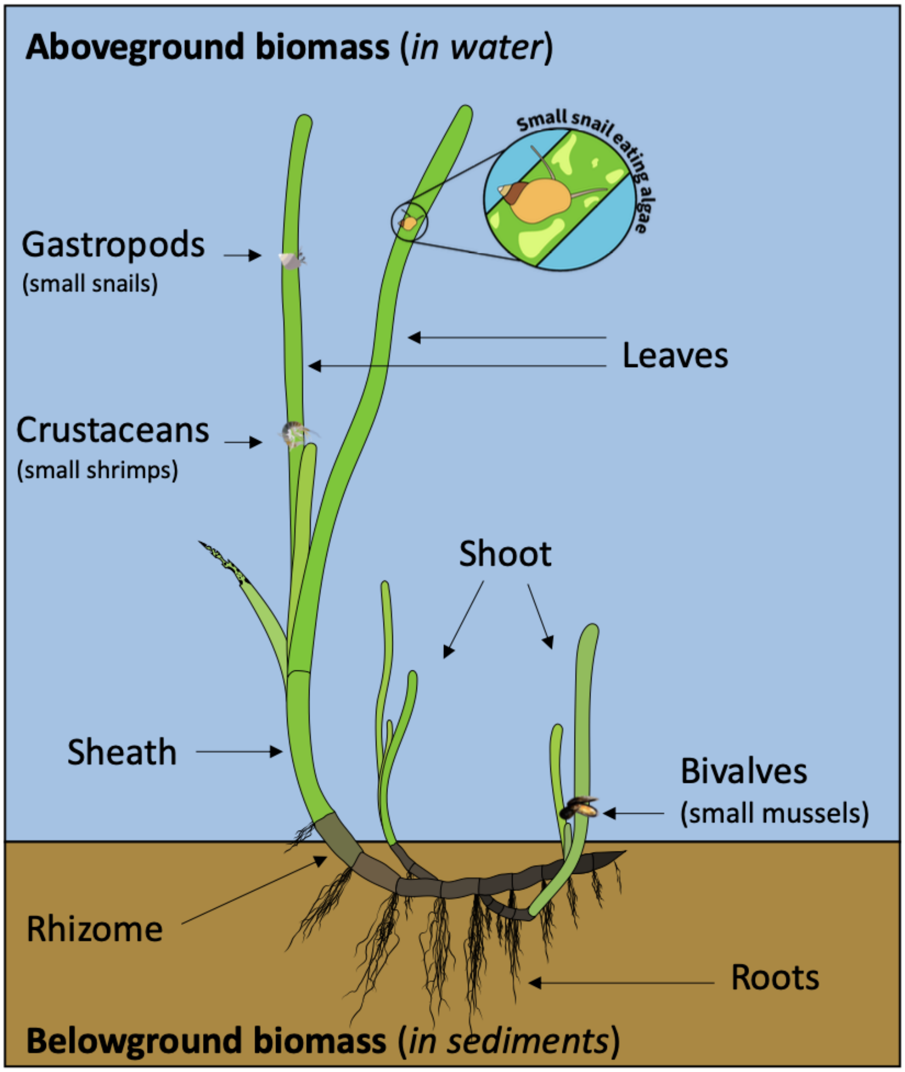

Figure 1 Eelgrass shoots have parts above the sediments and parts below the sediments. The sheath, which grows vertically from the rhizome, is a tube-like structure that protects the leaves from strong currents. An eelgrass shoot usually contains four to six leaves. Small invertebrates (different species of snails, crustaceans, and bivalves) live on the leaves, and some eat the algae growing on the leaves (known as epiphytes). Rhizomes, which are in the sediment, are separated into small segments known as internode. New shoots can emerge from the rhizomes. Internode length reflects growth and is often longer in the spring and summer and shorter in the winter when growth continues but is slower than in summer. Tiny roots attached to the rhizomes absorb nutrients from the sediments. Sea bottom sediments can be very hard or soft depending on the composition (the amount of silt, sand, clay, small rocks…). Eelgrass shoots need sediments soft enough to anchor their rhizomes and roots. Illustration credit: M.L. Leblanc

Where is eelgrass doing well?

We took measurements of eelgrass at 41 sites in 2019, 26 in 2020 (sampling led by the Cree team) and 13 in 2021 (in Chisasibi only due to COVID restrictions). At no site is eelgrass as long or as thick as it used to be, according to historical scientific observations and Cree reports. Still, we wanted to know where it is growing taller than other places, or thicker than other places, and therefore might be considered to be doing relatively well, compared to other sites in the region now. What we can say about where eelgrass is doing well and where it is not is influenced by how we chose to visit sites and the number of parameters we were able to assess. Choices about where to go were essential - the coastline is large and even when we were there for several weeks in the summer, we could only visit a few places each day. We chose sites to visit and check eelgrass for three reasons: 1) sites where land users told us eelgrass used to grow, and was still there recently (most sites that we visited), 2) sites where eelgrass used to grow and hasn't been growing recently (some sites), and 3) sites where land users said they didn't know if eelgrass ever grew (a few). This approach to site selection reflects our collaboration with the land users. This collaboration is a clear strength for this project, and it allows us to describe the current state of eelgrass in what are likely the best meadows. Though, notably, some land users did not allow us to visit eelgrass on their traplines (CH4, CH5, CH6) and these traplines are thought to have some of the best eelgrass in the region.

Our sampling method also limits what we can say. For example, it is not a stratified random sampling design with temporal resampling. This means that we cannot say *why* eelgrass grows well where it does, because we did not sample a full enough set of sites to sufficiently observe places where eelgrass is *not* growing. In addition to this, we cannot assess why the year-to-year variability as the number of sites resampled (3 years) is low. There are many places where eelgrass is not growing, where it used to grow (Figure 2). Furthermore, some Cree land users have recently observed that eelgrass was growing in areas where it had previously been absent before disappearing again. These observations show how James Bay eelgrass beds can be highly dynamic. There are additional limitations to our ability to explain why eelgrass grows well where it is growing have to do with the recent history of decline and recovery, and we explain those below.

Where did we observe eelgrass?

We observed eelgrass growing at far fewer locations in recent years than it was remembered to be at in the past by Cree (pre-1996's), and then it was documented by Hydro Quebec surveys in 1996 or before (Figure 2 *that shows eelgrass presence based on surveys and Cree knowledge*). We visited sites with land users where eelgrass used to grow well. At some of these sites there was no eelgrass, and at others, there was eelgrass but in different conditions.

A)

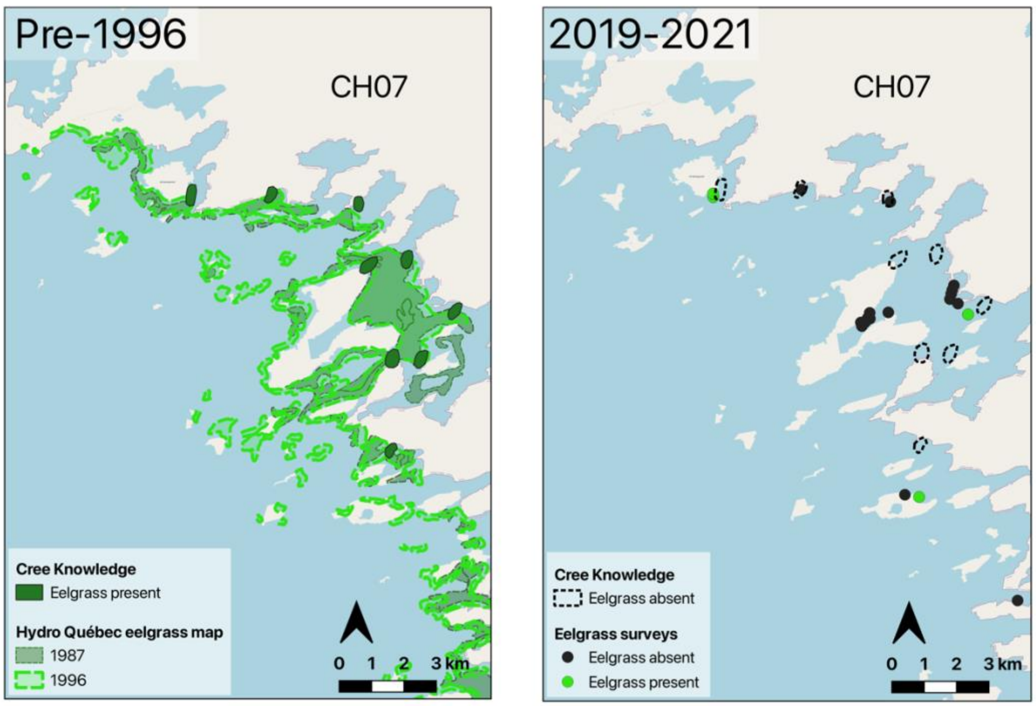

B)

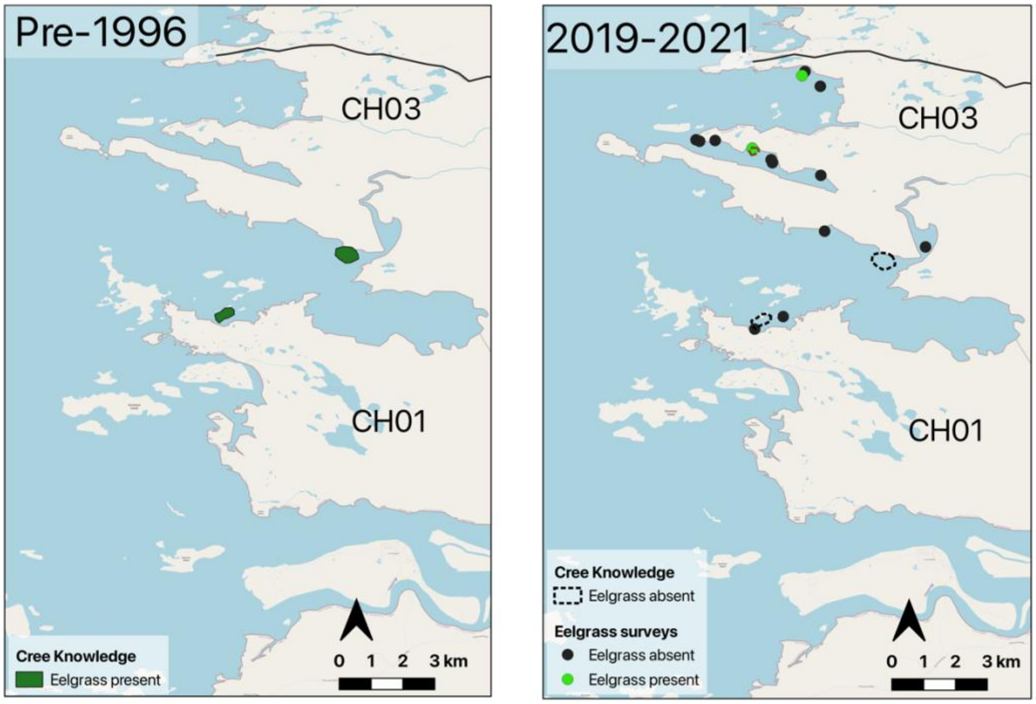
Pre-1996
CH03
CH01
Cree Knowledge
Eelgrass present
0 1 2 3 km
2019-2021
CH03
CH01
Cree Knowledge
Eelgrass absent
Eelgrass surveys
Eelgrass absent
Eelgrass present
0 1 2 3 km

C)

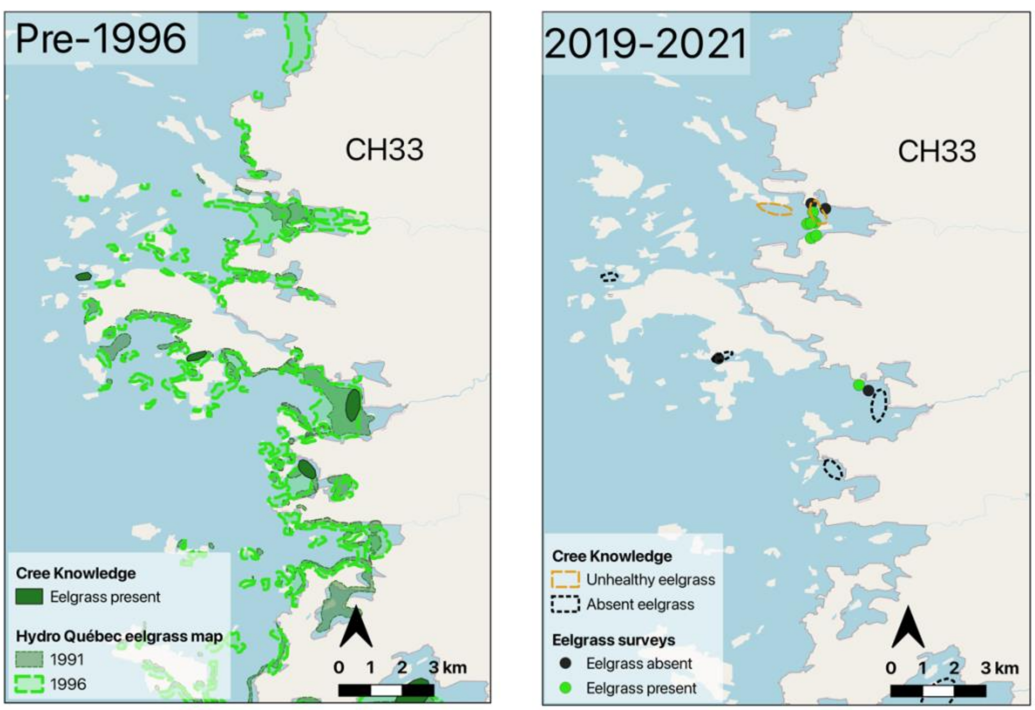
Pre-1996
CH33
Cree Knowledge
Eelgrass present
Hydro Québec eelgrass map
1991
1996
0 1 2 3 km
2019-2021
CH33
Cree Knowledge
Unhealthy eelgrass
Absent eelgrass
Eelgrass surveys
Eelgrass absent
Eelgrass present
0 1 2 3 km

D)

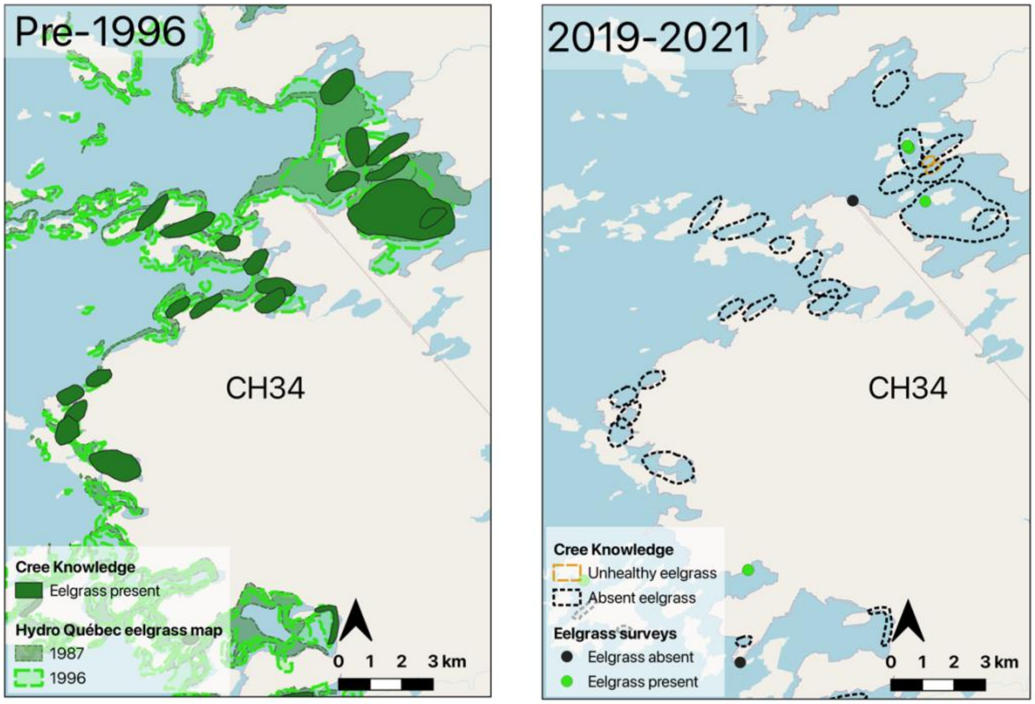
Pre-1996
CH34
Cree Knowledge
Eelgrass present
Hydro Québec eelgrass map
1987
1996
0 1 2 3 km
2019-2021
CH34
Cree Knowledge
Unhealthy eelgrass
Absent eelgrass
Eelgrass surveys
Eelgrass absent
Eelgrass present
0 1 2 3 km

E)

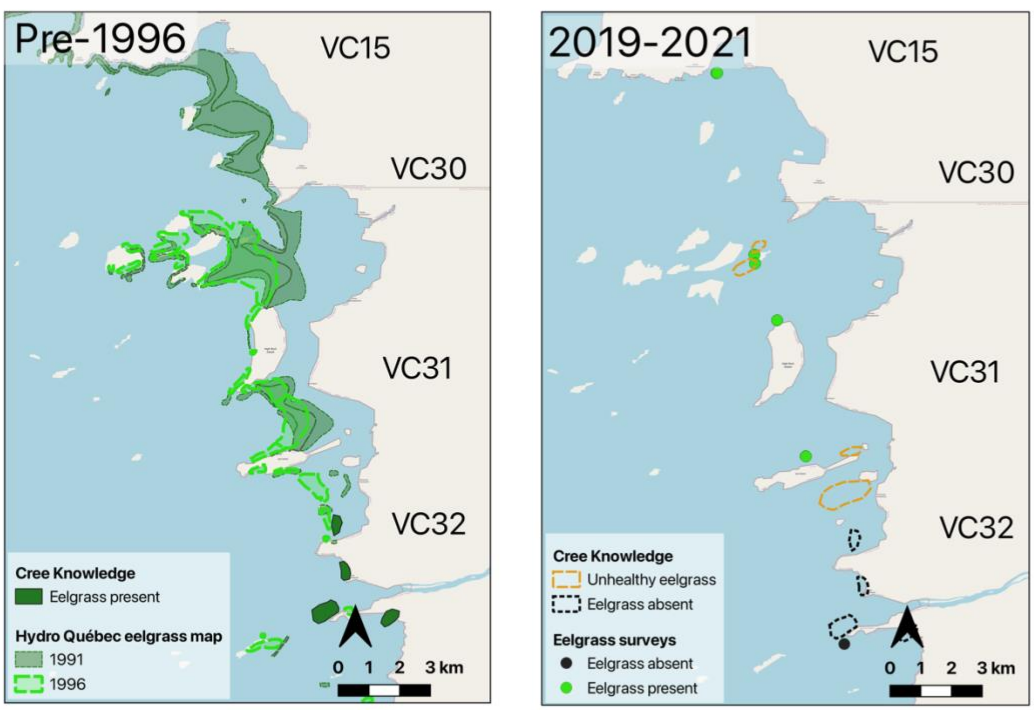
Pre-1996
VC15
VC30
VC31
VC32
Cree Knowledge
Eelgrass present
Hydro Québec eelgrass map
1991
1996
0 1 2 3 km
2019-2021
VC15
VC30
VC31
VC32
Cree Knowledge
Unhealthy eelgrass
Eelgrass absent
Eelgrass surveys
Eelgrass absent
Eelgrass present
0 1 2 3 km

F)

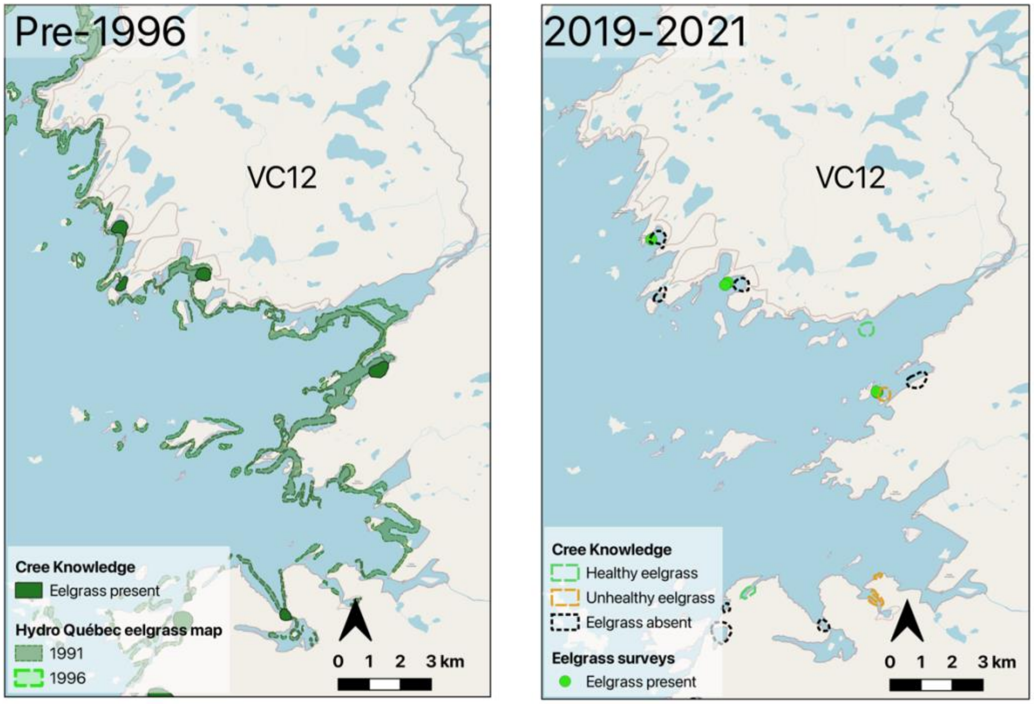
Pre-1996
VC12
Cree Knowledge
Eelgrass present
Hydro Québec eelgrass map
1991
1996
0 1 2 3 km
2019-2021
VC12
Cree Knowledge
Healthy eelgrass
Unhealthy eelgrass
Eelgrass absent
Eelgrass surveys
Eelgrass present
0 1 2 3 km

G)

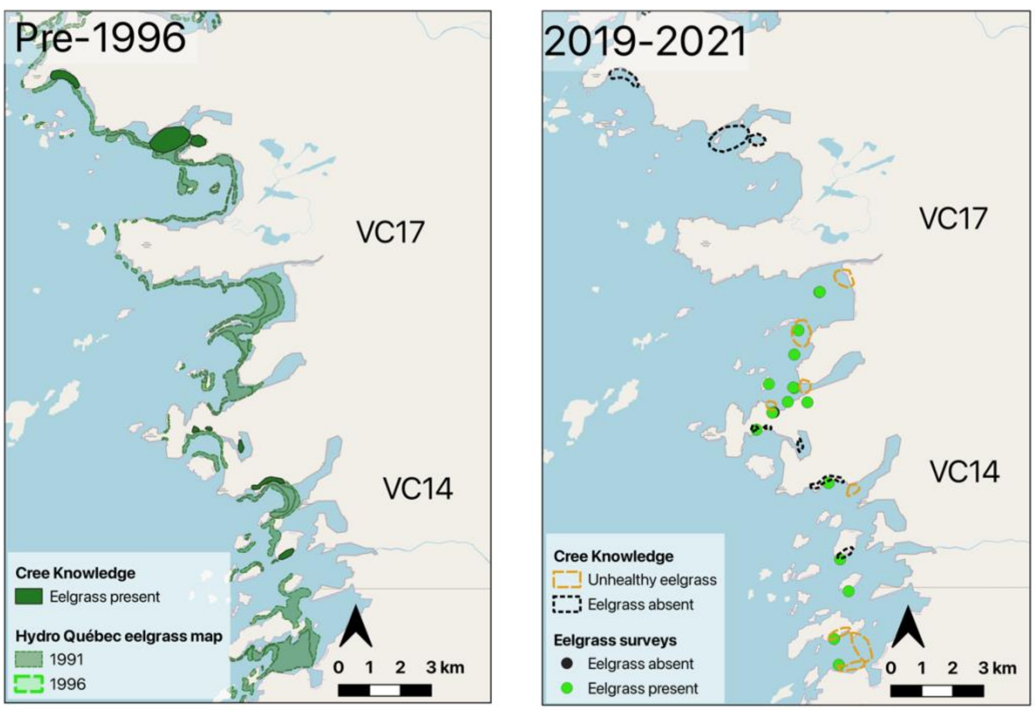
Pre-1996
VC17
VC14
Cree Knowledge
Eelgrass present
Hydro Québec eelgrass map
1991
1996
0 1 2 3 km
2019-2021
VC17
VC14
Cree Knowledge
Unhealthy eelgrass
Eelgrass absent
Eelgrass surveys
Eelgrass absent
Eelgrass present
0 1 2 3 km

H)

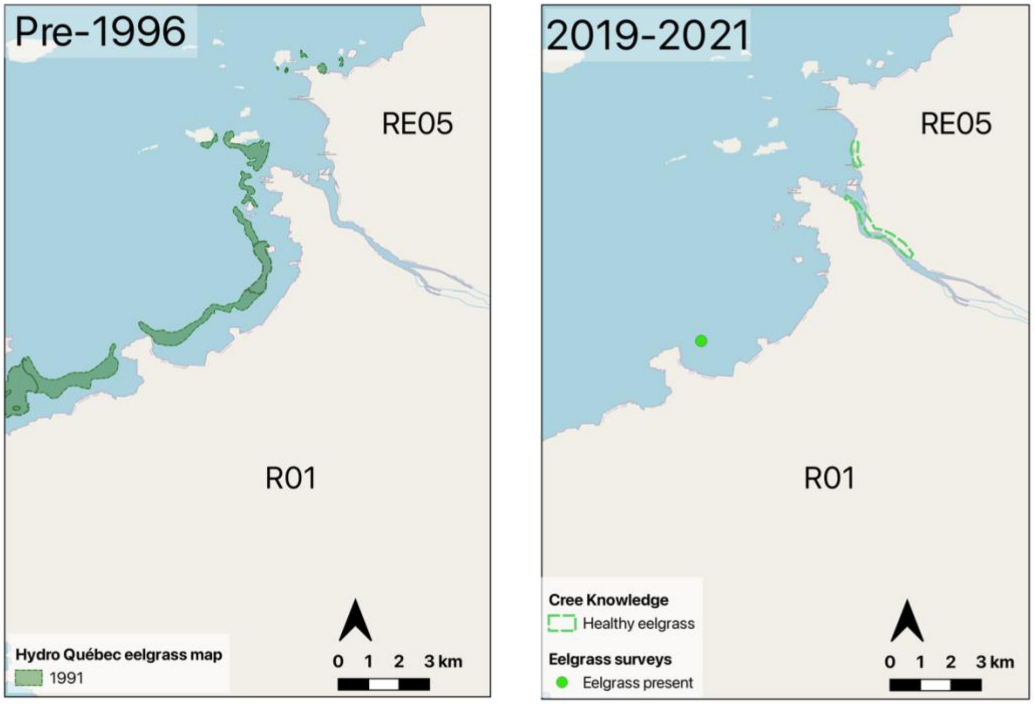

Figure 2 Eelgrass presence and absence based on eelgrass team dive and snorkel surveys from 2019-2021, on Cree knowledge (surveys conducted by Julián Idrobo) and Hydro-Québec eelgrass distribution map produced in 1996 (Lalumière et al. 1996) and 1991 (GEL 1992) along the eastern coast in A to H. Eelgrass was not mapped South of CH38 in 1996 - so we used 1991.

What was the eelgrass like, when it was present?

When we did observe eelgrass, its densities, length and biomass varied quite a lot within sites. Eelgrass that we observed ranged in size from very tiny shoots to shoots up to approximately 1 m in length (Figure 3). Based on measurement of 1439 shoots across 14 traplines, eelgrass shoots were much smaller in 2019-2021 (Figure 3) than the biggest shoots of ~250 cm documented in 1988-1991 dive surveys near Chisasibi (Lalumière et al. 1994).

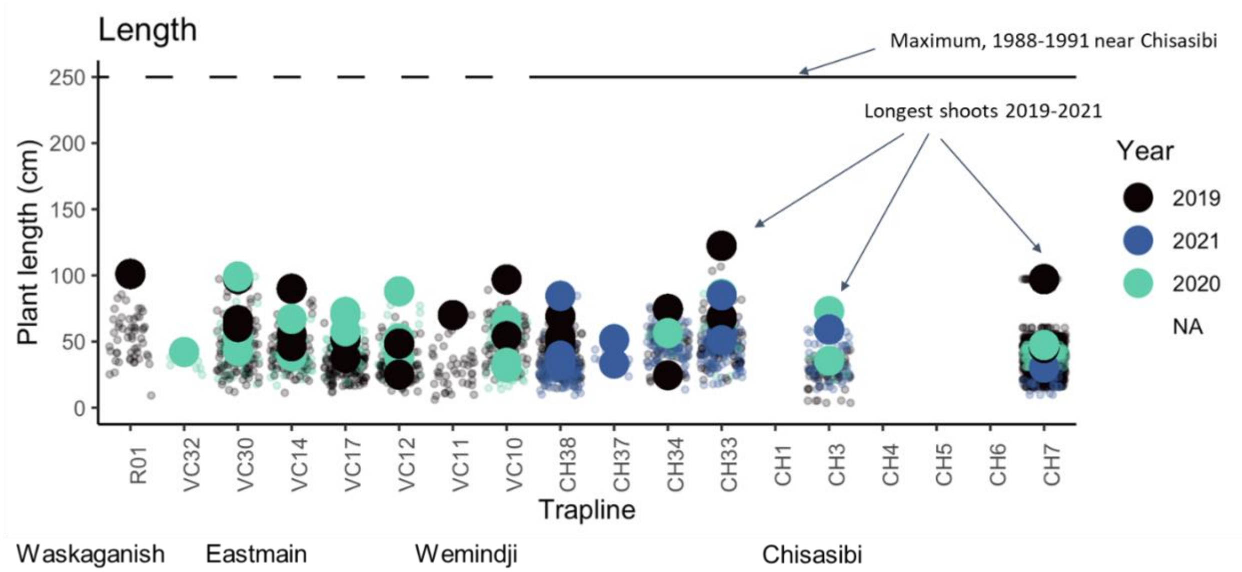

Figure 3 Eelgrass shoot lengths. Horizontal line shows the biggest shoots documented in 1988-1991 dive surveys near Chisasibi. Source: O'Connor et al. (in prep.)

One measure of eelgrass size is the length of the longest shoot, also called canopy height. The traplines with the longest eelgrass when we visited in 2019 were: VC10, VC17, CH34, and in 2020, CH33, CH3 and CH7 had long eelgrass (Figure 3). From year to year (between 2019, 2020 and 2021), eelgrass varied in size even at the same site, though CH34, CH33 and VC12 had the most consistent eelgrass over time. One thing that affects eelgrass length in the data is the date we visited the site, relative to when the ice melted. Indeed, canopy height usually peaks several weeks after the ice breaks, as the growth rate increases rapidly (Figure 4).

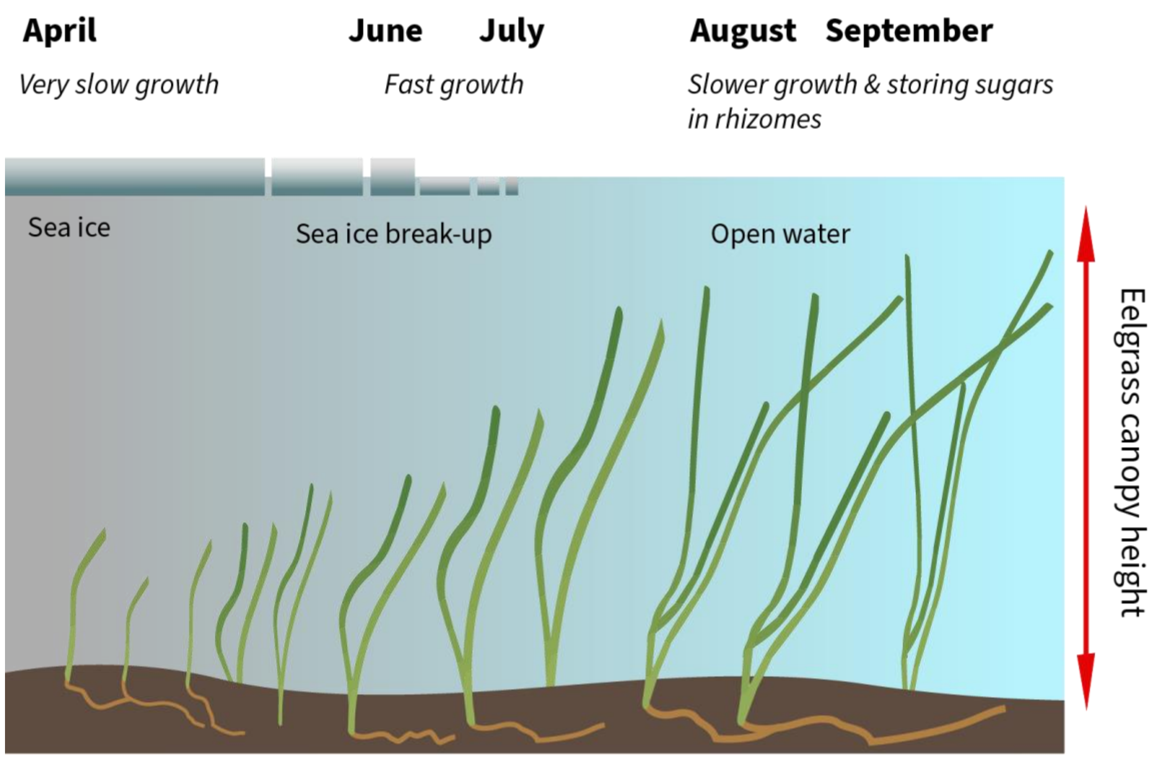

Figure 4. Seasonal pattern of eelgrass growth. Eelgrass survives and grows under the ice in winter, and when the ice breaks up it grows quickly until it reaches its maximum length for that year. Then, it spreads and stores sugars for the winter. The period of maximum *growth* is July, and the period of maximum *biomass* is August.

Shoot density is another measure of eelgrass meadow health. The densest eelgrass we observed was nearly 400 shoots m^{-2} (shoot m^{-2} - *number of shoots within a square meter*) at CH34 in 2021 (Figure 5). We observed densities greater than 200 shoots m^{-2} at three other traplines: R01, VC17 and VC30. The lowest densities we observed were at CH7 in 2021 and CH3 in 2019 and 2021. The low-density meadows in CH7 are areas known to historically have had high abundance (Figure 2 A), and CH3 do not have historical records of large meadows. We sampled density on SCUBA, manually counting each shoot and did this for 11 sites in 2019, four of them being revisited in 2021. CH3 and CH33 had similar densities in 2021 as in 2019, while CH34 had higher density in 2021, and CH7 had much lower density in 2021.

A flowering shoot is a shoot that develops flowers and releases seeds. We observed a high proportion of flowering shoots in R01, VC30 and VC17, and a few flowering shoots in CH34, CH38 and VC12. We observed no reproductive shoots in VC11, CH3, CH7, CH33, though at CH3 and VC11 we might have visited too early in the season. High proportions of flowering shoots (> 20%) can be a sign of stress (Figure 6).

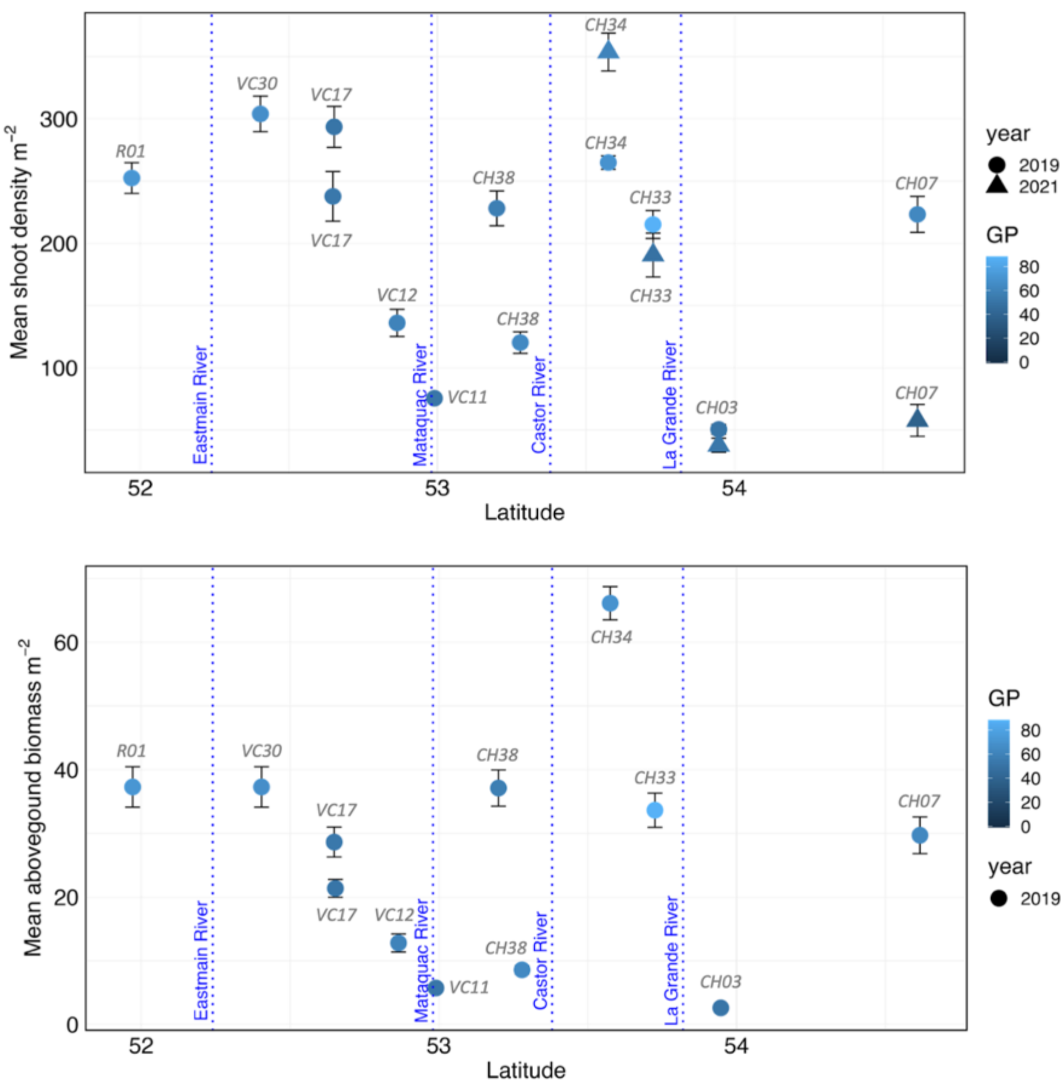

Figure 5 Density and above-ground biomass at 12 sites where we were able to dive and collect 9 replicate samples of seagrass. Color codes indicate growing period, which is the number of days between the date we visited the site and the date of ice melt.

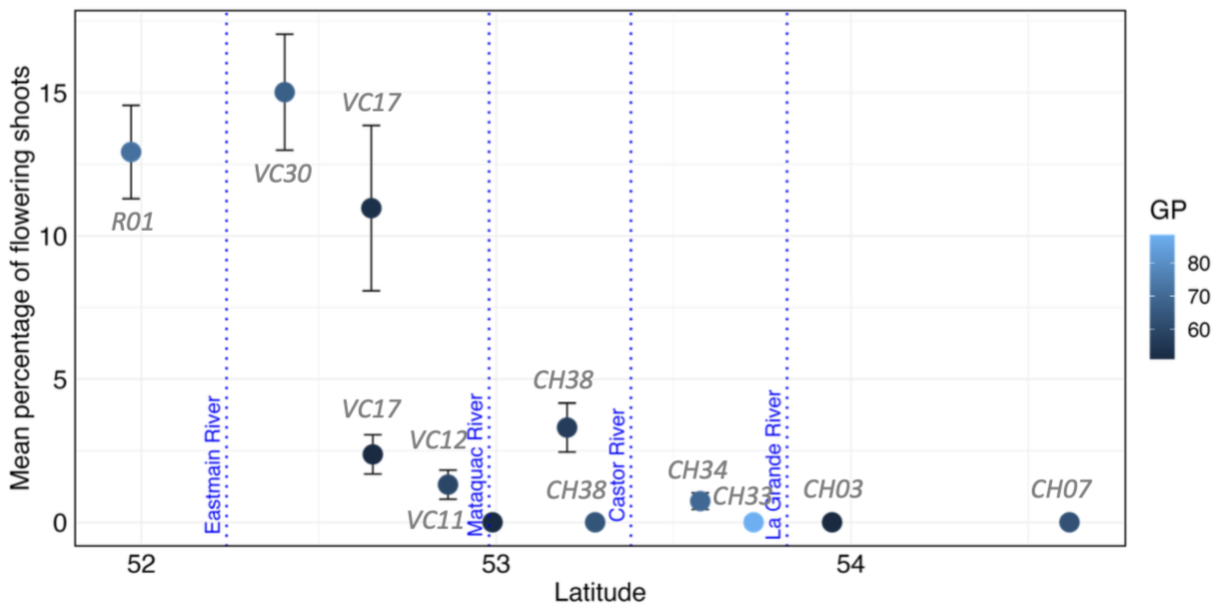

Figure 6 Mean percentage of flowering shoots in 12 dive sites. Color codes indicate growing period, which is the number of days between the date we visited the site and the date of ice melt.

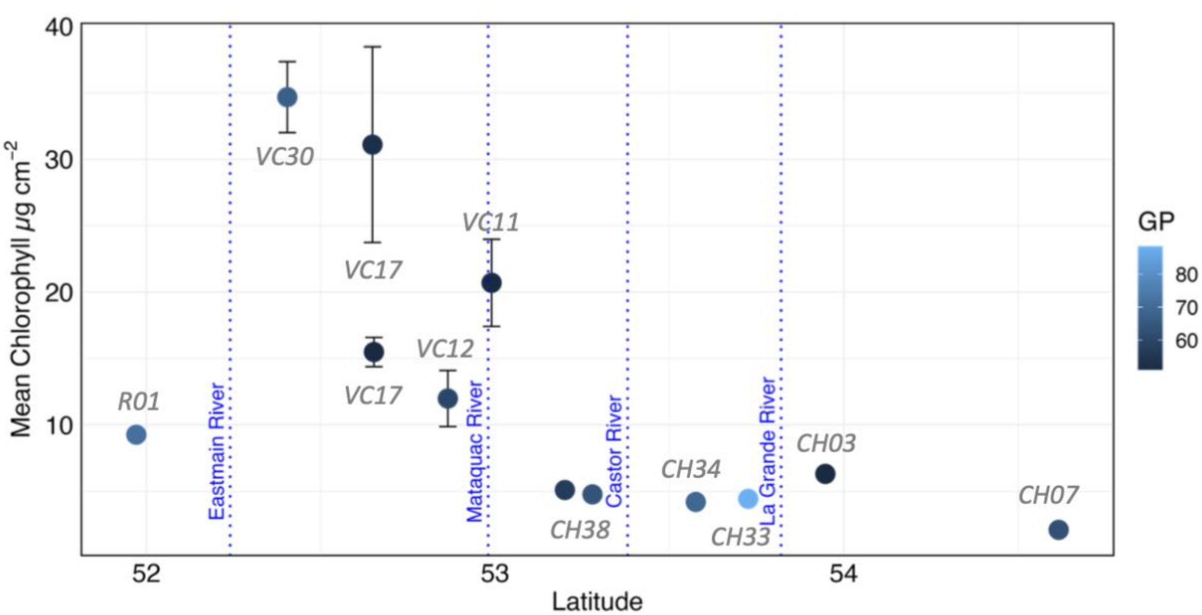

Figure 7 The epiphytic algae on eelgrass leaves was measures at 12 sites in 2019, using the chlorophyll a content as a proxy. Color codes indicate growing period, which is the number of days between the date we visited the site and the date of ice melt.

Where was it growing well?

Most of our observations are on eelgrass size or density, but we also wanted to know how well eelgrass is growing. This can help us understand, is it small shoots because it's still growing, or is it small because it's done growing. Measuring growth rate requires puncturing shoots with pins to follow the migration of the scar along the shoot with the formation of new tissues. The only way to do it in this project was to dive on the same sites repeatedly, finding the shoots identified with flags underwater. We were able to directly measure growth rates at two sites CH33 and CH34 in 2021 (Davis et al. in prep). We found that at these two sites, shoots were growing very quickly in July – between 0.5 and 1.0 cm per day (Figure 8).

We learned that eelgrass growth is likely affected by environmental conditions throughout the year. We saw evidence of fast growth in the six weeks or so preceding our sampling at CH4-DSS and VC10-F1, and even more recent fast growth (preceding four weeks or so) at CH33 sites and CH7 (high sheath length values) (Figure 9). In addition to this, we suspect that past winter growth is linked to spring growth. Using rhizome morphology, we were able to reconstruct growth in winter, and found that shoot growth in winter under ice (cm rhizome/node) is positively correlated with summer growth rate (cm rhizome/node), suggesting that eelgrass growth rates in winters is an indicator of spring growth rates (Figure 10). Overall, these results concerning growth indicate that poor conditions in the winter under ice, when eelgrass and the environment are difficult to observe, could potentially explain poor growth in the summer time. Additionally, we only measured growth rates in sites where we expected growth conditions to be good, and we found evidence of good growth. This means that overall low eelgrass abundance or biomass in these locations could be due to eelgrass loss, rather than limited growth.

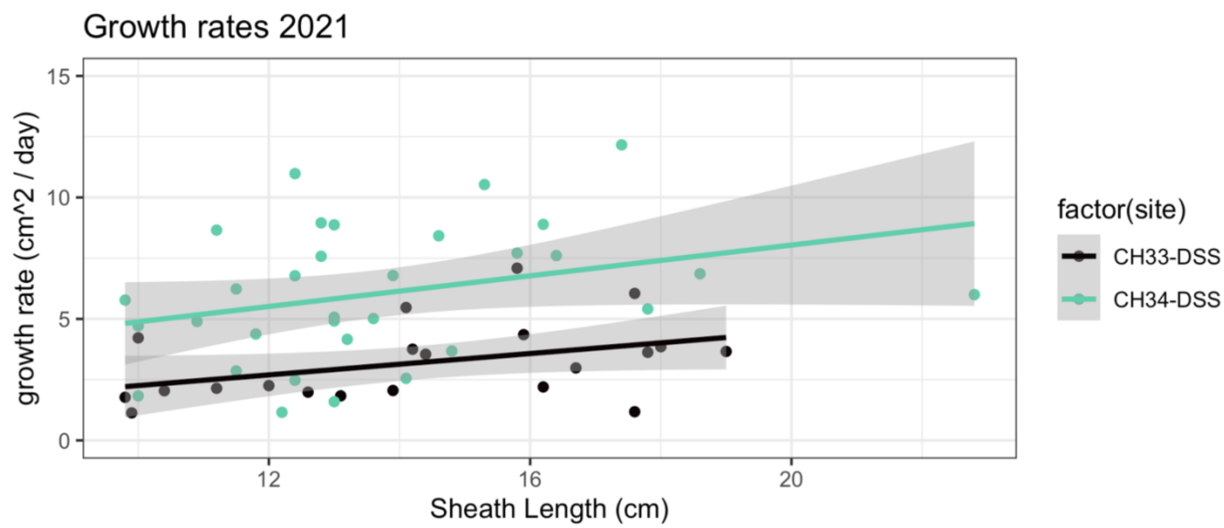

Figure 8 Eelgrass growth rates. Growth rates were measured on plants growing in the field underwater over a period of approximately 2 weeks, and growth is measured in cm^2 / day increase in surface area. We found that the length of the sheath, which is part of the shoot (Figure 1), is a good proxy for growth rate. This relationship allows us to estimate growth rates for other sites where we were not able to measure growth directly.

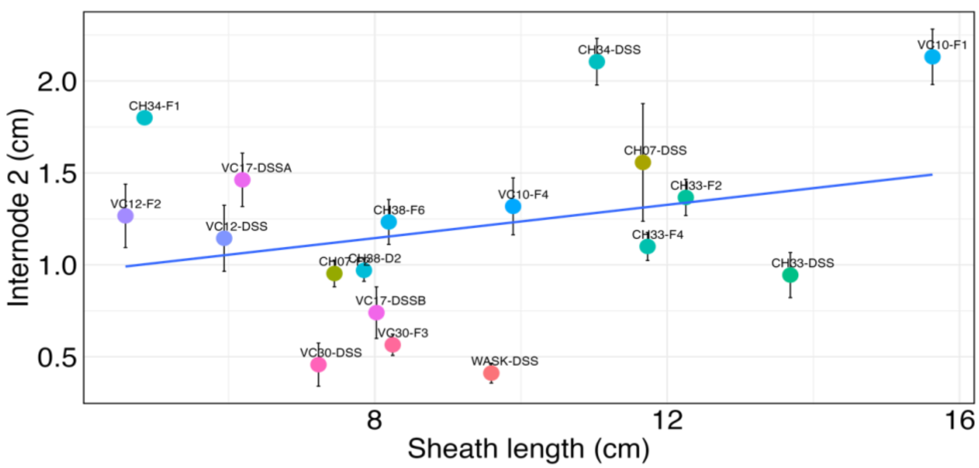

Figure 9 Morphological proxies of growth rate are correlated. Rhizomes, which are in the sediment, are separated into small segments known as internode. Internode length reflects growth. Here we assess the relationship between sheath length and the second internode (see Figure 1). Sheath length reflects recent growth rates, and internode 2 reflects growth rates in the recent past (1-2 months) (ajd. R 0.1207, p = 0.001517).

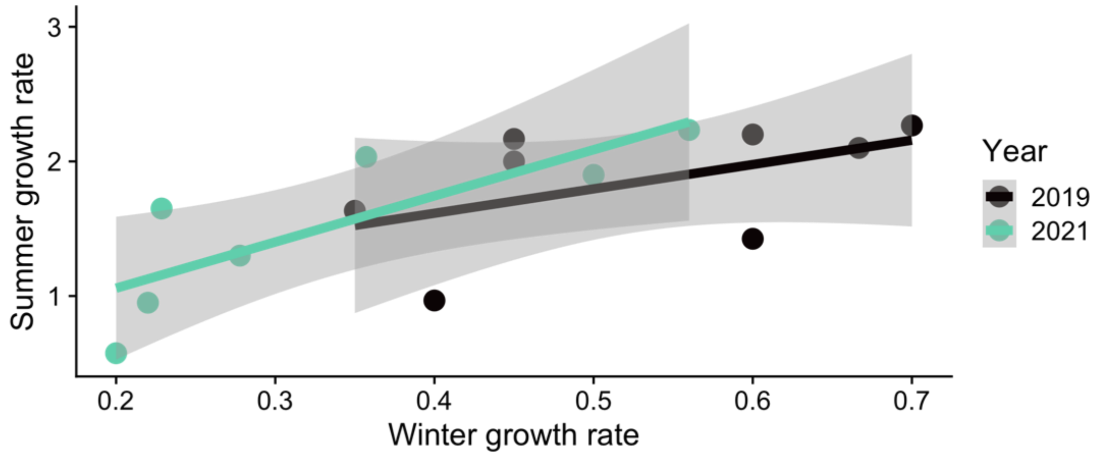

Figure 10 Using rhizome morphology, we were able to reconstruct growth in winter, and found that shoot growth in winter under ice (cm rhizome/node) is significantly related to summer growth rate (cm rhizome/node). Source: O'Connor et al. (in prep.)

Relationships between environmental factors and eelgrass growth, abundance and shoot length?

Eelgrass meadows are complex systems, generally affected by a combination of several environmental factors rather than a single driver. Environmental changes associated with climate, changes in hydrology and geomorphology, and water quality, can all change the growing environment for eelgrass and its competitors. Some changes can enhance growth, if light, temperature and nutrient conditions remain favorable. However, if light levels are reduced or salinity, temperature or water chemistry becomes intolerable to seagrasses, seagrass may no longer be able to grow well, or grow at all. Signs of stress or reduced growth in remaining meadows may be detected using analyses of seagrass morphology, reproductive features, recent productivity, and physiological conditions (Roca et al 2016). To better understand factors affecting eelgrass presence/absence and abundance, we tested several hypotheses for various present-day factors that could be associated with eelgrass surveys. These factors can be grouped into three types: 1- ice break up date, 2-landscape features, such as exposure to waves or proximity to rivers, and 3- environmental conditions, such as water temperature, salinity, turbidity, or other temporally dynamic conditions that could have affected on eelgrass loss and recovery.

1- Relationship between eelgrass shoot length and ice break up date

We estimated the number of days between ice break up dates and sample dates, referred here as the growing period. Growing period is the amount of time eelgrass would have had to grow, before we visited it to measure it. We found a positive relationship between the shoot length and growing period 2019 and 2020, meaning that sites we visited later in the summer (or where ice breakup occurred earlier in spring) where eelgrass had more time to grow had longer eelgrass (Figure 11). This was expected, and suggests that with enough light in a good environment, eelgrass is growing. However, there were no relationship in the 2021 dataset (Figure 11). The lack of relationship between shoot length and growing period in 2021 suggest that eelgrass had reached its mean height of ~ 50 cm earlier compared to 2019 and 2020. The number of free-ice days was determined for each year at each site from 1058 optical images acquired by Landsat-7 TM, Landsat-8 OLI, Sentinel-2A, Sentinel-2B, Sentinel-3A, and Sentinel-3B as well as 236 SAR imagery acquired by Sentinel-1A and Sentinel-1B. The images were acquired in spring and fall. They were orthorectified, filtered, and photo-interpreted by Armand LaRocque (Table 1).

Table 1 Distribution as a function of the satellite, year, and season of the number of images that were used for determining the number of free-ice days.

Satellite	Spring 2019	Fall 2019	Spring 2020	Fall 2020	Spring 2021	Fall 2021	Total
Landsat-7	17	10	16	21	16	19	99
Landsat-8	22	15	21	16	17	18	109
Sentinel-2A	45	34	66	69	53	61	328
Sentinel-2B	37	30	49	58	61	65	300
Sentinel-3A	0	0	19	32	27	36	114
Sentinel-3B	0	0	30	32	22	24	108
Sentinel-1A	9	13	10	19	10	13	74
Sentinel-1B	21	29	31	26	27	28	162
Total	151	131	242	273	233	264	1294

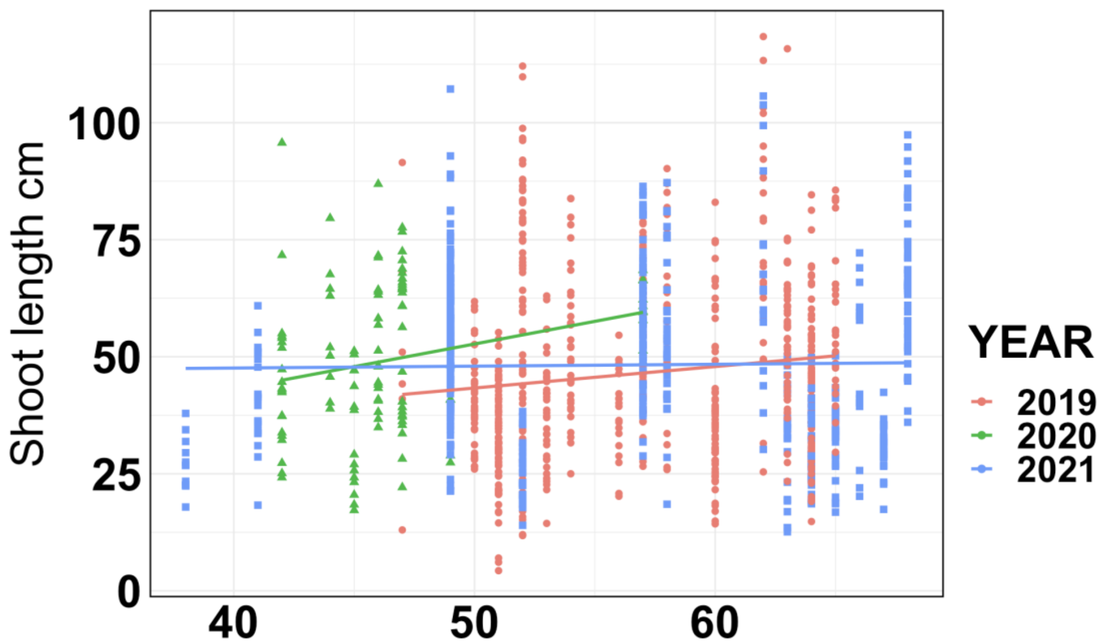

Figure 11 Eelgrass shoot length as a function of the growing period, which corresponds to the number of days between sea ice break-up and sampling dates for 2019, 2020 and 2021. Shoots are getting longer early in the season, and after that they stop getting longer and instead spread laterally. Site visits made before approximately 55 days after ice break up are likely to capture shoots still getting longer.

2- Relationship between eelgrass and landscape features

The potential effects of landscape features like exposure to waves are most straightforward to interpret because this feature is relatively constant over time. We tested a measure of exposure to waves, relative exposure index REI (Figure 12), that estimates how much exposure to wind-driven wave energy a site would experience based on the preceding 8 years of wind data from Environment and Climate Change Canada. Wind-driven wave energy would be expected to cause physical disturbance to the sediments, resuspending sediments and creating turbid water that would slow eelgrass growth by limiting light availability, as well as ripping of some shoots occasionally during extreme events. We found that eelgrass was present and absent at a similar range of exposure (REI) levels, though it was present at higher exposure levels than it was absent. Some of the sites with the lowest wind exposure were those in CH3 (Figure 2 B), and some of the highest wind exposure sites were in CH7 (Figure 2 A) and VC30 (Figure 2 D). We also tested whether ice break-up date was associated with eelgrass presence and eelgrass length. Eelgrass was present at sites with early and late ice break-up dates. We think that early ice break-up dates might have a negative effect on eelgrass growth by creating open water, exposure to wind in late spring and increasing sediment resuspension.

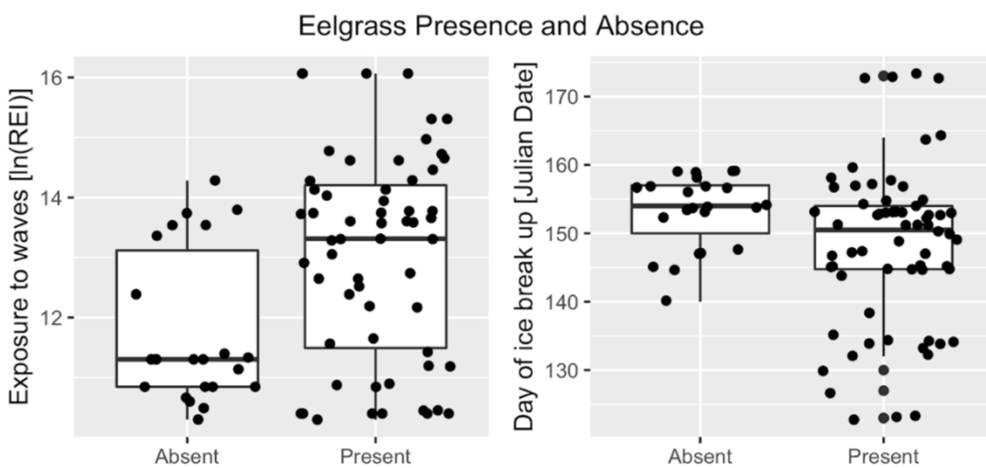

Figure 12 Eelgrass presence (n = 76) and absence (n = 30) varied somewhat with exposure to winds and ice break up date. This is the set of observations for sites that we visited at least 50 days after ice-melt. We excluded these because early in the growing season, eelgrass is very small and easy to miss, even if it is there. Of the sites we visited, which was not a systematic or random sample of the coastline, we found eelgrass to be absent at many sites. Our sampling design prioritized visiting sites where eelgrass was expected to be present. Sites with eelgrass tended to have, on average, **LEFT)** higher exposure (log(REI); t-test: $t = -3.54$, $df = 50.0$, $p < 0.001$); and **RIGHT)** earlier ice melt dates, expressed as Julian dates (t-test: $t = 2.70$, $df = 80.30$, $p < 0.05$). Includes observations from 2019, 2020 and 2021.

Sea bottom sediments can be very hard or soft depending on the composition (the amount of silt, sand, clay, small rocks…). Eelgrass shoots need sediments soft enough to anchor their rhizomes and take up nutrients by their roots. Sediment hardness, estimated by divers using a qualitative scale, seemed to be negatively related to shoot size (Leaf area index, LAI) (Figure 13). We observed fewer sites that had hard sediments and seagrass, so there is a much higher frequency of sites with eelgrass and soft sediments, as expected. We did tend to see smaller eelgrass at sites with very hard sediment, but we note that we also had fewer sites with eelgrass and hard sediment. We cannot exactly relate length to hardness because the sites with the shortest eelgrass lack hardness measures.

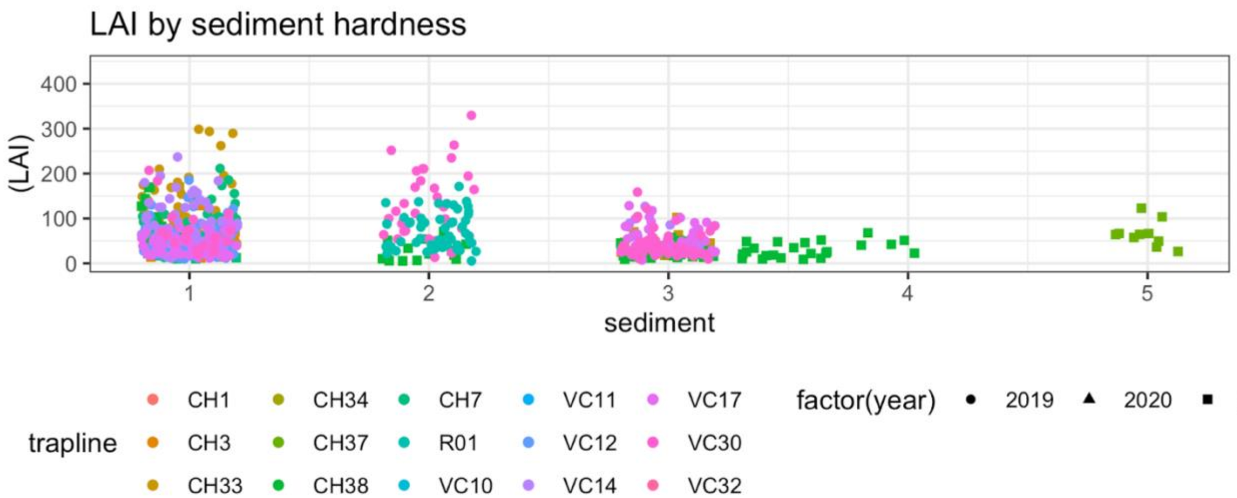

Figure 13 Leaf area index (LAI) is a measure of photosynthetic capacity for eelgrass. Sediment 1 soft to 5 hard, based on a qualitative scale developed by the CHRCP divers.

3- *Relationship between eelgrass and environmental conditions*

To determine which environmental factors influenced eelgrass growth and abundance, we tested the relationship between a few key water parameters and eelgrass aboveground biomass, density, shoot length and growth, using these growth rate proxies (rhizome node length). Discrete environmental parameters measured in the field as the eelgrass were sampled were associated with eelgrass density and recent growth (Table 2). However, we do not know whether these water properties are representative of these sites over the growing and ice-free periods. Based on the water samples we collected on the days we visited the sites to sample eelgrass density, there were positive relationships between eelgrass bed density and warmer, more highly coloured water as indicated by concentrations of CDOM. Warmer water was highly correlated with higher CDOM (R^2 = 0.72), higher SPM (R^2 = 0.42), and lower salinity (R^2 = 0.64). We suspect that the warmer, more coloured water is indicative of more summertime conditions, further advanced into the growing season, which we associate with larger plants and denser beds. We found that water conditions in the summer were associated with recent shoot growth rates, specifically temperature. The growth rates of the second rhizome internode exhibited an upward trend at colder water temperatures and suspended particulate matter (SPM), while it showed an upward trend with an increase in salinity (Figure 14). This suggests that combined factors of water temperature, salinity and water clarity may influence growth rates early in the spring. *It is to be noted that these are preliminary findings that may change following further investigation; one major limitation is that the temperature, salinity and water data used here are only from the day we visited the site to collect eelgrass; these measures of water conditions may not accurately reflect the growing conditions of eelgrass over the previous months.*

Table 2. Relationships between eelgrass properties and water parameters measured on the day of eelgrass collection at sampling sites in 2019. We used linear regressions and here show the adjusted R values, with values in bold above 0.10. Adjusted R above 0.10 suggests a possible relationship between the water parameter and eelgrass measurement. Non-significant statistical relationship between a water parameter and eelgrass measurement is indicated with NS (non-significant).

	Aboveground biomass (g m^{-2})	Shoot density (m^{-2})	Length (cm)	Rhizome internode 2 growth rate
Salinity	NS	NS	0	**0.2**
Water Temp (°C)	0.03	**0.11**	0.04	**0.18**
CDOM (442 m^{-1})	0.08	**0.16**	0.06	0.01
SPM (mg L^{-1})	NS	0.02	0	**0.19**
Turbidity (NTU)	NS	NS	0.02	0.03
Nutrients in water column*	0.01	0.01	0.00	NS
Nutrients in sediments*	0.03	0.05	0.04	NS
Chl *a* (μg L^{-1})	0.03	0.02	0.05	**0.13**

*nitrate+nitrite corrected for salinity

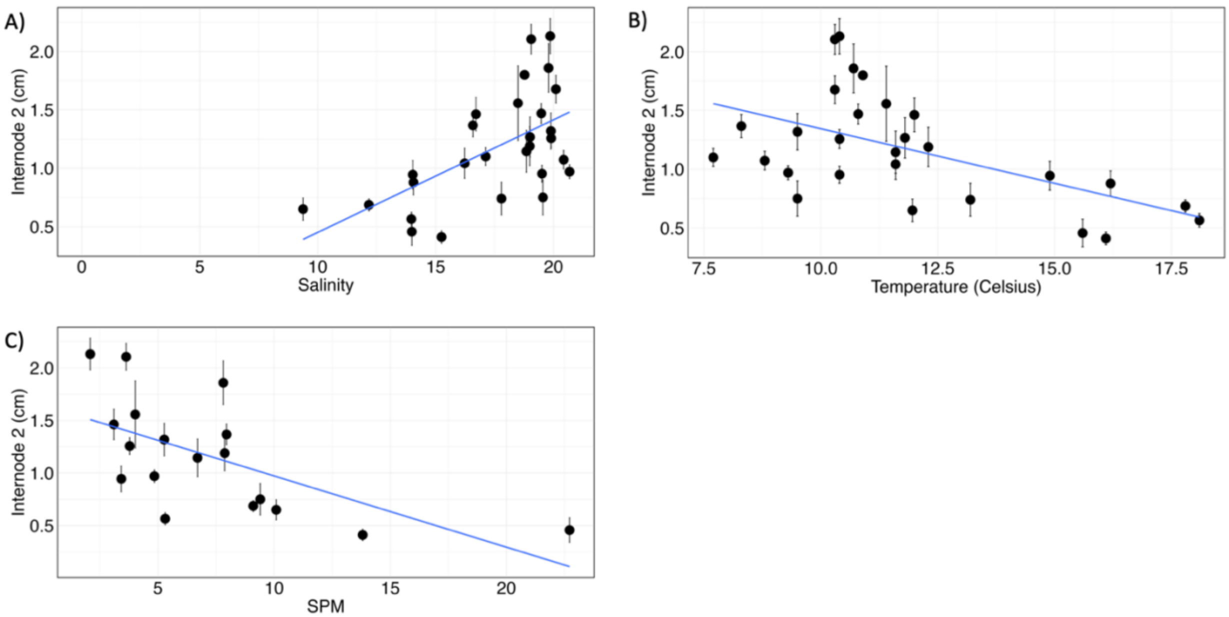

Figure 14 Relationships between (A) salinity, (B) water temperature, and (C) SPM and the recent growth rates of eelgrass estimated from length of internode 2 on the rhizome. Is to be noted that we found that warmer water is also highly correlated with higher CDOM (R^2 = 0.72), higher SPM (R^2 = 0.42) and lower salinity (R^2 = -0.64). Source: O'Connor et al. (in prep.)

Eelgrass beds still shelter a diversified community of epifauna

The current eelgrass beds still provide habitat for a wide variety of invertebrates that live on the eelgrass leaves (epifauna) including shrimp, amphipods, isopods, and snails (Figure 15, 16). The diversity and abundance of epifaunal organisms play an important role in the coastal food chain. Eelgrass meadows with high epifaunal diversity and abundance may support a greater number of fish species and potentially serve as an attractive habitat for larger predators such as seabirds that feed on small fish dwelling within eelgrass meadows. Additionally, the epifaunal diversity of these habitats can provide an indication of the environmental conditions and the disturbance history of the meadows. We observed invertebrate assemblages typical of eelgrass meadows elsewhere (Duffy et al. 2015; Gross et al. 2022) with a mix of crustaceans, snails and worms. We noticed that one common member of eelgrass animal assemblages, the limpet, was not present anywhere in our samples, but had been noted in the region by Lalumiere et al 1994. It is possible that this species was lost during the eelgrass decline of the late 1990s. Crustaceans and some of the larger worms (annelids) are good food for fish. Notably, we did observe a few species typical of very freshwater environments abundant in several meadows. These species are chironomids, a type of insect larvae. Their presence is an indication of persistent freshwater in these eelgrass meadows related to nearby rivers. In other meadows were inhabited by more marine (higher salinity) animals. This suggests that future research could investigate the fate of the limpets, to quantify the contribution of eelgrass-associated animals to fish populations by using isotope and fatty acid tracers, and to study the biodiversity and function of the animals living in the sediments near the eelgrass rhizomes. These below-ground animals generally play an important role in the health of eelgrass rhizomes.

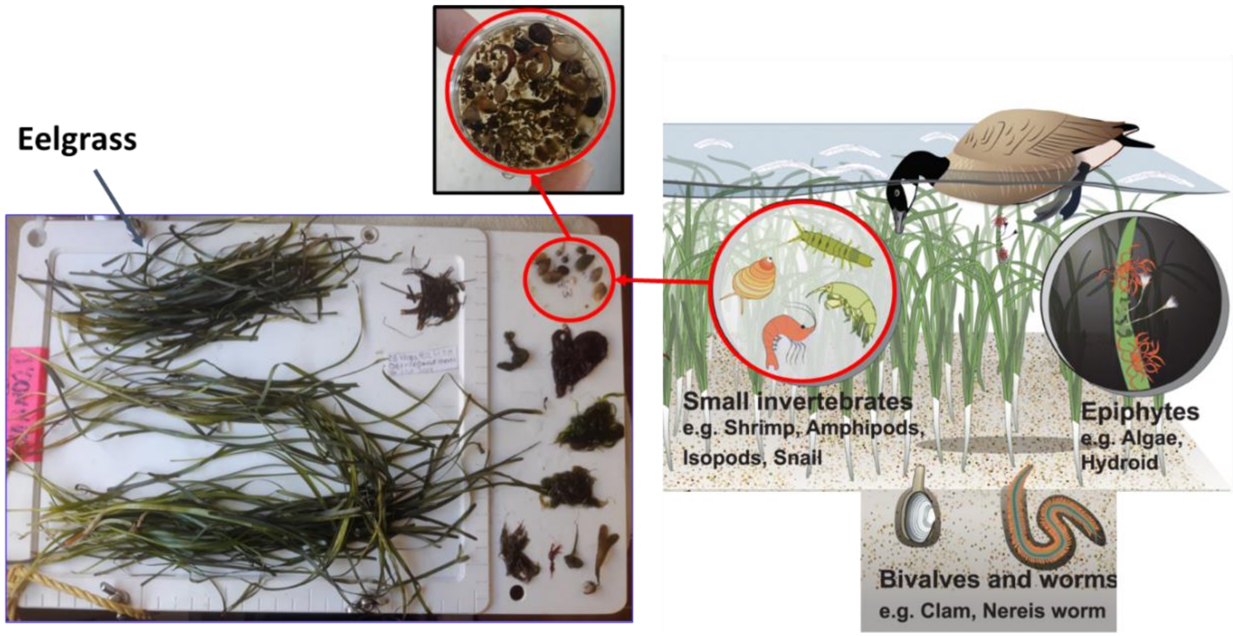

Figure 15 Examples of invertebrates living in and around the eelgrass and collected by the divers on SCUBA. Leblanc et al. (in prep.)

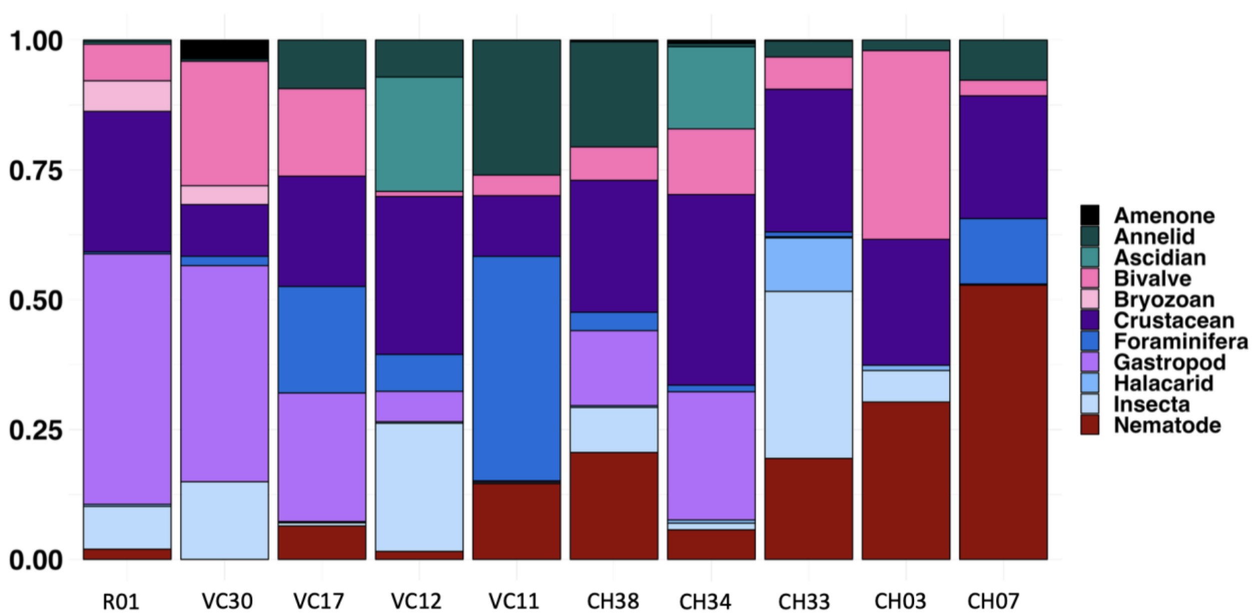

Figure 16 Relative abundance (%) of 11 taxonomic groups in each dive site. Gastropods are snails, nematodes and annelids are worms, crustaceans are little bugs. Foraminifera are signs of more ocean water, and insects (insecta) are signals of more freshwater. Source: Leblanc et al. (in prep).

Eelgrass physiological indicators

To study the eelgrass health, we used different chemical indicators and measurements in leaves and roots. These measurements help us see how the plant is storing energy and obtaining sufficient nutrients. If these properties were monitored consecutively for several years, the results could reveal locations that are persistently better (or worse) for eelgrass growth and show whether there are important inter-annual differences between “good” and “bad” growing seasons. In other words, we would be able to see how the growing season affect eelgrass abundance in the longer term.

Eelgrass stores energy reserves (measured as Carbon C content) in the roots and uses this energy to grow and survive in less favorable conditions (i.e., winter season). C content in percentage in eelgrass in James Bay ranged between 15 to 45; C content in eelgrass roots from CH7 and CH3 traplines were lower than in the other traplines in 2021 (Figure 17), indicating that eelgrass from these traplines had lower energy reserves for starting new growth in the spring. Nitrogen (measured as Nitrogen N content) in leaves is an indicator of whether the plant is obtaining enough nutrients. Eelgrass that are nitrogen-deficient have nitrogen values below 1.8 % (Short and McRoy, 1984). The eelgrass nitrogen values in eastern James Bay were typically above 1.8 % (Figure 17, middle panel), suggesting that eelgrass growth is not limited by nutrients. Lastly, nitrogen isotopic ratios (measured as delta 15N ratio; Figure 17, lower panel) in eelgrass shoots can help determine if eelgrass are taking up nutrients from the water column or sediments (Lepoint et al. 2004). Except for eelgrass in CH7, delta 15N ratio values were low, indicating that the nutrients are taken up from sediments. CH7 has very sandy seabed that may not contain many nutrients. Therefore, at this location, eelgrass growth may be limited by low nutrient availability in the water column.

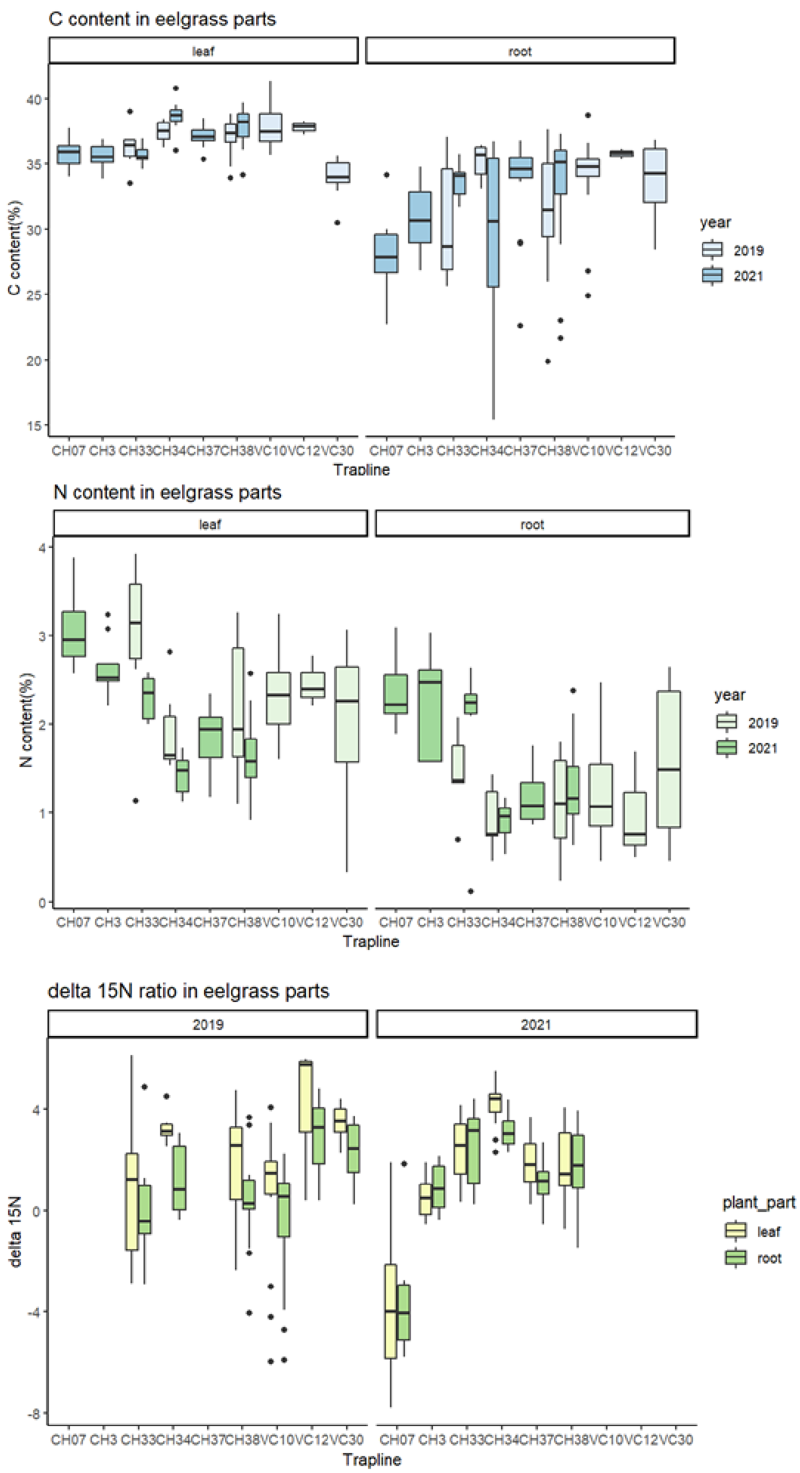

Figure 17 Eelgrass physiology results indicating the energy reserve and nutrient status of the eelgrass: Carbon C content (top), Nitrogen N content (middle), and delta 15N ratio (bottom) across traplines. Source: Noisette et al. (in prep.)

Light and nutrient experiments

Eelgrass growth and productivity are significantly impacted by various factors and light and nutrient availability are among the most influential factors. Through our research comparing growth and eelgrass presence in other sites, we suspected temperature and salinity in most areas were not limiting eelgrass growth; but there was still a possibility that light and nutrients were problematic. Given the time we had in the field in 2021, we could only experiment with water column nutrients, and we did not manipulate nutrients in the sediments. To test whether the light and nutrient levels in the water could be limiting eelgrass growth in eastern James Bay, we conducted experiments on eelgrass from two eelgrass beds in CH33 and CH34, where eelgrass was observed to be relatively healthy relative to other areas yet still well below historical sizes. To test for nutrient limitation, we experimentally manipulated water column nutrient concentration in the beds and compared eelgrass growth in manipulated (high nutrient concentration) and controlled (ambient nutrient concentration) locations at each site. Divers on SCUBA measured eelgrass growth rates using a standard growth measurement protocol. Overall, the experiment demonstrated that eelgrass shoots are growing quickly in both beds. We found no effect, either positive or negative, of nutrient addition on eelgrass growth rate (Figure 8). We did find a positive effect of nutrient addition on epiphyte accumulation rate suggesting that algae growth is limited by low nutrient availability in the water column (Figure 18). Because addition of nutrients to the water did not improve eelgrass growth, we conclude that the eelgrass takes up enough nutrients from the sediments at these locations. The concentration of nitrogen (measured as ammonium) in the sediments was about 10-times higher than in the water column (Figure 19), which is consistent with the conclusion that the sediments supply the nutrients to the eelgrass.

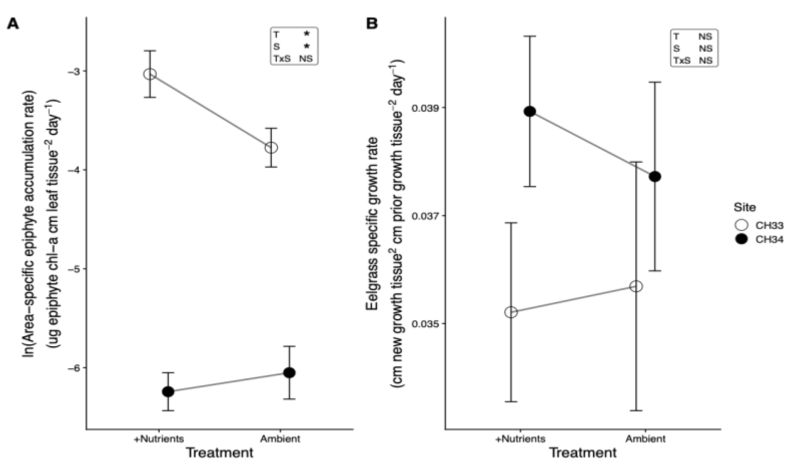

Figure 18 Experimental results for nutrient addition experiment. Panel A) effects on epiphytes (logged area-specific epiphyte accumulation rate); Panel B) effects on eelgrass (area-specific growth rate at each site). Panel legends indicate statistical results as significant (asterisk) or not significant (NS), where T = treatment, S = site, and TxS = treatment by site interaction. Source: Davis et al. (in prep.)

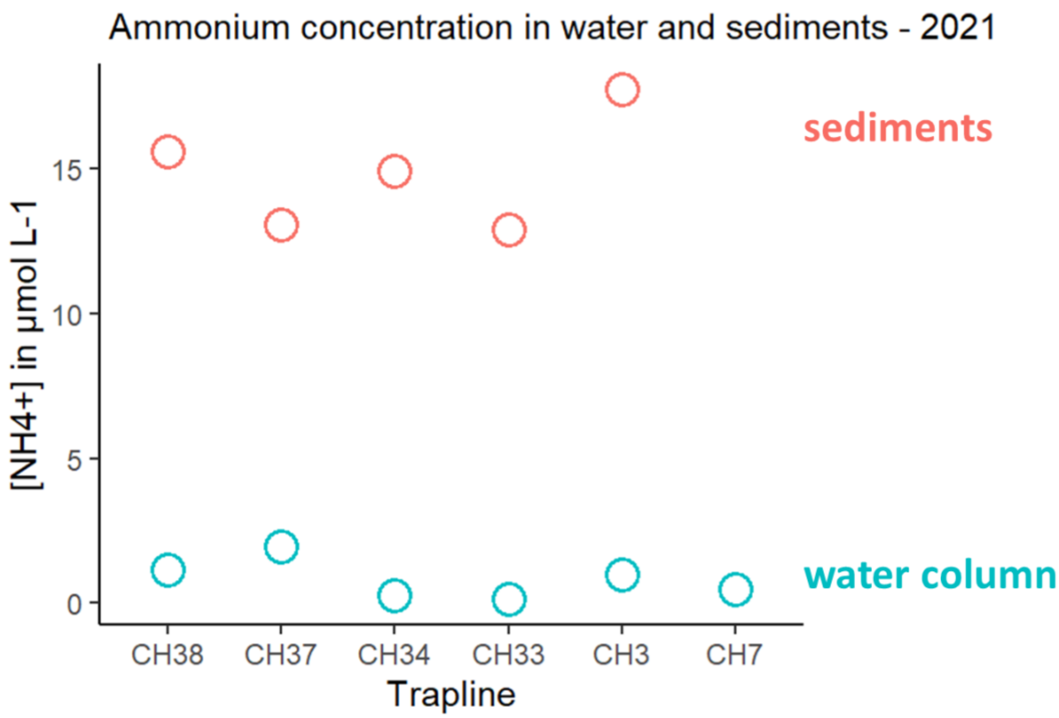

Figure 19 Concentrations of nitrogen measured as ammonium in sediments vs. the water column. Source: Davis et al. (in prep.)

To test for light limitation, we collected shoots from each eelgrass bed, brought them back to the field lab in Chisasibi, and experimentally manipulated light levels to test how the shoots responded. We found that eelgrass at both sites had high light requirements, i.e., they were not adjusted to be able to grow well in a low light environment.

Independent evidence that low light was limiting growth at CH34 was obtained by combining the knowledge about the light requirements of the eelgrass with light record collected at a CH34 eelgrass bed between April and August 2019 (Ehn, unpublished data). We found that light levels passed the minimum requirement for growth on 84% of the days where we measured light, but there was only sufficient light to *maximize growth* on 10% of these days (Figure 20). The results suggest that low light is holding back eelgrass growth during the summer. If growth is held back by low light, likely other important processes like storing carbon as energy for the winter *also* are being held back.

Severe and chronic light limitation can have consequences for eelgrass growth and survival (Bertelli and Unsworth 2018). These effects can vary throughout the ice-free season. Early in the growth season, eelgrass utilize light to synthesize new shoots and grow quickly. Light limitation during this period can reduce growth rate, leaf area, and density, leading to shorter, narrower and/or thinner leaves (Bertelli and Unsworth 2018; Schubert et al. 2018). Late in the growing season, eelgrass shoots utilize light to accumulate energy as carbon (carbohydrates) for winter survival in the dark. Light limitation during this period reduces these stores, threatening under-ice survival and early growth in the next season (Marsh et al. 1986; Bulthuis 1987).

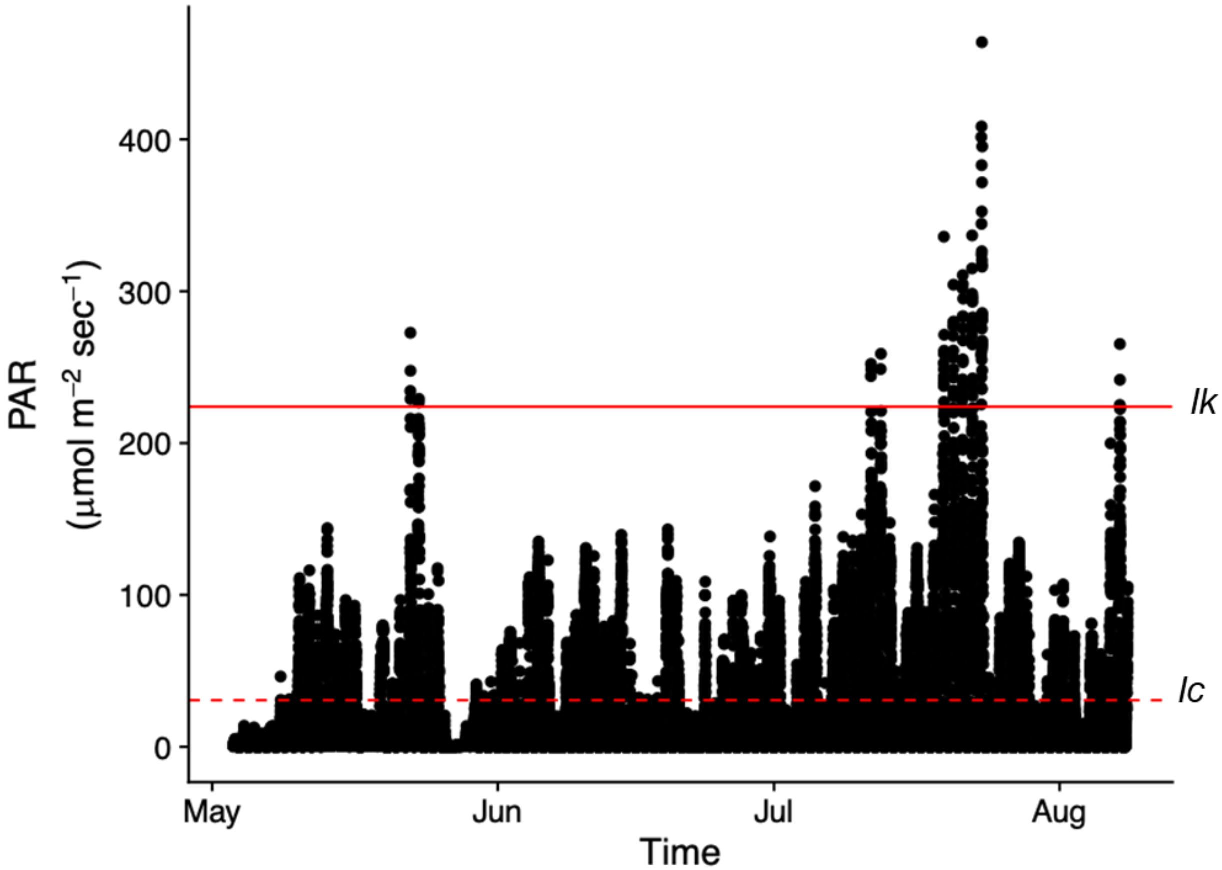

Figure 20 Light (measured as PAR) record at CH34 compared to light requirements of eelgrass. The minimum requirement for growth (compensation point, Ic) is shown by the dotted red line and the light requirement to maximize growth (saturating irradiance, Ik) is shown by the solid red line. Source: Davis et al. (in prep).

What are the characteristics of the healthier meadows?

Measures of eelgrass health include high density, tall shoots, high biomass, low percent of reproductive shoots, high growth rates and high surface area (leaf area index, or LAI). Sites that had values indicative of *relatively* healthy meadows (compared to the other meadows in our sample). We could only consider density for the 11 we sampled on SCUBA, and the highest ranking were CH34 (high density, high biomass, biodiversity, spatially consistent / not patchy), VC30 (high density, high biomass, tall shoots), and R01 (high density, high biomass, tall shoots) (Table 3). CH37, VC11 and VC32 had the shortest eelgrass; R01, VC30, VC10 and CH33 had the longest.

Table 3 Characteristics of the healthier meadows in eastern James Bay, 2019. Note, the term 'long eelgrass' in this table is only in reference to the length of eelgrass we observed in 2019. No eelgrass in our observations was long, by historical standards.

Community	Trapline	Characteristics
Waskaganish	R01	Long eelgrass shoots, high density, high biomass
Eastmain	VC30	Long eelgrass shoots, high density, high biomass
Wemindji	VC10	Long eelgrass shoots
Chisasibi	CH33	Long eelgrass shoots
Chisasibi	CH34	High density, high biomass; epifaunal biodiversity consistent/ not patchy

A note about rivers and eelgrass genetic diversity

The relationship between rivers and eelgrass health is not simple. We can see that very near some of the river mouths, other than the La Grande River, eelgrass can be shorter and less abundant (site VC11). These sites must consistently have low salinities because we observed *Ruppia maritima* (a low salinity plant) growing near *Zostera* in these areas, and we observed Chironomids, a freshwater invertebrate, on eelgrass in these places. However, eelgrass abundances were also very high at some sites near rivers (site CH33). Areas around river mouths can be suitable habitat for eelgrass if they are associated with clearer water, and as long as flow rates are not too high, and salinities are not too low (below 5) for extended periods.

The genetic analyses conducted on the 2021 eelgrass samples revealed that the James Bay *Zostera* is related to Atlantic eelgrass, and not Pacific eelgrass. Atlantic eelgrass is often shorter than what we observed in Eeyou Istchee, while Pacific eelgrass is often much longer and more consistent with what the Cree remember (Figure X). According to the study using 2021 eelgrass sample from two sites, Eeyou Istchee eelgrass populations had less genetic diversity than the populations of the Atlantic coast and the Gulf of St. Lawrence (Jeffrey et al. in revision). In addition, there were more clones per individual plant sampled suggesting a greater frequency of clonal reproduction in James Bay than in other Eastern Canadian sites. The James Bay population was found to be quite different genetically from other Atlantic populations, and most closely related to eelgrass in Rimouski, Quebec. This difference could reflect longer isolation of James Bay eelgrass from the rest of the Atlantic and potentially greater chance of local adaptation to James Bay environmental conditions of the past. The lower diversity of James Bay eelgrass could also reflect a loss of diversity associated with the late 1990s eelgrass decline. The eelgrass population in eastern James Bay may be at higher risk of climate change due to lower genetic diversity and a greater rate of change in ocean temperature. Future research that involves sampling genetics in more populations along the coast could help to determine whether the apparently low diversity is indeed low throughout the Eeyou Istchee region, and whether it reflects a genetic bottleneck in the 1990s or low diversity historically.

Coastal habitat mapping highlights

Mapping eelgrass

Using Landsat imagery, we learned more about the current distribution of eelgrass. Despite the relatively muddy waters of Eeyou Istchee, we were able to generate a map of eelgrass distribution for 2019 using Landsat-8 OLI images (Figure 21; Clyne et al. 2021). The 2019 map showed the absence of substantial eelgrass beds like those seen on the 1996 map (Lalumière et al. 1996), corroborating findings from a re-analysis of monitoring data showing a limited recovery since the decline in the late 1990s (Leblanc et al. 2022). However, we identified challenges with Landsat imagery. First, the spatial resolution of Landsat is limited. Landsat-8 images with 30 m pixel resolution may have difficulty identifying patchier eelgrass beds. Second, the 30 m spatial resolution makes pinpointing the coastline challenging. Third, the 30 m spatial resolution may be insufficient to distinguish eelgrass from other aquatic plants (Widgeon grass *Ruppia maritima*) and algae mats, which frequently co-occur with eelgrass beds in eastern James Bay (based on underwater photos from 2019 surveys). Sentinel-2 imagery that provides a bay-wide coverage at a resolution of 10 m could be a high-resolution multispectral alternative. True bathymetry data along with additional ground truth data could improve eelgrass mapping effort in eastern James Bay. We also reconstructed changes in eelgrass beds from 1988 to 2019 using a Landsat time series (Clyne 2022). The findings indicate that eelgrass appeared to decline over the research period with the decline starting in the late 1980's (Clyne 2022). Such observations agree with the Cree Land Users of Eeyou Istchee who have noted steady declines in eelgrass coverage along the coast in the late 1980s and then a drastic decline in 1997-1998 (Clyne et al. in revision). The satellite time series also revealed peaks in muddy water extents that were related to peaks in fire occurrence and extent, notably in 1989 and 2013 (Clyne 2022).

Mapping habitats

In addition to a greater understanding of the current distribution of eelgrass beds, we also mapped the distribution of several coastal habitats from Cape Jones to Ruppert Bay using Landsat and SAR imagery. We were able to use satellite imagery to examine changes in eelgrass and coastal ecosystems from 1984 to 2020 (Olatunji 2022) (Figure 22). Besides eelgrass bed declines, our study revealed a gradual drop in the surface area of shallow coastal waters and tidal flats, which is most likely due to isostatic rebound but could also be due to tide height differences. The study also revealed an increase in salt marsh and freshwater marsh, which was most likely caused by isostatic rebound. We also observed an increase in the extent of tree surfaces and a decrease in bare ground, shrubland, fen, and tundra, which could be attributed to global warming, favouring a northward migration of the tree line. The 2019-2020 mapping of coastal habitats was crucial in better understanding the habitat used by Canada Geese and Atlantic Brant in eastern James Bay (Sorais et al. 2022; Sorais et al. in revision).

Ground truth and auxiliary data – eelgrass

In the process of mapping various habitats or ecosystems such as forests, eelgrass beds, or salt marshes using satellite imagery or aerial photos, *ground truth data* are often used to verify the correspondence between the delineated habitats on the satellite images or photos and the actual conditions present at the corresponding locations. Ground truth data typically consist of field observations (e.g., photos, videos or detailed descriptions) with known GPS locations. Ground truth data is sometimes collected using a specific protocol to capture a variety of conditions (e.g., eelgrass, mud, algae, algae mixed with eelgrass, etc.). For the 2019 eelgrass map, we used field observations collected by the divers and snorkelers in 2019. The data consisted of single point observations (presence/absence of eelgrass) based on photos, videos or field notes. This data was used to produce and assess the accuracy of the eelgrass map. However, in cases where direct field observations are unavailable, alternative sources of information such as aerial photos or other maps can be used. To assess the eelgrass distribution in 1996, 1991 and 1988 using Landsat images, we used aerial photos (1996) and eelgrass maps (1996, 1991, and 1988) to generate ground truth data. We believe these were appropriate for auxiliary data because ground truth surveys were used to assess the accuracy of aerial photos and mappings (for additional information on previous mapping methods, see Appendix A).

Mapping validation for eelgrass

It is important to mention that even though ground truth surveys or auxiliary data were used in mapping, there might still be important discrepancies between what is "*actually there*", what is "*perceived to be there*" and what *is "shown on the maps*" for multiple reasons. First, the lack of ground truth data. In 2019, we had approximately over 150 single observation points collected by the divers and snorkelers. Ground truth data are critical for guiding mapping, and a lack of ground truth data can increase mapping inaccuracies (example mistake green algae for eelgrass). The single point sampling may not have captured the prevailing conditions in some areas. We therefore recommend that future mapping efforts plan ground truth surveys that aim to collect a greater number of *in situ* observations to capture a wider set of local conditions. For example, one of the most common techniques for collecting ground truth data for seagrass consist in recording underwater footage along many transects over seagrass beds. However, even with more ground truth data, the disparities between what is mapped and what is seen to be there may persist. If the eelgrass was long, covered the entire bay, and was visible at low tide, it would be interpreted as completely absent if it is now shorter and sparse. This situation emphasizes the importance of reviewing the maps with Cree land users to gain insights into eelgrass distribution and to discuss the mapping results. We had to skip this critical step due to COVID restrictions in 2020 and 2021. Nevertheless, before finalizing the maps, we recommend that in the next phase of the research, that all coastal maps produced be thoroughly reviewed by Cree land users. We also recommend that researchers meet with land users with photos or videos of ground truth surveys for use in conversations regarding mapping.

A)

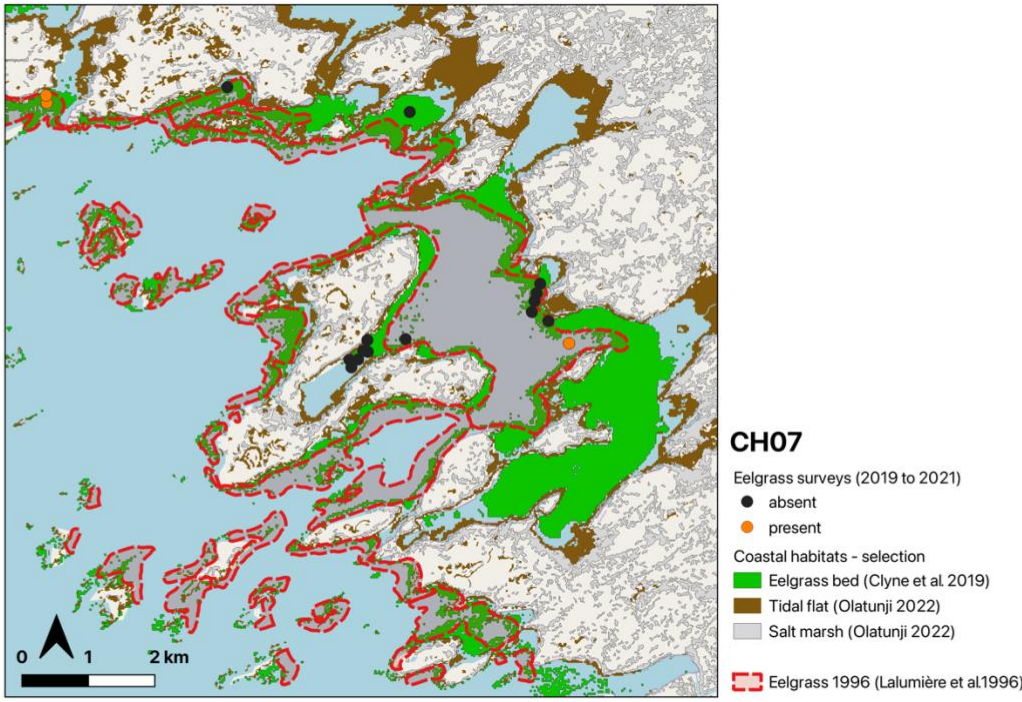

CH07
Eelgrass surveys (2019 to 2021)
absent
present
Coastal habitats - selection
Eelgrass bed (Clyne et al. 2019)
Tidal flat (Olatunji 2022)
Salt marsh (Olatunji 2022)
Eelgrass 1996 (Lalumière et al.1996)
0
1
2 km

B)

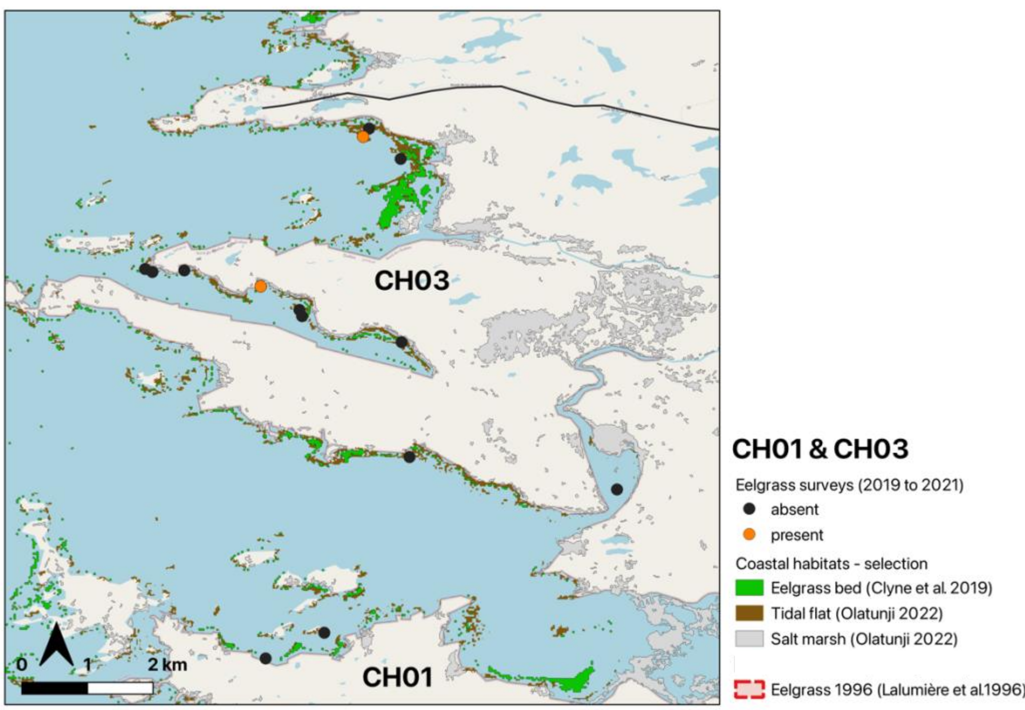

CH03
CH01
CH01 & CH03
Eelgrass surveys (2019 to 2021)
absent
present
Coastal habitats - selection
Eelgrass bed (Clyne et al. 2019)
Tidal flat (Olatunji 2022)
Salt marsh (Olatunji 2022)
Eelgrass 1996 (Lalumière et al.1996)
0
1
2 km

C)

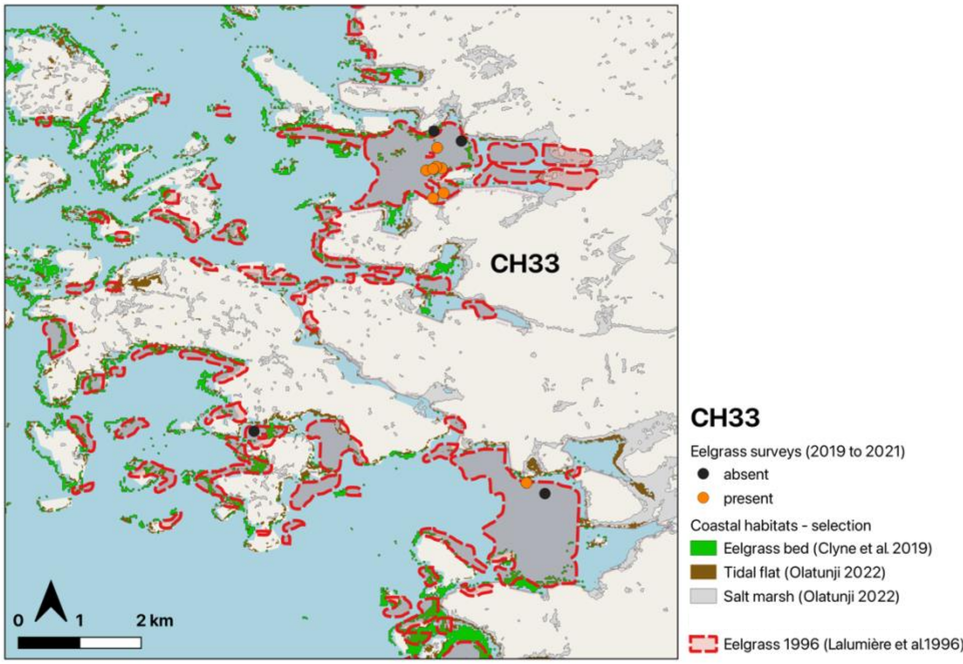
CH33
0
1
2 km
CH33
Eelgrass surveys (2019 to 2021)
absent
present
Coastal habitats - selection
Eelgrass bed (Clyne et al. 2019)
Tidal flat (Olatunji 2022)
Salt marsh (Olatunji 2022)
Eelgrass 1996 (Lalumière et al.1996)

D)

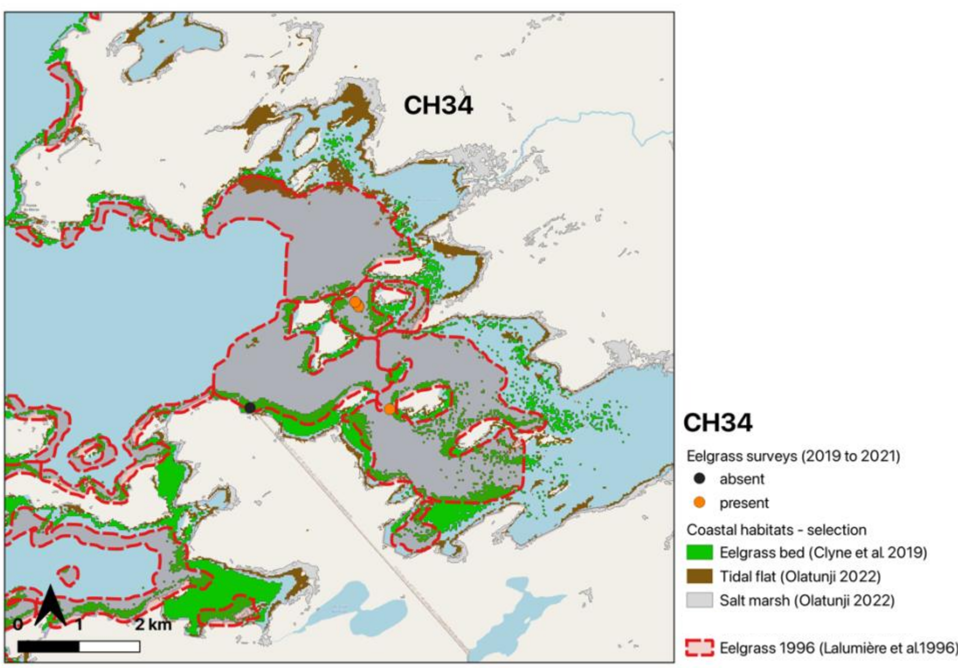
CH34
0
1
2 km
CH34
Eelgrass surveys (2019 to 2021)
absent
present
Coastal habitats - selection
Eelgrass bed (Clyne et al. 2019)
Tidal flat (Olatunji 2022)
Salt marsh (Olatunji 2022)
Eelgrass 1996 (Lalumière et al.1996)

E)

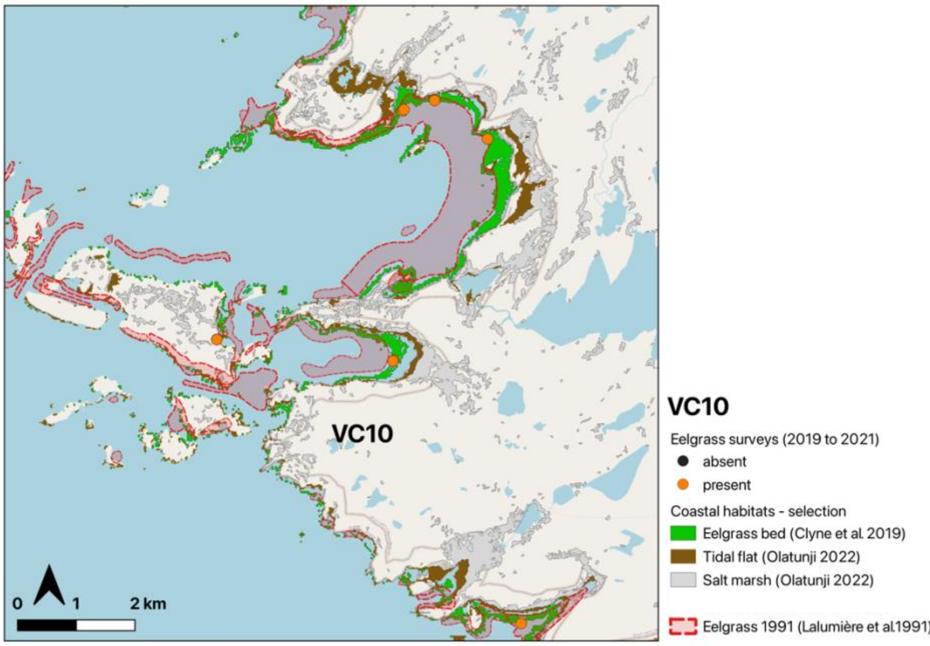
VC10
0
1
2 km
VC10
Eelgrass surveys (2019 to 2021)
absent
present
Coastal habitats - selection
Eelgrass bed (Clyne et al. 2019)
Tidal flat (Olatunji 2022)
Salt marsh (Olatunji 2022)
Eelgrass 1991 (Lalumière et al.1991)

F)

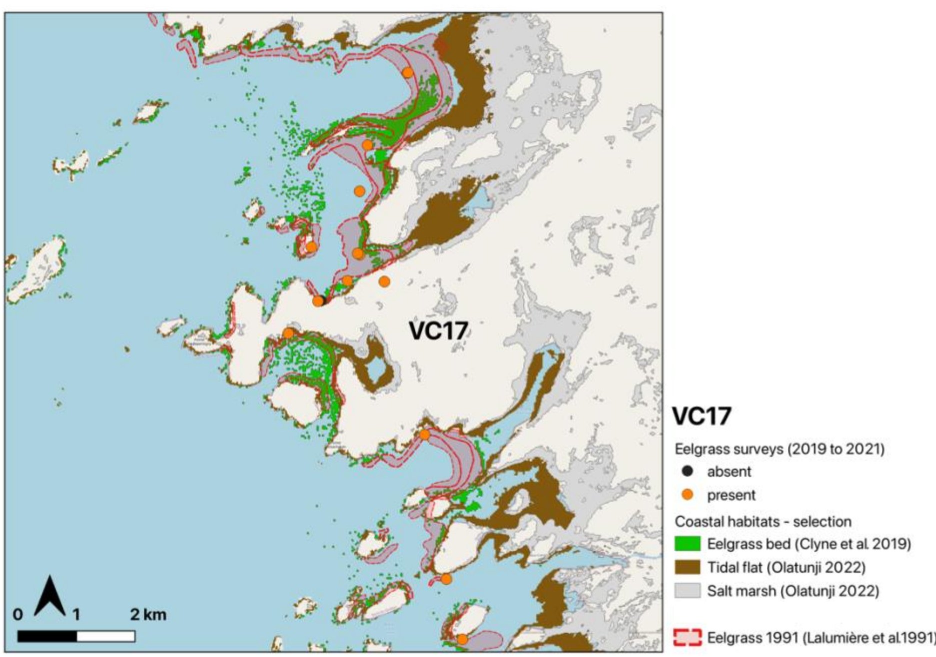
VC17
0
1
2 km
VC17
Eelgrass surveys (2019 to 2021)
absent
present
Coastal habitats - selection
Eelgrass bed (Clyne et al. 2019)
Tidal flat (Olatunji 2022)
Salt marsh (Olatunji 2022)
Eelgrass 1991 (Lalumière et al.1991)

G)

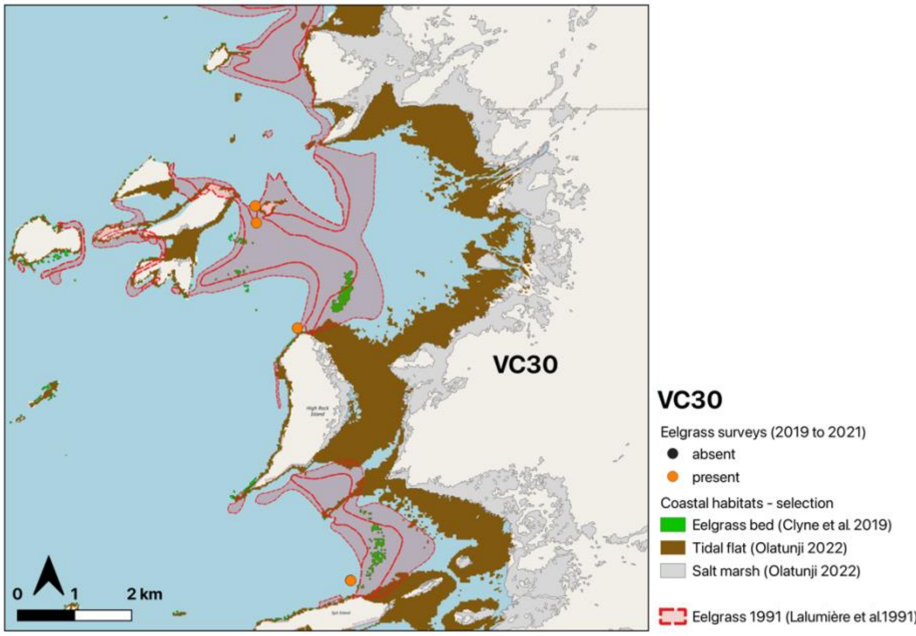

H)

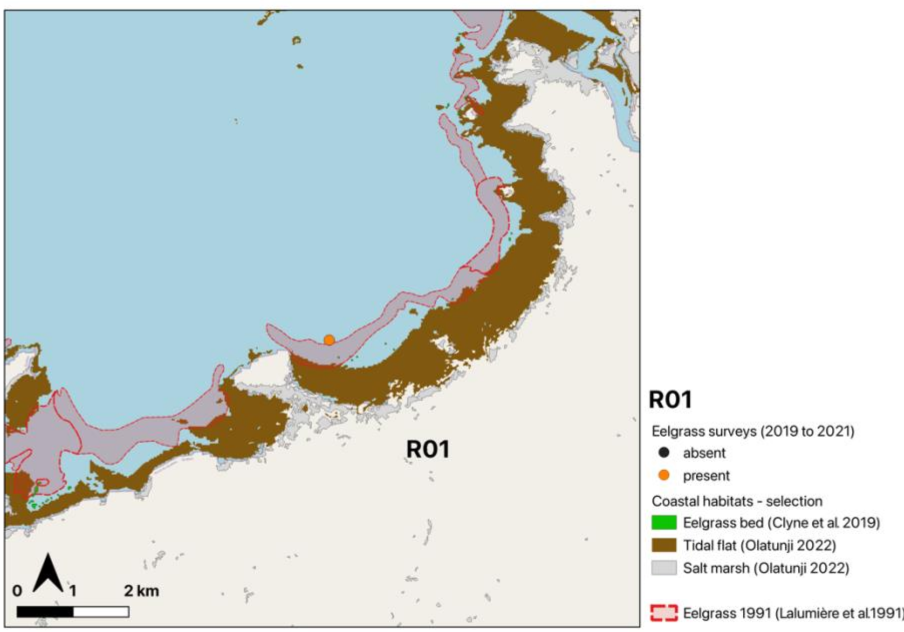

Figure 21 A-H Eelgrass presence/absence surveys from 2019 to 2021 (sub selection), with eelgrass distribution in 2019 (green) and eelgrass distribution in 1996 and 1991 (red). Tidal flats and salt marsh shown on maps are important habitat for Canada Geese (Sorais et al. 2022).

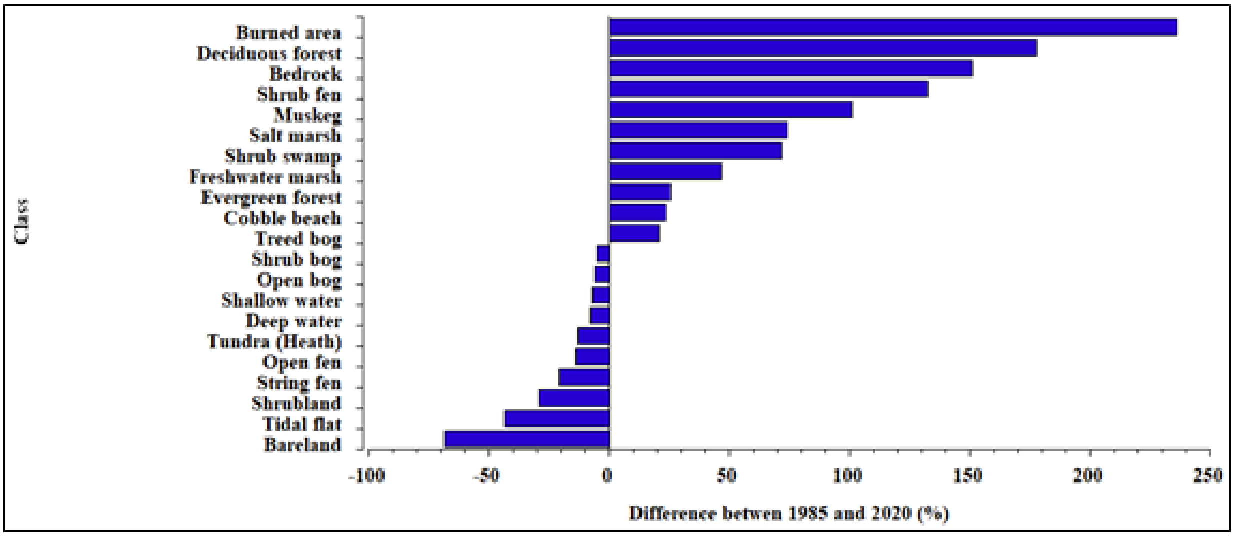

Figure 22 Changes in land cover classes between 1985 and 2020 in the coastal ecosystem of Eeyou Itschee as extracted from Landsat and SAR imagery classification (Olatunji 2022).

SECTION 2 FIELDWORK TO ASSESS EELGRASS GROWING ENVIRONMENTS AND CONDITION

In section 2, we presented a thorough description of the fieldwork undertaken in 2019, 2020, and 2021, as well as a complete list of type samples collected, and variables measured. To assess the present health of eelgrass, the eelgrass team surveyed eelgrass along the eastern coast of James Bay during the summers of 2019-2021. We surveyed a total of 124 sites and sampled eelgrass, algae, and associated invertebrates in a standard 25 x 25 cm sampling unit. We also conducted experiments to test the effects of light and nutrients of the water on eelgrass growth. Data were collected based on three different research objectives defined in the eelgrass team research proposal submitted to Niskamoon in 2019.

Summary of research objectives of the eelgrass team:

- **Objective 1:** Compare historical estimates with the current assessments of eelgrass.

- **Objective 2:** Quantify eelgrass distribution and condition at multiple sites within Eastern James Bay (biomass, density, condition, genetics, eelgrass-associated biodiversity).

- **Objective 3:** Assess if the coastal environmental factors, such as light and nutrients, influence eelgrass productivity

2.1 OBJECTIVE 1: COMPARING HISTORICAL ESTIMATES OF EELGRASS TO CURRENT ASSESSMENTS.

2.1.1 INTRODUCTION

To compare historical estimates of eelgrass with current ones, we aggregated, synthesized, and statistically analyzed data generated through previous monitoring activities conducted by Hydro-Québec (HQ) and Dr. Frederick Short's research team. These measurements were compared to eelgrass collected in 2019 and 2020.

2.1.2 METHODS

The compiled historical eelgrass monitoring data comes from various monitoring reports produced by various consulting firms hired by Société d'Énergie de la Baie James and Hydro-Québec. We compiled raw observations from 22 monitoring reports published between 1982 to 2019. We had access to Dr. Short's raw video footage and water parameters measurements at multiple sites. To compare observations among different years with minimal uncertainties due to how variables were estimated, we used the raw data (i.e., above ground biomass and shoot density records) and images (i.e., underwater photos and videos), and we collated, re-processed and analyzed the images. In total, we obtained 1664 observations covering 144 locations using systematic sampling strategies. The compiled historical data was used in one research paper.

In 1982, a monitoring program was established to assess the potential effects of hydropower development on eelgrass (Roche 1982). The locations of six permanent sampling sites were chosen based on two criteria: they were in embayments that harboured dense and continuous eelgrass meadows, and they were within the area expected most likely to be affected by the newly expanded La Grande River winter freshwater plume (Roche 1982, 1985). The original 1982 design included a control site 60 km south of the La Grande River that was only visited once (Roche 1982). Eelgrass monitoring was carried out by different consulting firms hired by HQ from 1982 to 2009. Eelgrass biomass monitoring was conducted during the first two weeks of August using similar sampling methods during the 13 years between 1982 and 2009 (though not every site was surveyed in each of the 13 years). Eelgrass was collected along transects perpendicular to the shore at 0.5 m, 1.0 m, 1.5 m, and 2.0 m water depths. Reports included estimates of above ground biomass (g dry weight m^{-2}), vegetative shoot density (# m^{-2}) and reproductive shoot densities (# m^{-2}) for each quadrat. We calculated the percent of reproductive shoots for each quadrat (number of reproductive shoots/total number of shoots * 100). Above ground biomass was not available in 1982 because the above and below ground biomass were not separated in core samples.

Table 4 List of variables compiled from Hydro-Québec monitoring reports from 1982 to 2009. Data were collected at six eelgrass biomass monitoring sites.

Variable	**Year**
Dry above ground and below biomass (DW g m^2)	1982, 1985, 1986, 1987, 1988
Dry above ground biomass (DW g m^2)	1985, 1986, 1987, 1988, 1989, 1990, 1991, 1993, 1994, 1995, 2000, 2009
Dry below ground biomass (rhizomes) (DW g m^2)	1985, 1986, 1987, 1988
Number of shoots (m^2)	1982, 1985, 1986, 1987, 1988, 1989, 1990, 1991, 1993, 1994, 1995, 2000, 2009
Number of reproductive shoots (m^2)	1982, 1985, 1986, 1987, 1988, 1989, 1990, 1991, 1993, 1994, 1995, 2000, 2009
Salinity (PPT)	1982, 1985, 1986
Water temperature (C°)	1982, 1985, 1986
Turbidity (NTU)	1982, 1985, 1986
Sediment Total Organic Carbon (%)	1982, 1985, 1986
Sediment Nitrogen Kjeldahl %	1982, 1985, 1986
Sediment assimilable phosphor %	1982, 1985, 1986
Sediment organic matter %	1982, 1985, 1986
Sediment Na mq/100 gr	1986
Sediment Ca mq/100 gr	1986
Sediment K mq/100 gr	1986
Sediment Mg mq/100 gr	1986
Sediment Total Hg	1986
Sediment Hg mg Kg Sec	1986, 1987
Sediment gravel (%)	1986, 1987
Sediment sand (%)	1986, 1987
Sediment silt (%)	1986, 1987
Sediment clay (%)	1986, 1987
Sediment Organic Carbon (%)	1986, 1987

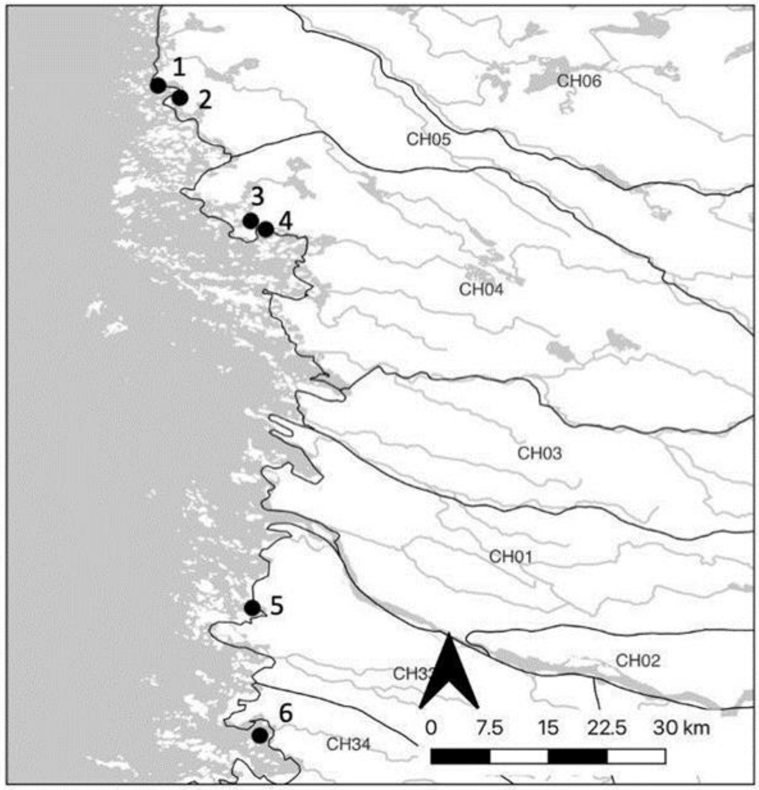

Figure 23 Location of Hydro-Québec eelgrass biomass monitoring sites. Sites 1 in trapline CH05 was surveyed from 1986 to 2009; site 2 in trapline CH05 from 1989 to 2009, site 3 in trapline CH04 from 1982 to 2009, site 4 in trapline CH04 from 1987 to 2009, site 5 in trapline CH33 from 1986 to 2009 and site 6 in trapline CH34 from 1982 to 2009.

Using the video footage from HQ eelgrass cover sites and Dr. Short's sites, we visually estimated the eelgrass cover (in %) in 10 % increments. The minimum cover of eelgrass when present was set at 5 % (0 % when eelgrass was absent). The eelgrass cover was estimated on 5 to 7 randomly selected image stills on each video, resulting in 5 to 20 observations per site per year. For the HQ eelgrass cover sites, we estimated eelgrass cover (%) in 12 sites for 2011, 11 sites for 2014, and 71 sites for 2019. We estimated eelgrass cover (%) in 61 sites in 2018 (Dr. Short's survey sites) and 21 in 2019.

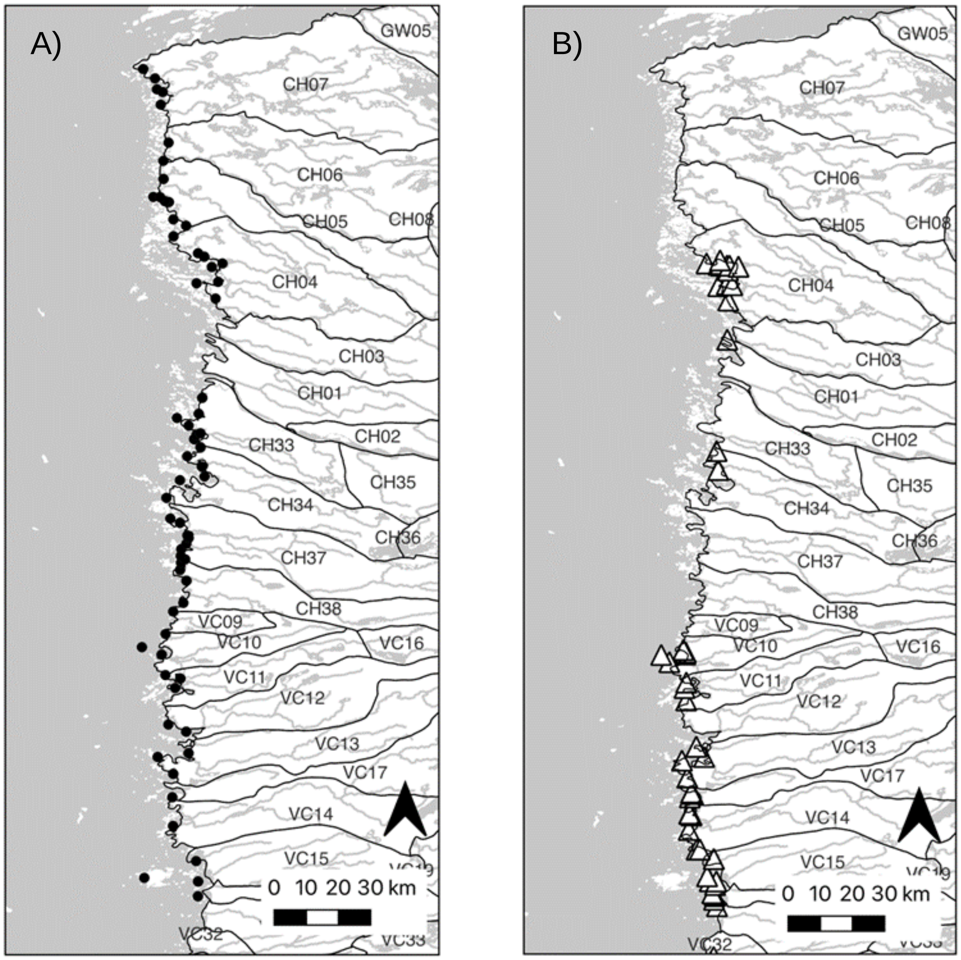

Figure 24 A) locations of Hydro-Québec eelgrass cover monitoring sites. We had access to the raw video footage from 12 sites for 2011, 11 sites for 2014, and 71 sites for 2019; B) locations of 61 sites surveyed by Dr. Short's team in 2018.

To quantify spatial and temporal variation in salinity and surface temperature, we compiled available water quality observations measured at HQ eelgrass cover sites from 1999 to 2019 and measurements of surface salinity and surface temperature from other sites surveyed in 2018, 2019 and 2020.

Table 5 Surface salinity and water temperature (T; ℃) mean ± SE based on estimates taken in the field during eelgrass observation trips from 1999 to 2020.

Water parameter	Year	n	Max	Min	Range	Mean ± SE	Median
Surface water salinity	2004	56	23.5	10.0	13.5	18.8 ± 3.21	19.8
	2009	40	24.0	11.0	13.0	18.9 ± 3.02	19.5
	2011	68	24.0	11.0	13.0	21.1 ± 2.70	22.0
	2014	88	23.2	1.70	21.5	19.2 ± 3.70	20.6
	2018	90	21.5	6.8	14.7	21.5 ± 0.31	17.9
	2019	132	21.2	2.2	19.0	17.1 ± 3.54	18.0
	2020	23	21.2	7.8	13.4	21.2 ± 0.97	17.9
Surface water T (℃)	1999	61	17.0	10.5	6.5	14.1 ± 0.17	14.0
	2000	55	22.0	11.0	11.0	14.8 ± 0.32	14.0
	2004	56	17.5	5.50	12.0	11.5 ± 0.35	12.0
	2009	40	16.0	7.00	9.0	12.2 ± 0.32	12.5
	2011	68	18.5	10.0	8.5	14.6 ± 0.20	14.5
	2014	88	18.5	9.70	8.8	14.2 ± 0.19	14.1
	2018	90	20.0	5.5	14.5	13.2 ± 0.35	13.2
	2019	135	19.9	6.97	12.9	12.1 ± 0.21	11.4
	2020	23	19.0	10.2	8.8	13.5 ± 0.62	13.8

2.2 OBJECTIVE 2: QUANTIFY EELGRASS DISTRIBUTION AND CONDITION AT MULTIPLE SITES

2.2.1 INTRODUCTION

To quantify eelgrass distribution and condition at several sites in James Bay, we used two sampling strategies: a detailed sampling strategy using SCUBA and an abridged sampling strategy using snorkeling and sampling from canoes. This is necessary because assessing some properties such as density, associated biodiversity, and total biomass require much more intensive field methods and usually requires work underwater using SCUBA or SNUBA-diving.

2.2.2 METHODS

We used a detailed sampling strategy to collect eelgrass above-ground biomass in three sets of three 0.0625-m^2 quadrats distanced 20 to 30 m apart (a total of nine quadrats per site) at 1 to 1.5 m depth. In general, one Detailed Sampling Site (DSS) would take around 2 to 3 hours to collect all the biomass. The second sampling strategy was an abridged sampling strategy that collected fewer data. Fast Sampling Sites (FSS) and Fast Fast Sampling Sites (FFSS) are sites where only a few eelgrass shoots were collected, and a few water parameters were measured. We also have Verification Sites (VS) where the presence or absence of eelgrass was determined.

We used the detailed sampling protocol at 11 sites in 10 traplines in 2019 and 2 sites in 2 traplines in 2021. The DSS locations were selected by considering community consultations that were held in June of 2019, published records of historical eelgrass presence or absence, and statistical considerations of distance from other sites, depth, and other shoreline attributes. DSS locations were also selected by considering sites that the Ocean Team had sampled in previous years and therefore had good water quality data. At each DSS, we sampled subtidal eelgrass using SCUBA or SNUBA. We collected all eelgrass and epifaunal invertebrates (2019 only) within a 0.625 m^2 PVC quadrat (0.25 m on a side). We sampled each site in three areas > 10 m apart (n = 3 quadrats in each area) for a total of 9 quadrats per DSS. All eelgrass within a quadrat was immediately placed in a mesh bag with minimal agitation to collect mobile invertebrates associated with the eelgrass. In the lab (back to the community), shoots were counted and measured. Invertebrates were removed from eelgrass and any algae collected within each quadrat and preserved in 95% ethanol. They were later identified to the highest level of taxonomic resolution possible (most to genus or species) and counted using a dissecting microscope. We sorted macroalgae, detritus, free-floating microalgae, and live eelgrass. Live eelgrass was dried and weighed to estimate above-ground biomass. Samples for estimating eelgrass condition (pigment, C/N ratio, δ15N, δ13C) as well as eelgrass shoots for genetics were also collected at some DSS in 2019 and 2021. To continuously monitor salinity, temperature, and light during the eelgrass growing season, 7 moorings were deployed at 7 DSS in 2019 and 2 moorings were deployed at 2 DSS in 2021 (CH33 and CH34). We also collected discrete water samples in the water column and in the sediments to quantify the nutrient concentration in seawater and porewater, respectively. Nitrates, nitrites (NOx) and phosphates (PO4) concentrations were measured in 2019 and 2021 while ammonium (NH4) was quantified in 2021 only.

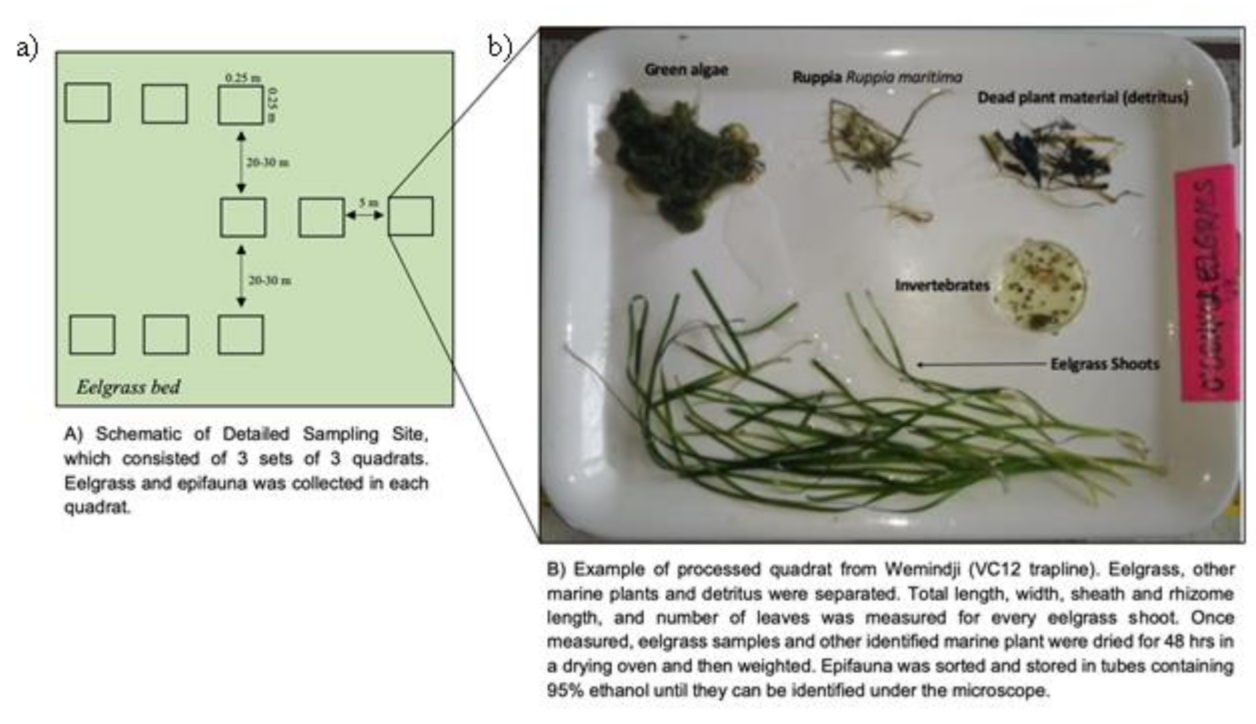

Figure 25 (a) schematic of DSS and (b) example of one sample collected at one quadrat.

In addition to the DSS, we conducted an abbreviated fast sampling protocol (FSS) at 43 sites in 2019, 24 sites in 2020 (Cree team) and 18 sites in 2021. The FSS were selected by considering input from the Cree land users based on their experience and knowledge of the area and other variables important to eelgrass health. At each FSS, we took photographs of eelgrass meadows using a method that allows comparison among sites to qualitatively assess eelgrass cover. We also collected 20 eelgrass shoots haphazardly. Shoots were selected independently by identifying a shoot at the sediment water interface and removing it and placing it in a mesh collecting bag. Visibility at most sites was very low (<2 ft, sometimes as low as 0 at the sediment), so selecting shoots at the sediment interface allowed random selection of shoots with regard to their length or reproductive status. The snorkeler swam around the boat in a radius of ~ 10 m.

At some sites, where it was impractical to collect eelgrass samples, we conducted further abbreviated protocols. In 2019, we collected data in 4 Fast Fast Sampling Sites and assessed eelgrass presence/absence in 15 Verification sites when traveling between sites or exploring different areas with Cree land users. These sites allow us to note that eelgrass was present, or likely absent, but because systematic methods were not used, we cannot be certain eelgrass was not there in small amounts if we didn't observe it. In total, we collected data from 11 DSS (two of which were visited twice), 85 FS, 4 FFS and 15 VS from 2019 to 2021. The data collected in 2019, 2020 and 2021 were used in two different research papers (see section 1.2 for additional information on the research paper). To assess the genetic diversity of eelgrass meadows in eastern James Bay, we collected samples in 2019 and 2021. The genetic analyses were conducted by France Dufresne (ISMER/UQAR). Because of the low quality of 2019 samples, only the 2021 were used for genetic analyses.

Finally, we calculated relative exposure index (REI) for each site. REI calculated for each site from 2019, 2020 and 2021 using methods of the Shore Protection Manual (1977), Keddy (1982), and Murphey and Fonseca (1995). The centroid of each site was used to determine the location for wave exposure analysis. For each location, 10 years of the most recent observed wind data from the closest Environment and Climate Change Canada weather stations for each site was downloaded using the weathercan package in R (LaZerte and Albers 2018, R Core Team 2022). Wind data were summarized to determine the mean monthly maximum wind speeds for 8 headings and the percent frequency with which wind occurred in each heading. Fetch is the unimpeded distance over which wind-driven waves can build a point in the ocean to land along a given heading (Shore Protection Manual 1977). We calculated fetch from 8 compass headings. Exposure was calculated as :

$$Exposure = \sum_{i=1}^{8}(V_i \times P_i \times F_i) \quad (1)$$

where, i is the i^{th} compass heading (1-8), V is the average monthly maximum wind speed in hr km^{-1}, P is the percent frequency which wind occurred from the i^{th} direction, and F is the effective fetch from i^{th} direction (Murphy and Fonseca 1995).

Table 6 List of variables generated from eelgrass samples collected in eastern James Bay in 2019, 2020 and 2021.

Variable	**Year**
Eelgrass morphometrics: shoot length, sheath length, blade width, and number of blades	2019, 2020, 2021
Eelgrass density: number of shoots per m^2	2019, 2021
Eelgrass biomass: wet and dry weight	2019, 2021
Epiphytic algae load	2019, 2021
Epifaunal diversity: number of invertebrate species, functional groups, present in quadrat (i.e. on or very close to eelgrass)	2019
Eelgrass tissue (leaves and roots) contents and isotopes: C/N ratio, $\delta^{15}N$, $\delta^{13}C$	2019, 2020 (under analyses), 2021
Eelgrass pigment content in leaves	2019, 2021
Rhizome morphometrics: total rhizome length, number of nodes and all internodal lengths	2019, 2020, 2021
Standardized density photographs: underwater photos of eelgrass meadows that include a 0.25 m^2 quadrat for cover estimation	2019, 2021
Temperature, Salinity, pH, Dissolved O2, CDOM, Turbidity	2019, 2020, 2021
Water characteristics: Suspended Particulate Matter, Chlorophyll a, nutrient concentrations, and Colored Dissolved Organic Matter	2019
Mooring water quality parameters (salinity, temperature, light)	2019 (7 sites) 2021 (two sites)
Nutrients in sediment	2019, 2021
Sediment to assess grain size and mineralogical composition	2019
Eelgrass genetics	2019, 2021
Relative Exposure Index	2019, 2020, 2021

Table 7 List of different sites per traplines visited in 2019, 2020 and 2021. DSS: Detailed Sampling Site; FSS: Fast Sampling Site; FFSS: Fast Fast Sampling Site, and VS: Verification Site.

	2019				2020	2021		
Trapline	DSS	FSS	FFSS	VS	FSS	DSS	FSS	**Total**
CH07	1	1		14	1	1	3	**21**
CH03	1	4	4	1	2	1	2	**15**
CH01		4						**4**
CH33	1	4			2		4	**11**
CH34	1	2			1			**4**
CH37							4	**4**
CH38	2	4					6	**12**
VC10		5			4			**9**
VC11	1							**1**
VC12	1	2		1	4			**8**
VC14		6			3			**9**
VC17	2	6			5			**12**
VC30	1	5			4			**10**
VC32					1			**1**
R01	1							**1**
Grand Total	**12**	**43**	**4**	**16**	**27**	**2**	**19**	**122**

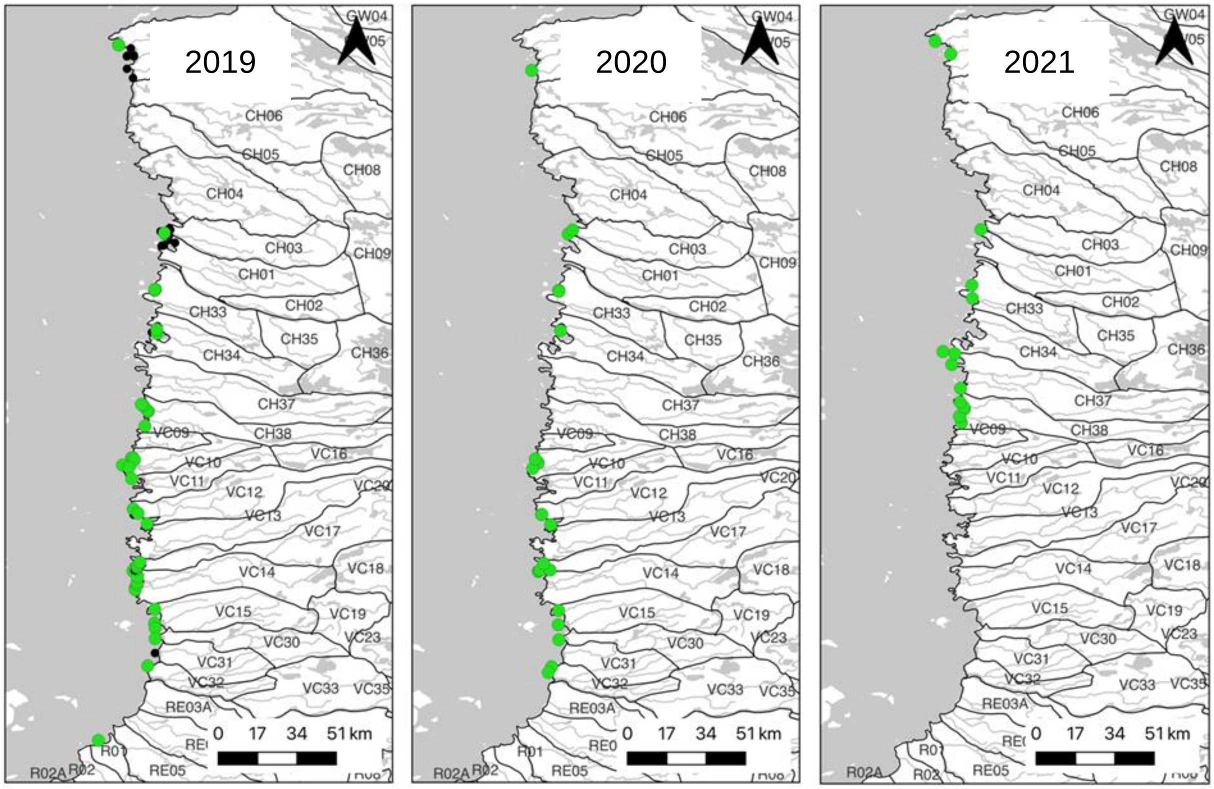

Figure 26 Locations of sampling sites in (a) 2019, (b) 2020 and (c) 2021. Green indicates eelgrass presence and black absence.

2.3 OBJECTIVE 3: ASSESS IF THE COASTAL ENVIRONMENTAL FACTORS, SUCH AS LIGHT AND NUTRIENTS, INFLUENCE EELGRASS PRODUCTIVITY

2.3.1 INTRODUCTION

We assessed performance of eelgrass in the conditions of today's coastal environment, specifically light and nutrient availability. We conducted two experiments on eelgrass and estimated eelgrass growth rates. The data from the experiments were used for one research paper.

2.3.2 METHODS

The light experiment aimed at measuring the primary production (oxygen fluxes) of eelgrass under increasing light levels, from dark to full daylight. Shoots from CH33, CH34 and CH7 were collected and used to establish production-irradiance curves. That allowed us to assess the efficiency of eelgrass in light limiting conditions and to determine light thresholds for optimal and sub-optimal growth. Preliminary results show that eelgrass seems to thrive above approximately 200 µmol photons m^{-2} s^{-1} and struggle in similar light conditions as observed for eelgrass from St Lawrence estuary.

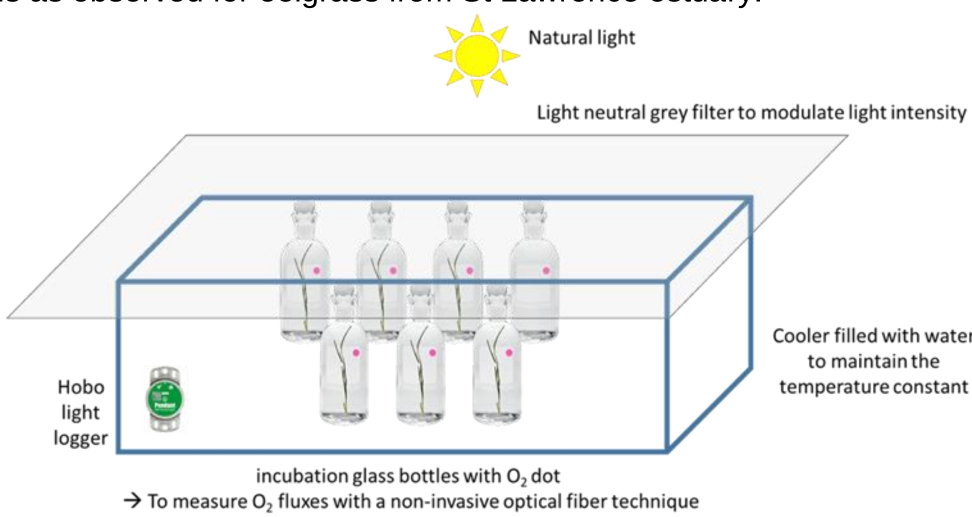

Figure 27 Methodological diagram for measuring photosynthesis-irradiance curves. Filters were applied in order of darkness to lightness.

The nutrient experiment was set up to help us understand how changes to nutrient concentrations in the water might influence the growth rate and condition of eelgrass. We expected that, because James Bay waters tend to be low in nutrients, adding nutrients would help them grow. We conducted the nutrient experiment at 2 sites (one site in CH33 trapline and another in CH34 trapline) that have moorings, to link our eelgrass observations with water measurements taken over the few months prior to the experiment. We placed nutrient packets into the eelgrass bed, attached to PVC pipe, and measured the eelgrass growth rate in response to the added nutrients.

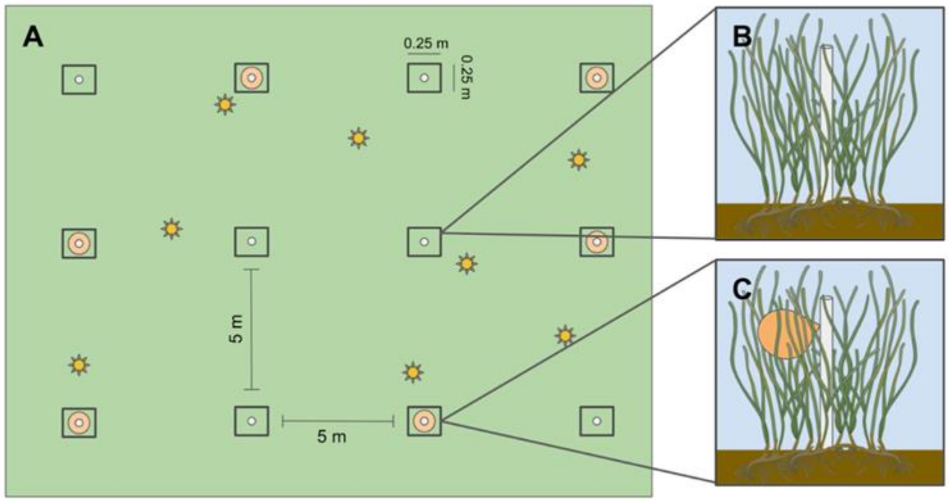

Figure 28 Experimental design for *in situ* nutrient addition and sampling for light experiment. Panel A shows the layout of the experimental array within the eelgrass meadow (green rectangle) from a bird's eye view. Each square represents an experimental quadrat. White circles represent PVC poles, which are present in every quadrat, and orange circles represent the nutrient addition treatments present in half of the quadrats. Panels B and C show zoomed in profile views of control and treatment quadrats, respectively. Sun icons represent hypothetical sampling locations for eelgrass shoots which are brought back to the research facility for production-irradiance measurements (i.e. light experiment).

To estimate the eelgrass growth rates, we visited each meadow (one in CH33 and CH34) twice, in order to measure how fast eelgrass was growing. At the first visit, we poked holes in the plants just above the meristem, and at the second visit we collected the plants to measure displacement of those holes away from the original location. At both sites, we also measured the water properties, including temperature, nutrient concentrations, and salinity. We also measured the nutrient concentrations in the sediments. This allowed us to link growth to environmental conditions and what we observe in biomass and abundance. To estimate eelgrass growth rates – we marked shoots and revisited them to measure growth two weeks later.

Table 8 Summary of eelgrass and environmental variables measured during experiments in 2021.

Experiment	**Variable**	**Sites**
Light experiment	eelgrass production in different light intensities	CH33, CH34, CH7
	pigment composition, morphometrics	CH33, CH34, CH7
Nutrient experiment	eelgrass growth rate	CH33, CH34
	epiphyte biomass and growth rate	CH33, CH34
	water column nutrients	CH33, CH34
	sediment nutrients	CH33, CH34
	water quality parameters	CH33, CH34

2.2 PEER-REVIEWED RESEARCH PAPERS

PAPER 1:

Title	Limited recovery following the greatest seagrass decline in subarctic eastern Canada (objective 1)
Authors	M. Leblanc, M.I. O'Connor, Z. Kuzyk, F. Noisette, K.E. Davis, E. Rabbitskin, L.L. Sam, U. Neumeier, R. Costanzo, J. Ehn, D. Babb, J. Idrobo, J.-P. Gilbert, B. Leblon, M.M. Humphries
Data	Hydro-Québec monitoring data (biomass and cover), eelgrass data collected in 2019 and 2020
Status	The manuscript published in Global Change Biology.
Reference	Leblanc et al. 2022. Limited recovery following a massive seagrass decline in subarctic eastern Canada. Global Change Biology. DOI: 10.1111/gcb.16499
Abstract	Over the last few decades, there has been an increasing recognition for seagrasses' contribution to the functioning of near-shore ecosystems and climate change mitigation. Nevertheless, seagrass ecosystems have been deteriorating globally at an accelerating rate during recent decades. In 2017, research into the condition of eelgrass (*Zostera marina*) along the eastern coast of James Bay, Canada, was initiated to respond to reports of eelgrass decline by the Cree First Nations of Eeyou Istchee. As part of this research, we compiled and analyzed two decades of eelgrass cover data and three decades of eelgrass biomass monitoring data to detect change and assess possible environmental drivers. We detected a major decline in eelgrass condition between 1995 and 1999, which encompassed the entire east coast of James Bay. Surveys conducted in 2019 and 2020 indicated limited recovery, e.g., low eelgrass cover (<25 %), low above ground biomass, smaller shoots than before 1995, and marginally low densities persisted at most sites. Overall, the 40 % loss of dense eelgrass meadows in eastern James Bay since 1995 demonstrated from the synthesized data sets represents the largest scale eelgrass decline documented in eastern Canada. Using biomass data collected since 1982 but geographically limited to the sector of the coast near the regulated La Grande River, generalized additive modeling revealed eelgrass meadows to be affected by local sea surface temperature, early ice breakup and higher summer freshwater discharge. The results caution against assuming subarctic seagrass ecosystems have avoided recent global declines or will benefit from ongoing climate warming.

PAPER 2:

Title	Eelgrass community structure along a subarctic latitude gradient (objective 2)
Authors	M. Leblanc, F. Noisette, K.E. Davis., M. I. O'Connor
Data	Eelgrass, epiphytes, epifauna and environmental data collected in 2019
Status	Structure drafted, writing in progress. Preliminary results presented to the steering committee in December 2019 in Halifax.
Abstract	Eelgrass (*Zostera marina*) is an important foundation species throughout the northern hemisphere, providing food and habitat for invertebrates, fish, and waterfowl. Its abundance and distribution has been sensitive to anthropogenic climate and land use change. We document eelgrass biomass, density, epiphyte load in 13 meadows in subarctic James Bay, Quebec, to contextualize this region's *Zostera* meadows along a latitudinal gradient. We also estimated invertebrate biodiversity across 9 of these subtidal meadows. Our approach employs standard methods, allowing comparison with other *Zostera* meadows throughout the world. In late July to early August), eelgrass shoots bore epiphyte loads that were lower than observed in other sites later in the season. We observed 78 epifaunal invertebrate taxa, surely an underestimate. We also observed substantial variation among locations in the eelgrass and animal communities, driven by a small number of environmental variables. Our observations provide a rare contribution to global efforts to understand *Zostera* ecology and biogeography in remote and rarely sampled locations, and also contribute an estimate to ongoing efforts to understand change in eelgrass in James Bay over time.

PAPER 3:

Title	Physiological condition of eelgrass and nutrients concentration in eastern James Bay (objective 2)
Authors	F. Noisette, L. Richer, M. Leblanc, K. Davis, M. I. O'Connor
Data	2019, 2020, 2021
Status	Structure drafted, writing in progress. Data collected and analysed by Lou Richer. Lou Richer completed her master at ISMER (Richer 2022).
Abstract	Healthy seagrass meadows are critical environments as food source or shelter for numerous species along the trophic chain (i.e birds, fishes, algae,

invertebrates...) in coastal zones. At the end of the nineties, the members of the Cree communities reported a major decline in seagrass meadows (*Zostera marina*) all along the eastern James Bay coast. The meadows have not recovered yet as the current coverage, abundance and plant height are well over the historical data from before the 90s, likely linked to changes in environmental conditions. To investigate what prevented eelgrass to recover as before the 90's, we coupled physiological proxies, morphometric measurements, and physico-chemical measurements of water masses to investigate how seagrass allocates energy according to the environmental conditions. During the summer of 2019, we sampled 83 sites along the eastern James Bay coastal communities of Chisasibi, Wemindji, Eastmain and Waskaganish. Seagrass shoots were collected for quantifying morphological and physiological traits. Physico-chemical variables were measured with discrete water sampling (e.g. organic matter content, chl. a. concentration, nutrients concentrations and CDOM) or recorded on a high frequency thanks to moorings deployed on 7 sites from early July to mid-August (bathymetry, conductivity, temperature and light intensity). Investigating the energetic allocation of seagrasses by measuring the energetic content (starch) in the rhizome, the photosynthetic pigments saturation (chl. a.) in leaves, as well as the carbon and nitrogen content in both plant parts, according to the concentration and fluctuation of environmental variables, especially nutrients in the water and the sediments, will allow us to better understand the limitations that may prevent any recovery of James Bay meadows.

PAPER 4:

Title	Temporal and spatial patterns of eelgrass meadows in Eeyou Istchee (objective 2)
Authors	M.I. O'Connor, K.E. Davis, F. Noisette, M. Leblanc, M.I., L.L. Sam, E. Rabbitskin
Data	2019, 2020 and 2021
Status	Writing in progress.
Abstract	*Writing in process*

PAPER 5:

Title	Effects of light and water column nutrients on eelgrass (*Zostera marina*) productivity in eastern James Bay, Québec (objective 3)
Authors	K.E. Davis, F. Noisette, M.I. O'Connor
Data	Experiments to test how eelgrass shoots grow in current light and nutrient conditions, 2021
Status	Manuscript presented to Steering Committee. Davis, E.K., Noisette, F. and M.I. O'Connor. 2022. Effects of light and water column nutrients on eelgrass (*Zostera marina*) productivity in eastern James Bay, Québec. Marine Ecology Progress Series (*in prep.*).
Abstract	Eelgrass (*Zostera marina*) meadows provide valuable ecosystem services to coastal communities. These shallow-water ecosystems in Eeyou Istchee (eastern James Bay, Quebec, Canada) provide waterfowl foraging habitat, nurseries for fish, and natural storm buffers, supporting Cree ways of life. In 2019-2021, Eeyou Istchee eelgrass extent and shoot size remained well below historical baseline levels following a major decline in the mid 1990's. We experimentally tested the potentially limiting roles of current-day nutrient and light conditions for eelgrass productivity during the growing season. We tested the hypothesis that eelgrass growth is limited by water column nutrient concentration, using an *in situ* manipulative nutrient addition experiment in two eelgrass meadows. Eelgrass growth rate did not respond to nutrient addition at either site, but epiphytic algae biomass increased with nutrient addition at one site. With shoots from each meadow, we assessed eelgrass response to low light conditions by producing *ex situ* production-irradiance curves. Eelgrass at both sites showed no evidence of low light acclimatization with a saturating irradiance about 230 µmol photons m^{-2} s^{-1} and a compensation point between 30 and 60 µmol photons m^{-2} s^{-1}. We observed eelgrass growth rates of 2.8 day^{-1}, high rates compared to a global synthesis. Together, our results suggest that Eeyou Istchee eelgrass is growing despite low water column light and nutrient conditions. However, they may have a shorter, faster growing season compared to eelgrass in other regions, leaving them vulnerable to stressful conditions and extreme climate events during this period.

PAPER 6:

Title	Variation in genomic vulnerability of climate change across temperate populations of eelgrass (*Zostera marina*) (objective 2)
Authors	Jeffery, N., Vercaemer, B., Stanley, R., Kess, T., Dufresne, F., O'Connor, M. I., Noisette, F., Wong M.
Data	2019
Status	The manuscript reviewed by the Steering Committee April 21, 2023.
Abstract	A global decline in seagrass populations has led to renewed calls for their conservation as important providers of biogenic and foraging habitat, shoreline stabilisation, and carbon storage. Eelgrass (Zostera marina) occupies the largest geographic range among seagrass species spanning a commensurately broad spectrum of environmental conditions. However, relatively little is known about their fine-scale genetic structure and broad-scale genomic signatures of environmental adaptation, and in Canada, eelgrass is considered a single phylogroup despite occurring across three oceans. We used a pooled whole-genome re-sequencing approach to characterise population structure, gene flow, and adaptation of 23 eelgrass populations ranging from the Northeast United States, to Atlantic, subarctic, and Pacific Canada. We identified over 500,000 SNPs, which when mapped to a chromosome-level genome assembly revealed six broad clades of eelgrass across the study area, with pairwise FST ranging from 0 among neighbouring populations to 0.54 between Pacific and Atlantic coasts. Genetic diversity was highest in the Pacific and lowest in the Arctic, consistent with colonisation of the Arctic and Atlantic oceans from the Pacific. Using redundancy analyses and two climate change projection scenarios, we found that subarctic populations are more vulnerable to climate change through genomic offset predictions. Conservation planning in Canada should ensure that representative populations from each identified clade are included within a national network so that latent genetic diversity is protected, and gene flow is maintained. Northern populations may require stronger protective measures given their susceptibility to change climate.

SECTION 3 COASTAL MAPPING

In section 3, we provide a full description of the different methods used to assess the distribution of eelgrass from satellite imagery. Understanding ecosystem changes in time and space requires reliable coast effective methods. The first eelgrass distribution maps for James Bay, produced by photo-interpretation of color aerial photographs combined with field data (e.g., Curtis 1974, Lalumière et al. 1996). Satellite imagery offers a cost-effective alternative for eelgrass bed mapping, providing superior coverage for a reduced cost compared to aircraft surveys (Hossain et al 2015).

Summary of proposed research objectives of the remote sensing team:

- **Objective 1:** Evaluating the capability of Landsat-8 Operational Land Imager (OLI) imagery to establish a baseline map of eelgrass distribution in 2019, despite the relatively turbid waters of Eeyou Istchee.
- **Objective 2:** Evaluating the capability of Landsat-5 TM and Landsat-8 OLI imagery to reconstruct the changes in eelgrass bed extent and distribution between 1988 and 2019
- **Objective 3:** Evaluating the capability of Landsat-8 OLI and Sentinel-1 SAR imagery to map the current coastal habitats along the coast of Eeyou Itschee.
- **Objective 4:** Evaluating the capability of Landsat-5 TM, Landsat-8 OLI and Sentinel-1 SAR imagery to map the changes in the coastal habitats along the coast of Eeyou Itschee between 1984-1985 and 2019-2020.

3.1 OBJECTIVE 1

Evaluating the capability of Landsat-8 Operational Land Imager (OLI) imagery to establish a baseline map of eelgrass distribution in 2019, despite the relatively turbid waters of Eeyou Istchee

3.1.1 INTRODUCTION

Due to the inaccessibility of much of the coastline, quantifying and mapping eelgrass extent within the bay presents a major challenge. Multispectral satellite imagery offers the only source of continuous data spanning the entire extent of the coastline, and much of it is freely available. The objectives of this study are to assess the capability of the Landsat-8 Operational Land Imager (OLI) imagery to detect eelgrass in Eeyou Istchee waters and assess and map the eelgrass distribution along the eastern coastline of James Bay in the summer of 2019. Temperate and subarctic water, such as in Eeyou Istchee, poses additional challenges for mapping eelgrass compared to tropical and subtropical waters because this region tends to have lower water clarity and, therefore, low light penetration. Local indigenous knowledge about the eelgrass beds is also included in the analysis. This study is the subject of the first chapter of Clyne (2022)'s thesis and was published in a peer-reviewed conference paper (Clyne et al., 2021).

3.1.2 METHODS

The study used freely available imagery obtained from the USGS website and acquired by the Landsat-8 Operational Land Imager (OLI) when the eelgrass reached its peak biomass. We used three images acquired on September 16, 2019. Still, given that there was cloud cover over Chisasibi on the September image, we used an additional cloud-free image acquired on August 26, as close to the September image.

The September and August images were converted into surface reflectance images using ACOLITE, a free atmospheric correction application developed by the Royal Belgian Institute of Natural Sciences. This application was designed for the simple and fast processing of coastal scenes, with a sun glint correction and the mosaicking of the three images acquired in September. Once processing was completed, the resulting image mosaic was clipped to keep only the water located from a short distance to the coastline.

Additional layers were created during the atmospheric correction and used as input for the image classification. First, ACOLITE module provides the option to compute the Turbidity, the Suspended Material Concentration, the Floating Algal Index, and the Orange reflectance. Second, eleven vegetation indices and four bathymetric ratios were computed. These computed layers were finally combined with the surface reflectance mosaic from ACOLITE and used as inputs for the RF classifier.

The September mosaics and the August imagery were classified using the Random Forests (RF) supervised classifier, which requires training areas. Representative training areas were delineated through photointerpretation of the satellite imagery for the four following classes: Eelgrass (EG), Turbid Water (TW), Highly Turbid Water (HTW), and Optically Deep Water (DW). In the images, a large part of the eastern coastline of James Bay contained turbid water, either within bays near the coastline or out in deeper waters at the southern end of the bay, as exhibited in Figure 29. It is why a "Turbid Water" class was created through a manual selection of visibly turbid waters. Another class was created as "Highly turbid water, " which encompasses the reflectance signal of optically shallow, sandy, James Bay, and visually highly turbid waters. These waters appeared brownish on the RGB composite image created with the visible bands.

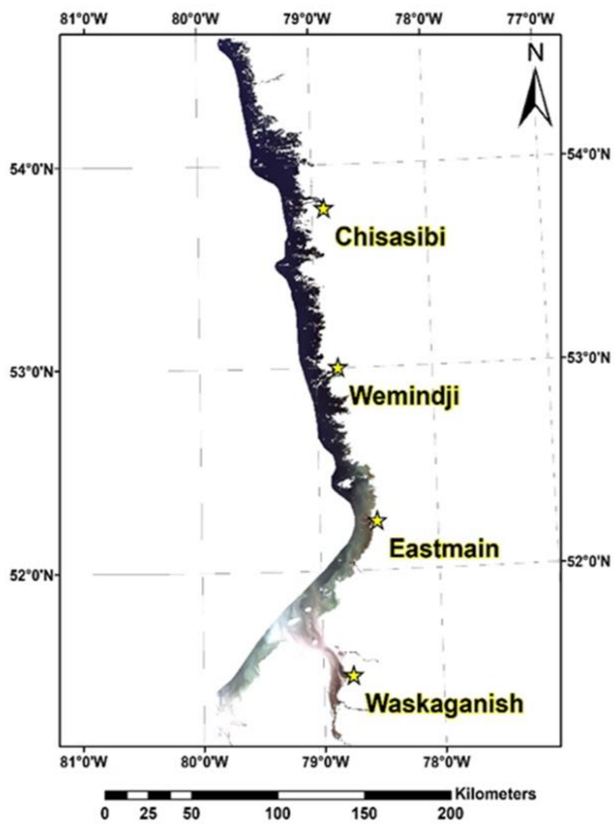

Figure 29 RGB composite for the mosaic created using ACOLITE with the Landast-8 OLI images acquired over James Bay on September 16, 2019 (Clyne et al. 2021).

3.1.3 RESULTS

A classified image was produced with RF, in applying the training areas to the 6 first Landsat-8 OLI bands and all the derived variables. According to the confusion matrix produced by RF, the classification accuracy is very high, with an overall accuracy (OA) of 99.3% (Table 9). The user's accuracy (UA), i.e., how the map produced from the classified image is real on the ground, is very high, except for the Eelgrass class (EG) with an accuracy of 89,5%, which is still a pretty good value.

Table 9 Confusion matrix for the classification of the training pixels computed with the Random Forests classifier. Bold values represent well-classified pixels (Clyne et al. 2021).

Class	**EG**	**TW**	**HTW**	**CW**	**Total**	**UA (%)**
EG	**3139**	56	43	268	3506	89.5
TW	28	**33129**	78	197	33432	99.1
HTW	58	55	**96688**	65	96866	99.8
CW	69	274	74	**37866**	38283	98.9
Total	3294	33514	96883	38396	**172087**	
PA (%)	95.3	98.9	99.8	98.7		OA = 99.3%

The classified image for the whole study area is shown in Figure 29. From this classified image, detailed maps were created at a resolution of 1:250,000 around each of the main Cree coastal communities: Chisasibi (Figure 30), Wemindji (Figure 31), Eastmain (Figure 32), and Waskaganish (Figure 33).

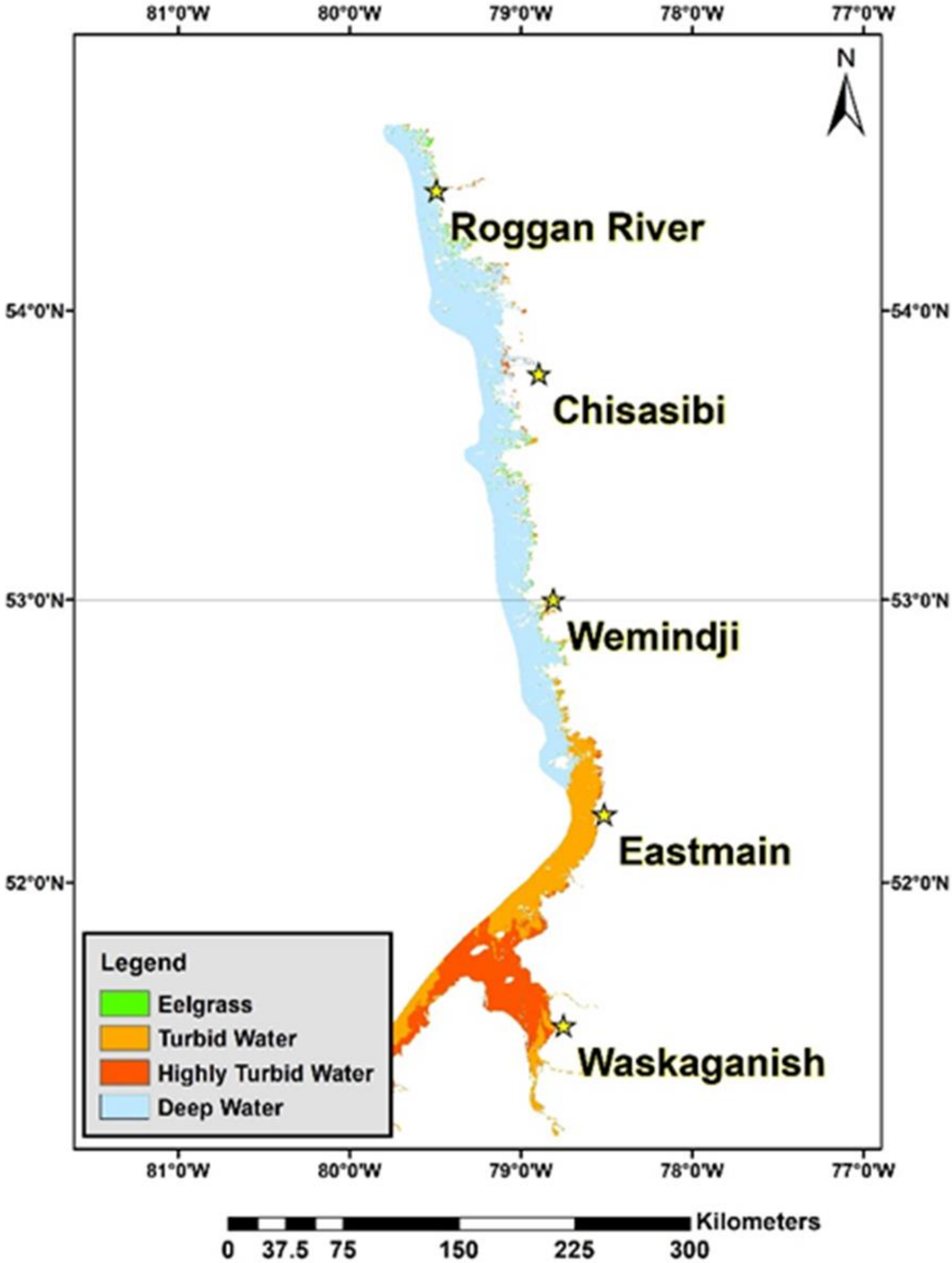

Figure 31 Map produced by classifying the 2019 Landsat-8 OLI images over the whole study area (Clyne et al. 2021).

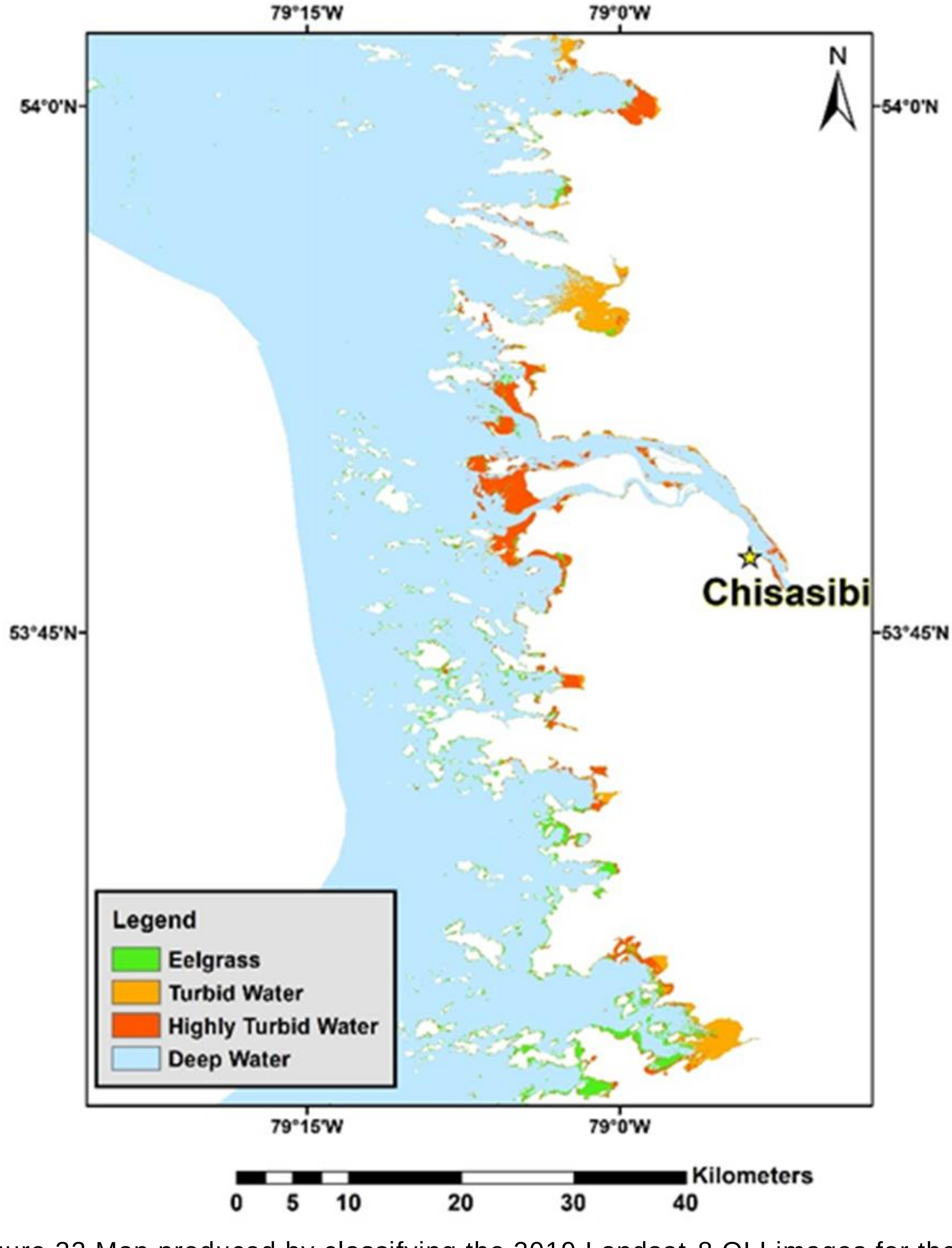

Figure 32 Map produced by classifying the 2019 Landsat-8 OLI images for the coastline around Chisasibi (Clyne et al. 2021).

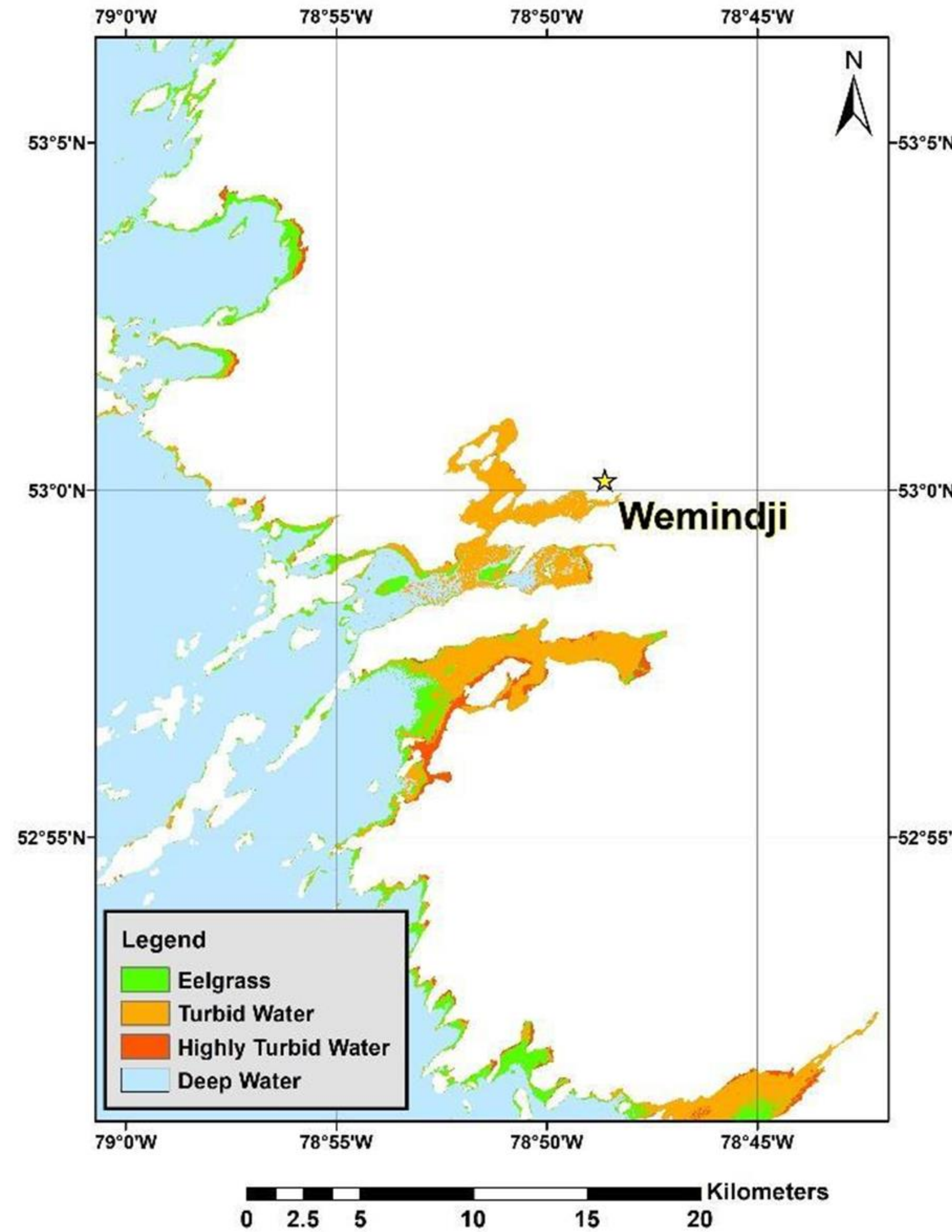

Figure 33 Map produced by classifying the 2019 Landsat-8 OLI images for the coastline around Wemindji (Clyne et al. 2021).

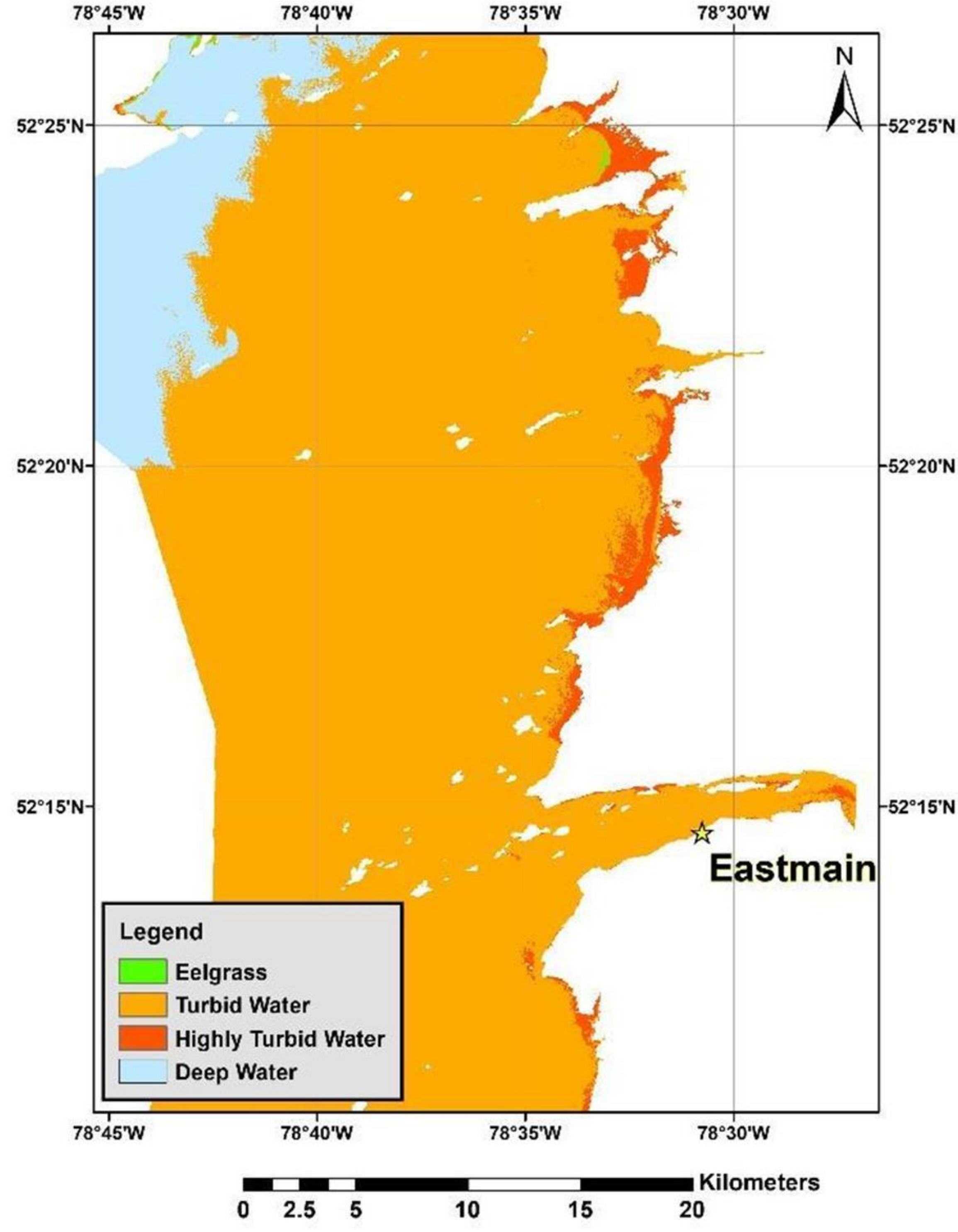

Figure 34 Map produced by classifying the 2019 Landsat-8 OLI images for the coastline around Eastmain (Clyne et al. 2021).

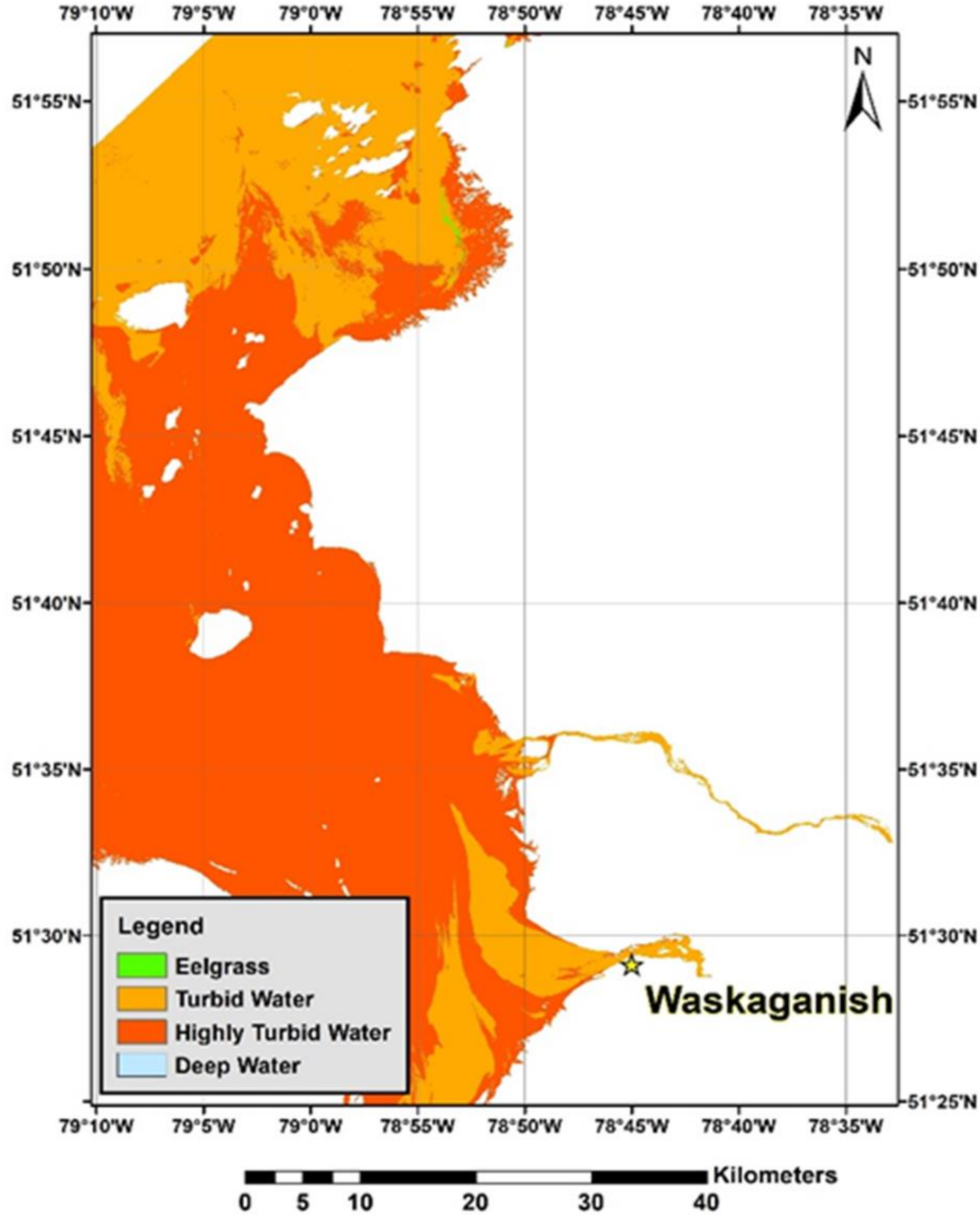

Figure 35 Map produced by classifying the 2019 Landsat-8 OLI images for the coastline around Waskaganish (Clyne et al. 2021).

The resulting classified image was validated against 108 ground truth data obtained from both the eelgrass health and Hydro-Quebec research team. The resulting overall accuracy was 78.7% (Table 10), indicating the potential of the Random Forests classifier to estimate baseline eelgrass coverage in James Bay using Landsat-8 imagery.

Table 10 Validation accuracies obtained by comparing field-based ground-truth sites with the classified image. Bold figures indicated well-mapped sites (Clyne et al. 2021).

Class	Present	Absent	Total	User's Accuracy (%)
Present	**69**	13	82	84.2
Absent	10	**16**	26	61.5
Total	79	29	**108**	
Producer's Accuracy (%)	87.3	55.2	Overall Accuracy = 78.7%	

3.1.4 CONCLUSION

This study shows that the Landsat-8 OLI imagery can be used to map the eelgrass distribution along the eastern coastline of Eeyou Itschee. In this imagery, eelgrass can be spectrally distinguished from optically deep and turbid waters. The spectral signature of eelgrass was not shown to be detectable underneath suspended material in the water column since the red and green reflectance of turbid waters is dominated by particulate matter in the water column. The overall accuracy for the classification was 99.3% and for the validation was 78.7%. Our map did not show extensive eelgrass beds where it was possible to map them with the Landsat8-OLI imagery. Such observations agree with the Cree Land Users of Eeyou Istchee who have noted steady declines in eelgrass coverage along the coast in the late 1980s and then a drastic decline in 1997-1998 (Cycle et al. in revision). Cree reported that since the decline in the late 1990s, the recovery of the eelgrass has been very slow. Such a study is therefore a good example of how local indigenous knowledge can be combined with Western science in a case study.

Landsat-8 imagery, while providing exceptional temporal coverage, is limited in its spatial resolution. The 30 m pixel size of Landsat-8 imagery limits the creation of training areas to only large beds and may have trouble classifying patchier eelgrass or smaller patches of turbid/clear water. The 30 m spatial resolution also makes an accurate location of the coastline difficult. This was not too much of an issue in James Bay, where optically shallow waters suitable for eelgrass extend far past the coastline-however it could present an issue if applied to a coastline with only a small strip (< 30 m width) of shallow enough water for eelgrass growth. Besides, while James Bay contains geographically large eelgrass beds, areas dominated by other types of submerged aquatic vegetation may have similar spectral characteristics. Therefore, this study framework may not be applicable for locations where multiple submerged aquatic vegetation may encompass a geographic area larger than 30 m. While this study provided a framework for mapping eelgrass beds on a large spatial scale in turbid waters, more work should be done researching the accuracy of the Random Forests classifier on smaller spatial scales using higher resolution imagery. Sentinel-2 imagery could potentially offer bay-wide coverage at a 10 m resolution and should be explored as a high-resolution multispectral alternative.

Lansat-8 OLI imagery has a limited number of bands and high-resolution hyperspectral imagery would be a suitable option for mapping sections of the Bay, but the unpredictable bay-wide turbidity could also make hyperspectral imagery acquisition not feasible. Lastly, substituting true bathymetry data for the ratio decay algorithms used in this study may improve classification; however, in the absence of bathymetry data, the high spectral separability between deep clear water and eelgrass makes the bathymetric ratios an excellent choice for adding information to the classifier. Our classified image was validated against 108 points and there is a need to add more validation points in further work.

3.2 OBJECTIVE 2

Evaluating the capability of Landsat-5 TM and Landsat-8 OLI imagery to reconstruct the changes in eelgrass bed extent and distribution between 1988 and 2019.

3.2.1 INTRODUCTION

The coastline of Eeyou Itschee is known to be home to sizeable beds of eelgrass (*Zostera marina* L.), which thrive in the James Bay's shallow, subarctic waters. The region was subjected to substantial hydroelectric dams, large fires, and other human activities in the past half-century. The Cree Land Users of Eeyou Istchee have noted steady declines in eelgrass coverage along the coast in the late 1980s and then a drastic decline in 1997-1998. They have also reported that, since the decline in the late 1990s, eelgrass recovery has been very slow, and the eelgrass currently observed in some areas seems unhealthy.

To evaluate the decline of eelgrass beds along the coast, some mapping attempts have been made in the past. In 1974, the Canadian Wildlife Service drew the first large-scale map of eelgrass in James Bay, utilizing black and white aerial photography to create a distribution map at a scale of 1:125,000. All major beds along the coast were recorded and generalized spatially into one of four distribution classes based on estimated percent cover. In 1987, 1991 and 1996, the Société d'énergie de la Baie James, in charge of the construction of a hydroelectric development in this area, deemed it necessary to update the map with distribution changes over the past 12 years using color aerial photography at a scale of 1:10,000 as well as field validation using divers to ascertain the limit of eelgrass distribution along a large part of the coast. In addition to the large-scale mapping, Hydro-Quebec initiated six permanent sampling stations in their monitoring effort, nearly all of them around Chisasibi, to estimate the impact of the hydrological changes in the bay's effect on eelgrass (since the most pronounced impact would be around Chisasibi).

The inconsistencies in data collected by Hydro-Quebec outline the need for continuous and independent monitoring of eelgrass distribution along the Eeyou Istchee coastline. Due to the many limitations on researchers to perform field surveys in James Bay (i.e., harsh winter conditions, the extent of coastline, shallowness of coastline limiting the operating capacity of ships, etc.), satellite image analysis presents the best option for cost-effective, routine monitoring of the entire extent of the coast. Previous attempts to map eelgrass distribution along the bay using satellite imagery have been scarce and varied in their methodology. While they could detect a change in the eelgrass distribution using image differentiation techniques, they could not correctly classify the images.

In this study, we aim to present a mapping approach for evaluating the distribution of eelgrass along the eastern coast of James Bay utilizing both freely available imagery from the Landsat-5 Thematic Mapper (TM) and Landsat-8 Operational Land Imager (OLI), in conjunction with pre-existing field data collected by Hydro-Quebec. This study is the subject of one chapter in Clyne (2022) M.Sc. thesis and one paper in preparation for Remote Sensing (Clyne et al. in revision).

3.2.2 METHODS

In this study, we considered only two zones of the whole coastline where historical maps existed because they were used as ground-truth data for the classification. The first zone is north of Chisasibi and the second one is south of Chisasibi (Figure 35). Both zones excluded the plume of the La Grande River and its immediate vicinity since there is no ground-truth data for that zone.

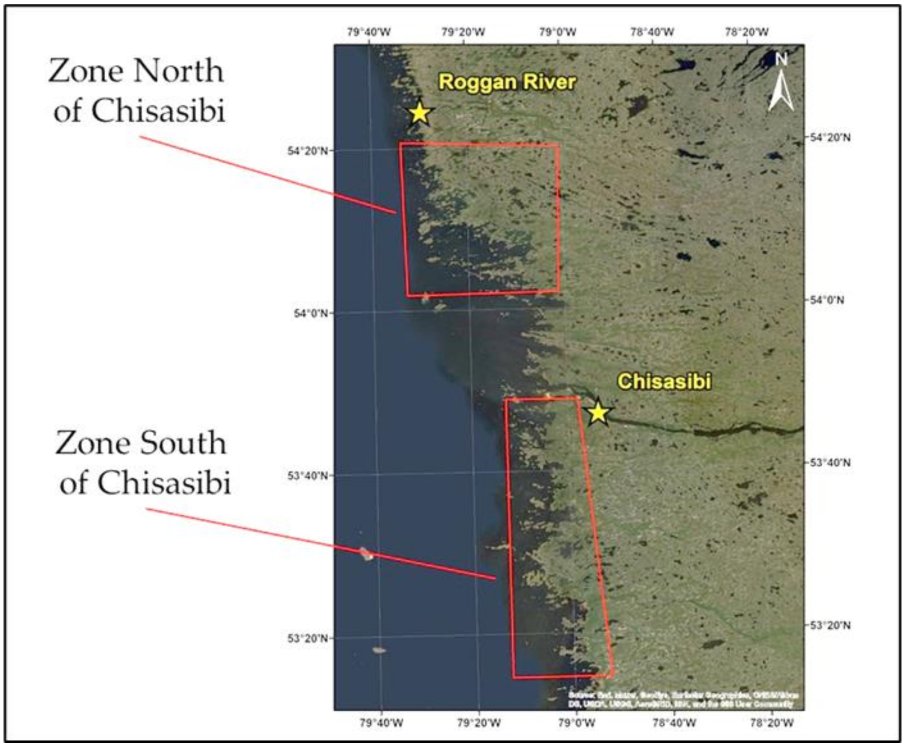

Figure 36 Study area showing the two zones where eelgrass distribution was evaluated: North and South of the Cree community of Chisasibi.

The study used Landsat imagery acquired for each year where existing eelgrass distribution data intersected with the availability of cloud-free Landsat imagery along the eastern coastline of James Bay (Table 11). Images selected were prioritized according to two criteria: (i) images were as free of cloud cover as possible; and (ii) images were acquired as close as possible to peak eelgrass biomass season (late summer). Due to the limited amount of cloud and ice-free scenes available that covered the full extent of the coastline, tidal level was not accounted for when selecting imagery. In addition, tidal data for this region was not consistent until the 21st century, so accurate tidal measurements do not exist for the historical study period (1988 to 1996). Imagery from the Landsat-5 Thematic Mapper (Collection-2) was acquired as close as possible to the years of the aerial photos and field surveys used for establishing the historical maps. We also used Landsat-8 Operational Land Imager (OLI) (Collection-2) imagery in 2019 that covers both zones and coincides with the 2019 summer field survey by the James Bay Coastal Habitat Comprehensive Project (CHCRP) team.

Table 11 List of the images used in the study and associated date and cloud cover.

Sensor	Image Acquisition Date	Image Path / Row	Scene Cloud Cover (%)
Landsat-5 MSI	24-Jul-1988	020 / 022	26
		020 / 023	2
	17-Jul-1991	020 / 022	7
		020 / 023	48
	16-Sep-1996	020 / 022	0
		020 / 023	0
Landsat-8 OLI	16-Sep-2019	020 / 022	0
		020 / 023	0

For the 1988, 1991, and 1996 classifications, the ground-truth data were extracted from eelgrass distribution maps established over the two zones, based on aerial photo interpretation, helicopter-based aerial surveys, and snorkeling/diving survey in summer. For the 2019 classification, the field data were acquired the same year via a snorkeling/diving survey, and eelgrass presence/absence was recorded using a GPS at each evaluation site. Each point location was saved, and the dataset was converted to a point shapefile dataset. This dataset was only used for validating the classified image. To account for varying survey extents by Hydro-Quebec between each of their distribution maps, we limited our study area to only where survey extent was the same during all three years North of Chisasibi (northern zone) and South of Chisasibi (southern zone), except for the 1988 southern zone (Figure 36). To account for this, the 1988 image was assessed for accuracy only as far south as the published distribution maps for Hydro-Quebec.

Eelgrass generally grows in areas of less than 5 m water depth, as such a depth mask was defined to minimize error on the image classification. Because bathymetric data are unavailable for all the bay, we estimated the water depth, using the digital terrain model (DTM) derived from the Shuttle Radar Topographic Mission (SRTM) data from the United States Geological Survey (https://earthexplorer.usgs.gov/). Two “relative depth” layers were created from the DTM as follows. The elevations of the land mass were transformed into a slope layer defining the extent to the water area. The resulting slope layer was converted to an elevation layer as a function of the coast distance to estimate the water depth. This allows the ability to create additional input features for the classifier, defining the deep water zone (water depth higher than 5 m) and the shallow water zone with a water depth of less than 5m. Both zones were only delineated where there were no islands along the coast. The island zone was considered a shallow water zone.

	1986	1991	1995
North of Chisasibi			
South of Chisasibi	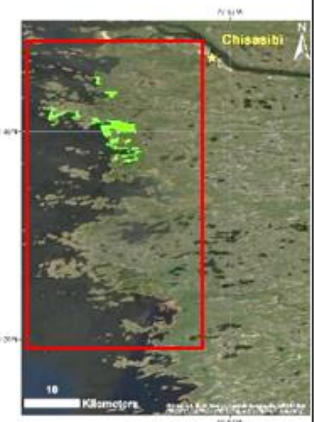	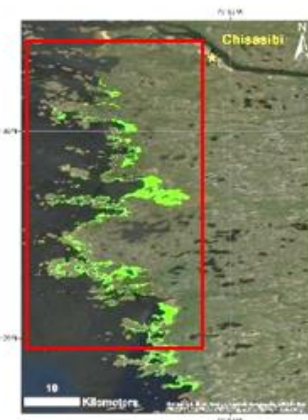	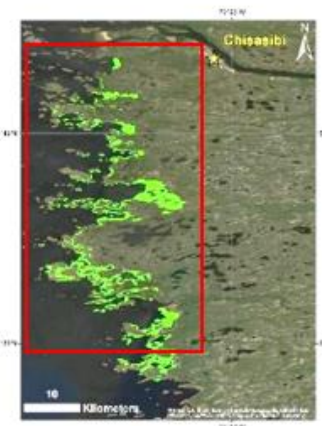

Figure 37 Digitized historical eelgrass bed distribution maps overlaid over a Google Earth image as a function of the year. Data outside of the red box was excluded from the study area due to varying survey extents.

The Landsat images were converted into surface reflectance images using ACOLITE, a free atmospheric correction application developed by the Royal Belgian Institute of Natural Sciences. This application was designed for the simple and fast processing of coastal scenes, with a sun glint correction and the mosaicking of the three images acquired in September. Once processing was completed, the resulting image mosaic was clipped to keep only the water located from a short distance to the coastline. Additional layers were created during the atmospheric correction and used as input for the image classification. First, ACOLITE module provides the option to compute the Turbidity, the Suspended Material Concentration, the Floating Algal Index, and the Orange reflectance. Second, eleven vegetation indices and two bathymetric ratios were computed. These computed layers were finally combined with the surface reflectance mosaic from ACOLITE and used as inputs for the RF classifier.

The Landsat images were classified using the Random Forests (RF) supervised classifier, which requires training areas. Representative training areas were delineated through a photointerpretation of the multispectral satellite imagery for the five following classes: Eelgrass (EG), Low Turbid Water (LT), High Turbid Water (HT), Bare Seafloor (SF), and Optically Deep Water (DW). The Eelgrass class was created where field surveys recorded eelgrass presence in that respective year or where large eelgrass beds were visible on the satellite imagery. Where field data were derived from the historical distribution maps, eelgrass training polygons were created in areas with large, high-density eelgrass beds were recorded on the map. In the images, a large part of the eastern coastline of James Bay contained turbid water, either within bays near the coastline or out in deeper waters at the southern end of the bay. It is why two classes of water turbidity were created through a manual selection of visibly turbid waters.

To examine how the classified images perform at smaller scales, a subset of the aerial photos taken by Hydro-Quebec that were used to derive the eelgrass distribution maps was compared visually with our classified image at specific locations. Each photograph was annotated with the limit of continuous and discontinuous eel-grass distribution for each site. These annotated aerial photographs correspond to field surveys from 1986 and 1995, so the classifications from 1988 and 1996 were compared to these photographs. This comparison was used to examine how closely our image classifications match the ground-truth data at more fine resolutions than a bay-wide scale, as well as to assess the accuracy of our image classifications.

3.2.3 RESULTS

A separability analysis was performed on the training data to estimate the spectral separability between the five classes considered in the study. The resulting Jeffries-Matusita distances show that the five classes used in the study were well spectrally separated, whatever the Landsat image used (Table 12).

Table 12 J-M distances computed with the combination of original spectral bands for each Landsat sensor. Values range from 0-2, with 2 representing perfect class separability.

Year	Average	Class	Eelgrass	Low Turbidity	High Turbidity	Seafloor
1988	1.950	Low Turbidity	1.936			
		High Turbidity	1.901	1.923		
		Seafloor	1.974	1.981	1.968	
		Deep Water	1.980	1.906	1.931	1.998
1991	1.983	Class	Eelgrass	Low Turbidity	High Turbidity	Seafloor
		Low Turbidity	2.000			
		High Turbidity	1.966	1.999		
		Seafloor	2.000	2.000	2.000	
		Deep Water	1.987	1.904	1.979	2.000
1996	1.996	Class	Eelgrass	Low Turbidity	High Turbidity	Seafloor
		Low Turbidity	2.000			
		High Turbidity	1.997	2.000		
		Seafloor	1.994	2.000	1.996	
		Deep Water	1.999	1.992	1.986	2.000
2019	1.997	Class	Eelgrass	Low Turbidity	High Turbidity	Seafloor
		Low Turbidity	2.000			
		High Turbidity	1.999	2.000		
		Seafloor	2.000	2.000	1.999	
		Deep Water	1.999	1.984	1.985	2.000
Average	1.982	Class	Eelgrass	Low Turbidity	High Turbidity	Seafloor
		Low Turbidity	2.000			
		High Turbidity	1.999	2.000		
		Seafloor	1.999	2.000	1.991	
		Deep Water	1.999	1.946	1.970	2.000

A classified image for each studied year was produced by applying RF to the Landsat band reflectance and the derived variables (vegetation indices and bathymetric ratios). According to the confusion matrix produced by RF, the classification accuracy is very high, between 94.51% for the 1996 classification and 99.85% for the 2019 classification (Table 13). Producer's accuracies for the "Eelgrass" class were the lowest for the 1996 classification (89.29%) and the highest for the 2019 classification (99.95%). By all three metrics stated, the 2019 classification using Landsat-8 imagery was the most accurate of the four classified images, and the 1996 classification was the least accurate. The various classified images are displayed in Figure 37.

Table 13 Confusion matrices (in number of pixels) obtained by applying the Random Forests classifier to Landsat band reflectance and the derived variables (vegetation indices and bathymetric ratios) as a function of the year. Bold values represent well-classified pixels.

1988	Eelgrass	Low Turbidity	High Turbidity	Seafloor	Deep Water	Total	UA (%)
Eelgrass	**4142**	40	15	35	4142	4586	90.32
Low Turbidity	68	**9041**	10	24	68	9224	98.02
High Turbidity	14	8	**1859**	1	14	1951	95.28
Seafloor	36	15	3	**2620**	36	2678	97.83
Deep Water	239	25	26	2	**239**	119791	99.76
Total	4499	9129	1913	2682	120007	**Overall Accuracy (%) = 99.23**	
PA (%)	92.06	99.04	97.18	97.69	99.58		
1991	Eelgrass	Low Turbidity	High Turbidity	Seafloor	Deep Water	Total	UA (%)
Eelgrass	**2881**	15	10	19	103	3028	95.15
Low Turbidity	27	**37016**	3	23	1431	38500	96.15
High Turbidity	14	5	**361**	2	35	417	86.57
Seafloor	15	45	0	**974**	0	1034	94.2
Deep Water	26	1335	10	0	**54651**	56022	97.55
Total	2963	38416	384	1018	56220	**Overall Accuracy (%) = 96.85**	
PA (%)	97.23	96.36	94.01	95.68	97.21		
1996	Eelgrass	Low Turbidity	High Turbidity	Seafloor	Deep Water	Total	UA (%)
Eelgrass	**3367**	0	136	58	450	4011	83.94
Low Turbidity	0	**12240**	0	0	2323	14563	84.05
High Turbidity	146	5	**3385**	45	160	3741	90.48
Seafloor	71	0	31	**1624**	0	1726	94.09
Deep Water	187	2031	65	0	**77617**	79900	97.14
Total	3771	14276	3617	1727	80550	**Overall Accuracy (%) = 94.51**	
PA (%)	89.29	85.74	93.59	94.04	96.36		
2019	Eelgrass	Low Turbidity	High Turbidity	Seafloor	Deep Water	Total	UA (%)
Eelgrass	**12906**	0	0	1	25	12932	99.8
Low Turbidity	0	**31055**	1	0	178	31234	99.43
High Turbidity	1	1	**9674**	0	300	9976	96.97
Seafloor	0	0	0	**3618**	0	3618	100
Deep Water	4	175	3	0	**414701**	414883	99.96
Total	12911	31231	9678	3619	415204	**Overall Accuracy (%) = 99.85**	
PA (%)	99.95	99.44	99.96	99.97	99.88		

(PA = Producer's accuracy; UA = User's accuracy)

<table>
<tr><th>Year</th><th>North of Chisasibi</th><th>South of Chisasibi</th></tr>
<tr><td>1988</td><td>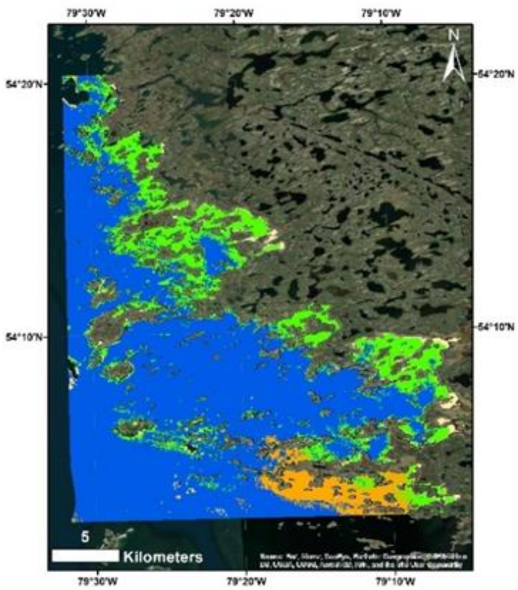
</td><td>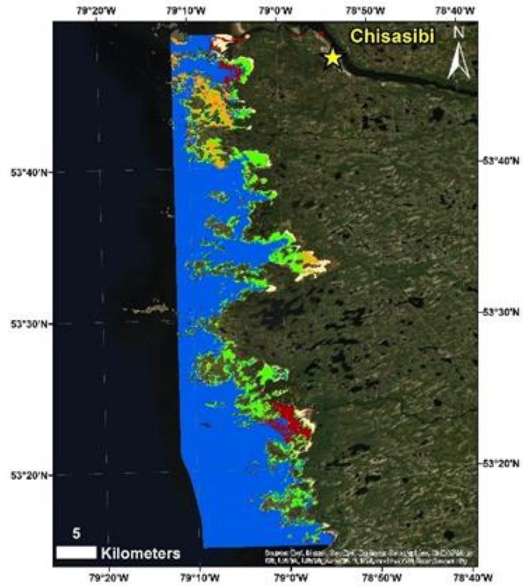
</td></tr>
<tr><td>1991</td><td>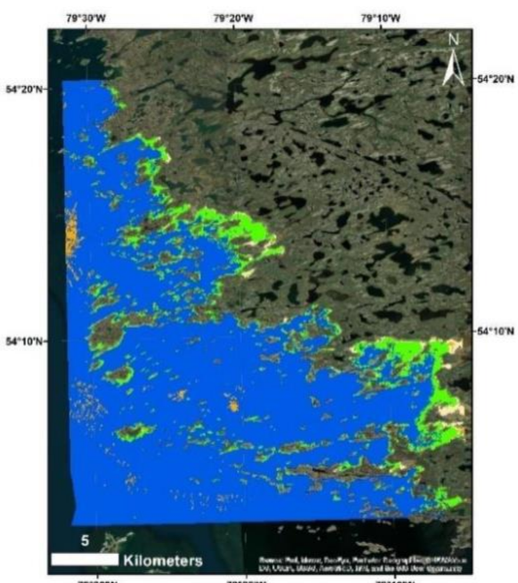
</td><td>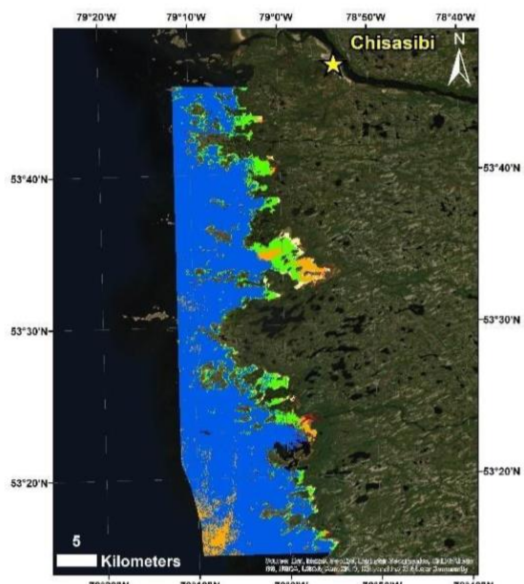
</td></tr>
<tr><td>Legend</td><td colspan="2">= Eelgrass = Low Turbidity = High Turbidity = Bare Seafloor = Deep Water</td></tr>
</table>

<table>
<tr><th>Year</th><th>North of Chisasibi</th><th>South of Chisasibi</th></tr>
<tr><td>1996</td><td>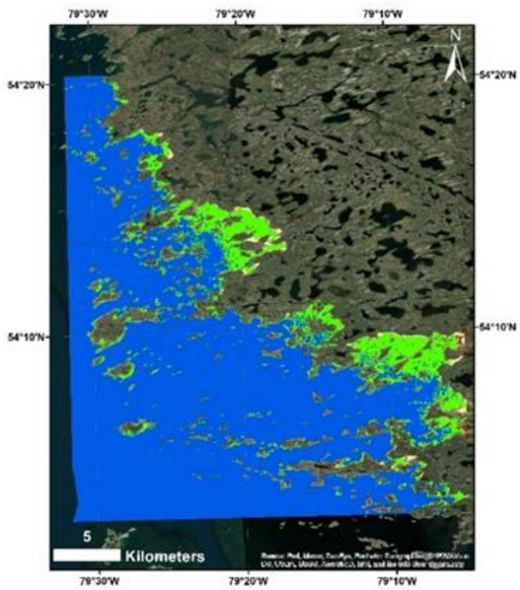
</td><td>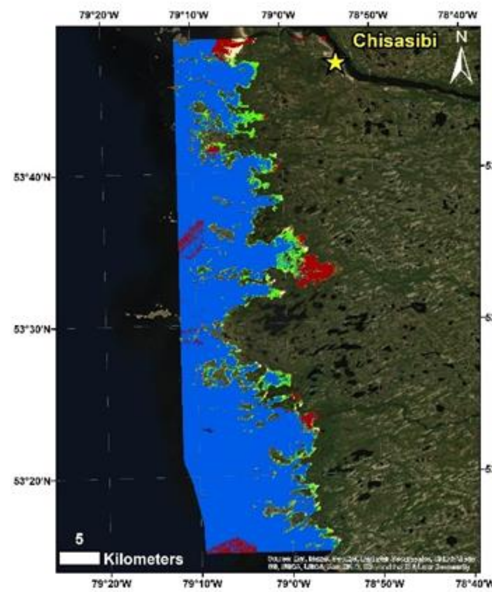
</td></tr>
<tr><td>2019</td><td>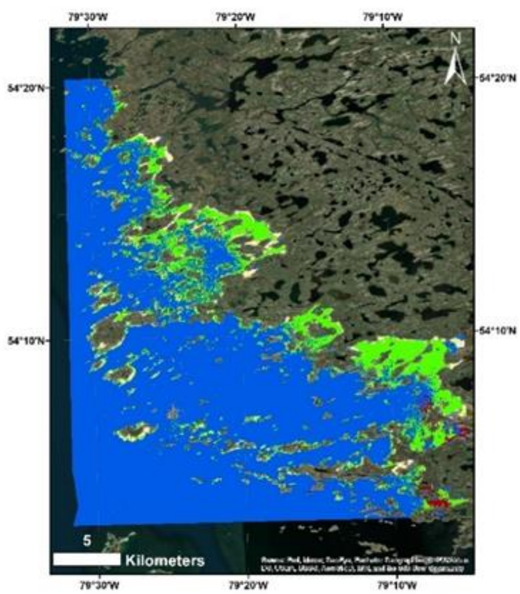
</td><td>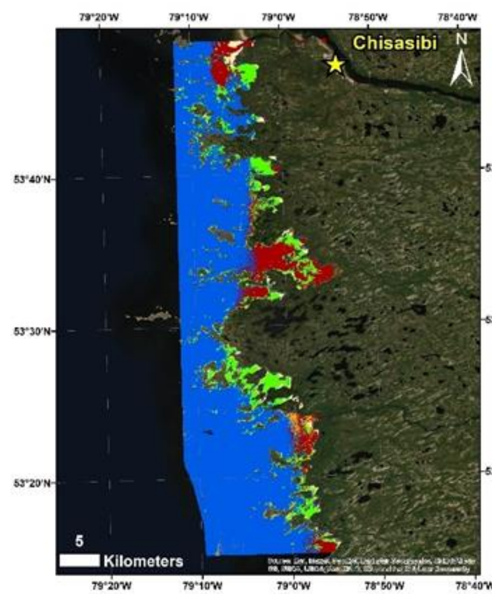
</td></tr>
<tr><td>Legend</td><td colspan="2">= Eelgrass = Low Turbidity = High Turbidity = Bare Seafloor = Deep Water</td></tr>
</table>

Figure 38 Classified images produced by applying the Random Forests classifier to the reflectance bands, associated vegetation indices, and bathymetric ratios for each year.

Classified images were further assessed for accuracy using validation points (eelgrass present/absent) derived from historical Hydro-Québec eelgrass distribution maps for 1988, 1991, and 1996 as well as the James Bay Coastal Habitat Comprehensive Project team's field validation set for the 2019 classification. The assessment was done using a confusion matrix that is presented for each classified image in Table 14. The overall validation accuracy was the highest for the 1988 classification (84.5%) and the lowest for the 2019 classification (74.5%). Producer's accuracies of the eelgrass present class ranged from 73.3% with the 1996 classification to 84.0% with the 1988 classification, while the corresponding User's accuracies ranged from 79.2% with the 1988 classification to 91.1% with the 2019 classification, indicating reasonable consistency between classification results. The 1988 classification and the 2019 classification had significantly fewer validation points compared to the 1991 and 1996 classifications due to lack of data availability in 1988 and 2019. Yet, the validation results do not show any distinct trends relative to the number of validation points.

Since the aerial photograph delineations were not available for 1991, only the 1988 and 1996 classifications were compared at individual sites to aerial photographs with delineations of eelgrass distribution produced by Hydro-Québec. Both data sources (classified imagery and historical aerial photographs) showed a general agreement that eelgrass was present along the entire eastern coastline of James Bay based on a visual comparison of the two images for each study site. Both datasets showed large eelgrass beds in locations where eelgrass have been historically recorded to be present, such as the Bay of Many Islands and Dead Duck Bay. A slight variation was observed between the two years on either the historical distribution maps or the multispectral image classifications between the presence and general distribution of the most major beds, while higher variation was shown for smaller beds on the classified Landsat imagery. However, the distribution and shape of eelgrass meadows, as extracted from the classified image of 1996, are generally in good agreement with those extracted from the aerial photographs of 1995, as shown for the three among the Hydro-Québec (HQ) sites presented in Figure 38.

Table 14 Validation accuracies obtained by comparing field-based ground-truth sites with the classified images. Bold figures indicated well-mapped sites.

		Ground-Truth			
1988	Class	Eelgrass Present	Eelgrass Absent	Total	UA (%)
Classified	Eelgrass Present	**42**	11	53	79.25
	Eelgrass Absent	8	**62**	70	88.57
	Total	50	73	123	
	PA (%)	84.00	84.93	Overall Accuracy (%) = 84.55	
		Ground-Truth			
1991	Class	Eelgrass Present	Eelgrass Absent	Total	UA (%)
Classified	Eelgrass Present	**75**	16	91	82.42
	Eelgrass Absent	25	**84**	109	77.06
	Total	100	100	200	
	PA (%)	75.00	84.00	Overall Accuracy (%) = 79.50	
		Ground-Truth			
1996	Class	Eelgrass Present	Eelgrass Absent	Total	UA (%)
Classified	Eelgrass Present	**66**	12	78	84.62
	Eelgrass Absent	24	**78**	102	76.47
	Total	90	90	180	
	PA (%)	73.33	86.67	Overall Accuracy (%) = 80.00	
		Ground-Truth			
2019	Class	Eelgrass Present	Eelgrass Absent	Total	UA (%)
Classified	Eelgrass Present	**41**	4	45	91.11
	Eelgrass Absent	11	**3**	14	21.43
	Total	52	7	59	
	PA (%)	78.85	42.86	Overall Accuracy (%) = 74.58	

(PA = Producer's accuracy; UA = User's accuracy).

HQ Site	Classified Landsat Imagery (1996)	Aerial Photograph (1995)
3	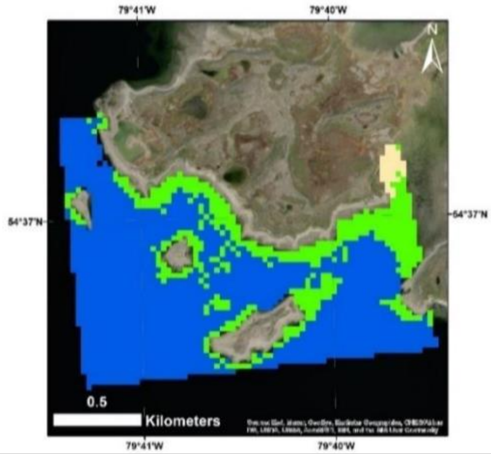	
4	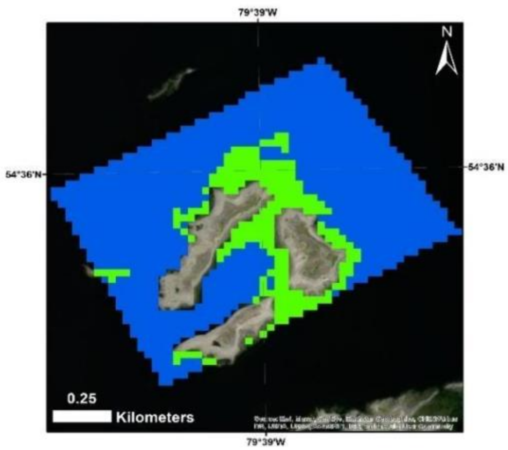	
5	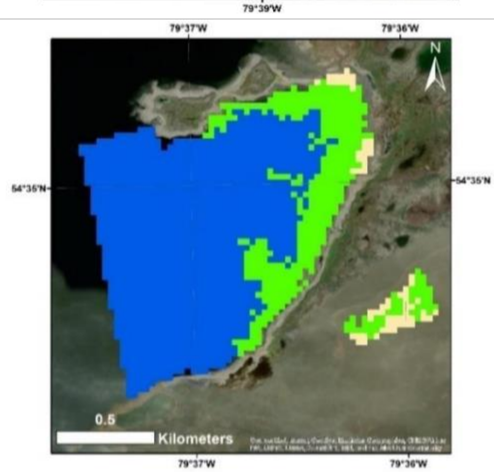	

Figure 39 Comparison between the classified Landsat imagery of 1996 and the aerial photographs of 1995 for the eelgrass distribution mapped for three sites mapped by Hydro-Québec (HQ site). Green lines on the aerial photos represent the extent of continuous eelgrass beds, while the red lines represent the discontinuous bed limit.

The area of classified eelgrass beds mapped with the classified images over each zone was quantified (Table 15) and plotted (Figure 38). This last figure shows the declining trend in eelgrass extent observed throughout the study period for both zones as well as the total study period, although the 2019 extent was slightly higher than the 1991 and 1996 extents. The area covered by eelgrass mapped by Hydro-Québec in 1991 and 1996 is also shown. The classified image area well compared with the Hydro-Québec area in 1991 for the South of Chisasibi zone but not for the North of Chisasibi zone. The difference was the most important with the 1996 dataset.

Table 15 Total classified eelgrass area, assessed with turbid water points from any classified image omitted from all other images, as well as with turbid water points included.

	Turbid Pixels Included			Turbid Pixels Excluded		
	North	South	Total	North	South	Total
1988	82.39	86.89	169.28	79.39	62.82	142.21
1991	50.47	59.35	109.82	23.58	25.87	49.45
1996	60.00	45.51	105.51	30.24	14.81	45.05
2019	66.37	59.31	125.68	47.95	44.06	92.01

a) North of Chisasibi

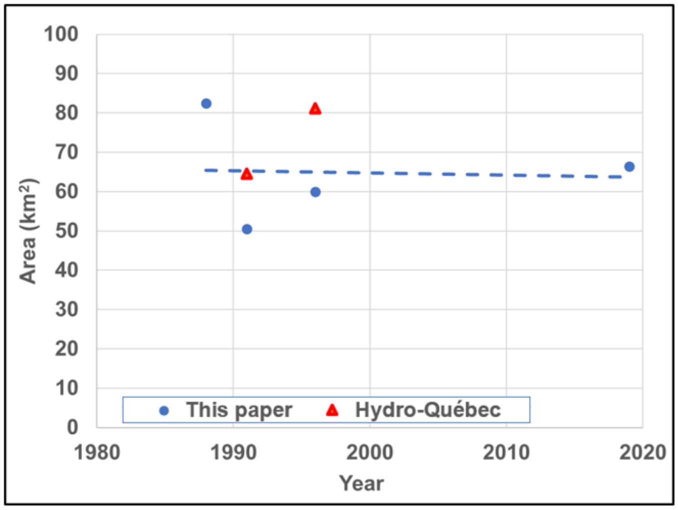

b) South of Chisasibi

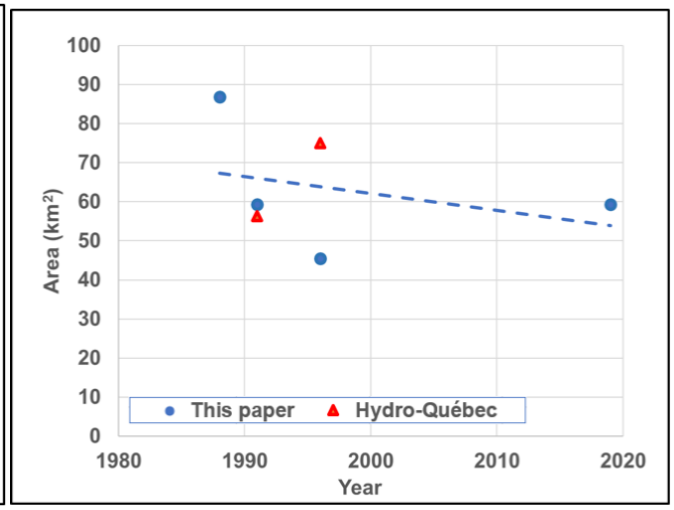

c) Total

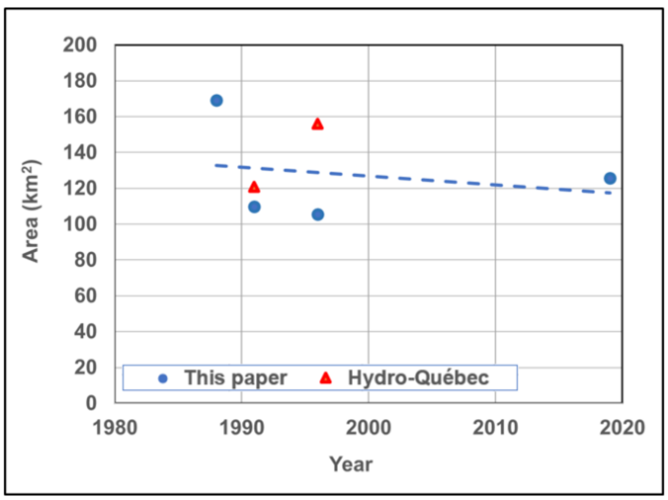

Figure 40 Evolution of the eelgrass area extracted from the classified images and the HQ aerial photographs as a function of the classification year (Clyne 2022).

Due to variable extents of turbid water in each classification year, the total area having potentially eelgrass beds varies between the four classified images. To determine if this impacted the overall trend, the total area classified as eelgrass was also determined where all pixels classified as turbid water during any of the four image classifications were removed from all the classified images. This allowed us to determine the total eelgrass area independent of the quantity of turbid water pixels present for each individual classification year. Table 15 gives the resulting eelgrass area with and without the turbid water pixels. The difference between the two cases is the largest for 1991 and 1996, indicating that the influence of water turbidity extent is the most important for both years. Besides the hydroelectric development occurring in the area, another factor that could explain the water turbidity is extensive wildfires. The statistics of the area affected by wildfire in the study area (Figure 40) show that a peak of extensive wildfires occurred not very long before the acquisition of the images used, particularly in 1989. According to the forest fire map of the Quebec Ministry of Forests, Wildlife and Parks, a large portion of that burned area occurred on or around watersheds of major James Bay tributaries, A comparison of satellite images acquired before and after the 1989 fires on these major James Bay tributaries showed a distinctive higher water turbidity on the post-fire images than on the pre-fire images (Figure 40).

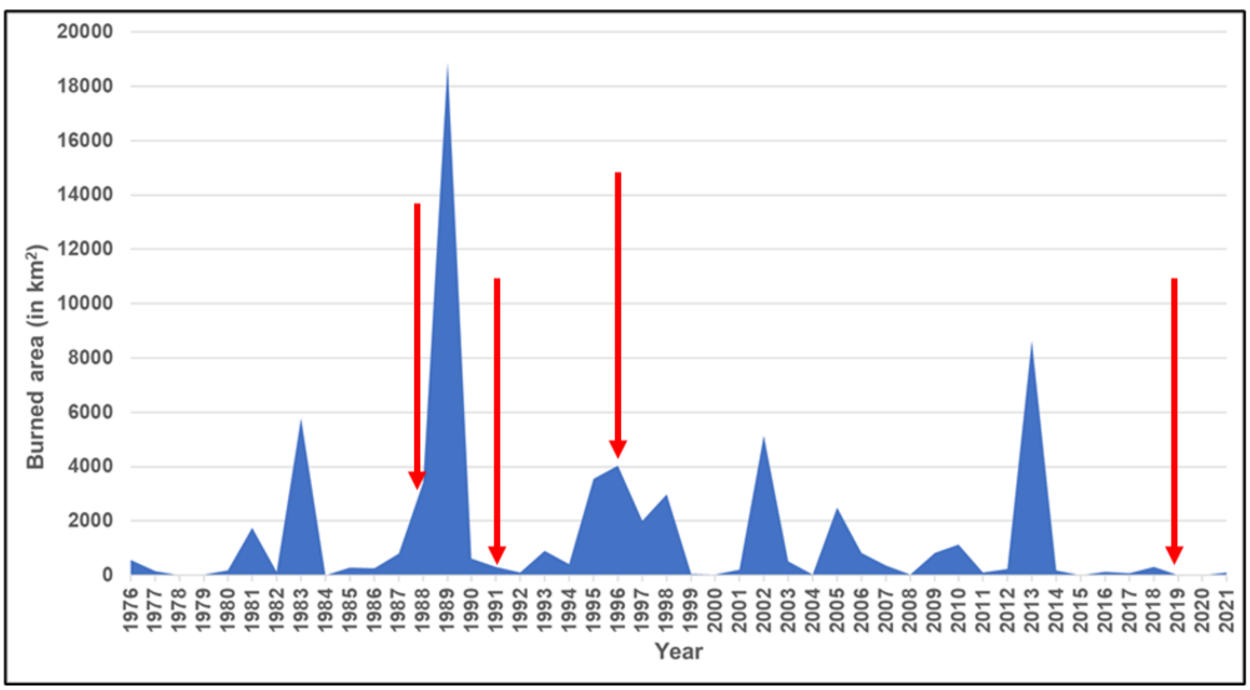

Figure 41 Evolution of the yearly burned areas extracted from the forest fire map of the Quebec Ministry of Forests, Wildlife and Parks website (https://mffp.gouv.qc.ca/). The red arrow indicates the year when eelgrass beds were mapped on the classified images.

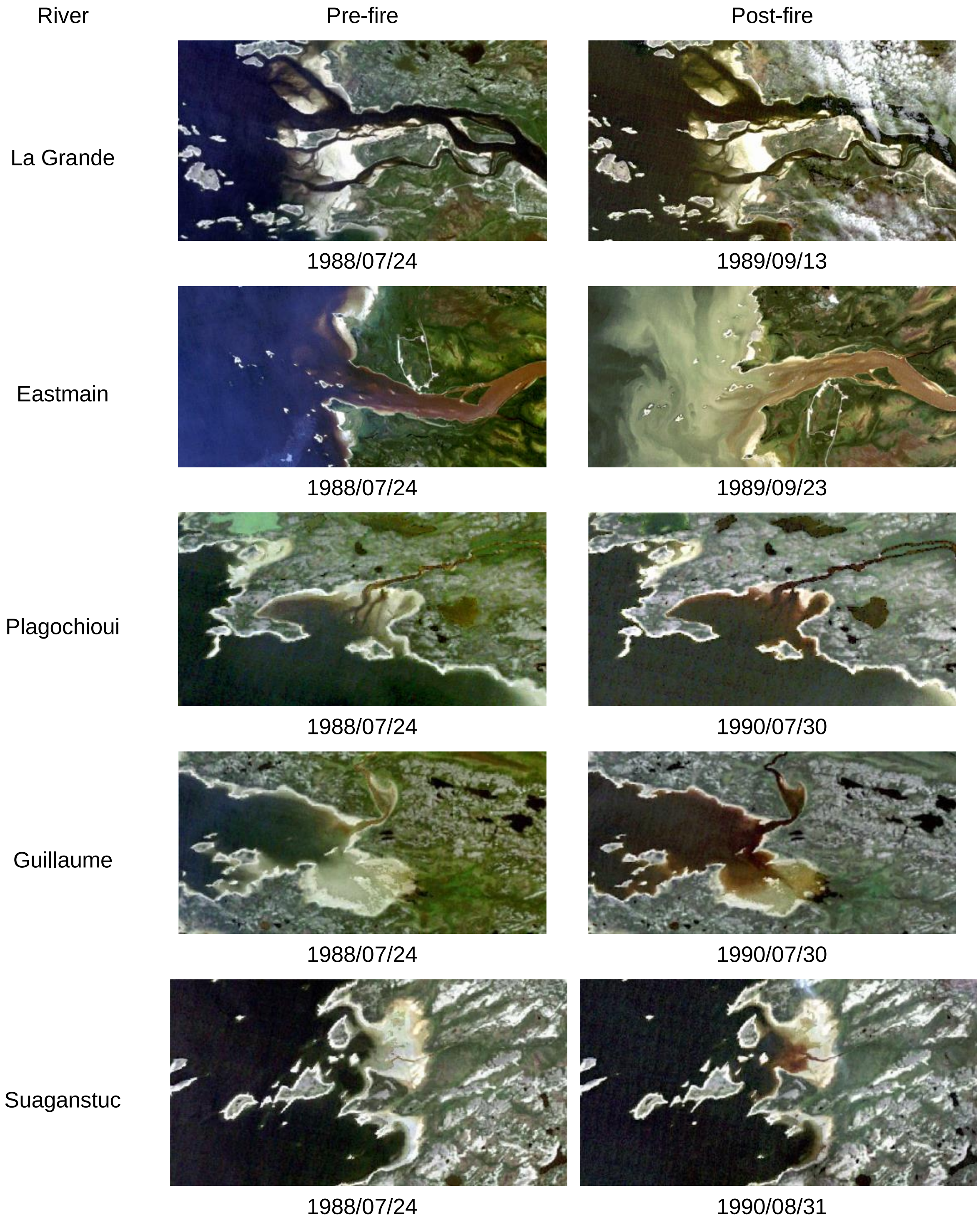

Figure 42 Comparison between Landsat RGB composites over major tributaries of the eastern coast of James Bay before and after the 1989 wildfires.

3.2.4 CONCLUSION

Satellite image analysis offers users the unique ability to evaluate data retroactively and in real-time, which can be a precious tool for scientists looking to add depth and consistency to temporal change analysis. The overall accuracy of our classified Landsat imagery assessed using the training data subset ranged from 94% (lowest) for the 1996 classification to 99% (highest) for the 2019 classification, indicating exceptionally high accuracy. When evaluated using independent field data sets, classified image accuracies for eelgrass presence/absence ranged between 76% for the 2019 classification (lowest) and 85% for the 1988 classification (highest), which, while slightly lower, is still very accurate for the classification of multispectral imagery. Our results present better overall validation accuracies than previous studies carried out over the eastern coast of James Bay.

This study was limited by multiple factors, including: the availability of suitable ice and cloud-free imagery covering the whole of the study area and correct temporal period, tidal differences between images, limited image spatial resolution and the quality of available ground-truth data. Indeed, some of the images acquired (i.e., 1988 and 1996) were acquired within two years of the aerial photographs and data collected for the Hydro-Quebec maps, limiting the precision with which we can compare our image classifications to pre-existing historical data. Tidal differences, which can affect the depth at which eelgrass can be detected, are reluctantly apparent between the three historical image classifications. This difference likely affects the extent to which eelgrass can be detected by the Landsat sensor, as eelgrass extent can be measured further out when the tidal level is lower, and there is less water column above the eelgrass to obfuscate the reflectance signal. Fortunately, the ACOLITE module automatically filters out “land pixels” during the atmospheric correction step, so we can use a total number of pixels in each image as a proxy for tidal levels. Landsat-derived image classifications, while effective for change detection in large areas, have many limitations on their applicability. The moderate spatial resolution presents an advantage in covering a large swath. However, mapping accuracy comes at a cost compared to utilizing imagery with higher spatial resolutions.

The imagery classified in this present study was acquired after the completion of most of the La Grande Complex, making it difficult to determine the potential effects of this hydroelectric project on eelgrass distribution in the bay. Even though historical data could exist before the complex’s construction, such as Curtis 1974’s map, they are too broad and not detailed enough. In particular, there is no multispectral satellite imagery from the Landsat collection to perform a detailed analysis such as the one presented in this report. However, our results were in agreement with Cree’s observations on eelgrass decline from the late 1980’s. Also, our study was able to show the forest fires occurring in 1989 which burned the highest area since 1974 in the study area have an impact on the water turbidity in rivers and in the coastal water of the bay. It is still necessary to analyze how the water turbidity can influence the health status of eelgrass beds. Also, it is necessary to assess where climate changes will have an influence on fire occurrences in the study area and thus on the water turbidity.

Overall, in this study, we showed that multispectral image classification could be a valuable tool for detecting and mapping large eelgrass beds along the eastern coast of James Bay, even in locations with variably turbid water. Data from the Landsat archive is continuously collected and consistently updated within the USGS database, giving this type of study widespread applicability for both past and future change detection analysis. Multispectral image classification can be used on its own but is best used in conjunction with one or multiple field surveys or other datasets. Our maps extracted from classified images can and should be used to inform and guide future eelgrass distribution monitoring along the eastern coastline of James Bay.

3.3 OBJECTIVE 3

Evaluating the capability of Landsat-8 OLI and Sentinel-1 SAR imagery to map the current coastal habitats along the coast of Eeyou Itschee.

3.3.1 INTRODUCTION

In Eeyou Istchee, the Cree inhabitants who are living there for time immemorial consistently rely on geese hunting as a form of subsistence. The Cree Land Users have observed a decline in geese abundance, explained by a steady decline in eelgrass coverage along the coast in the late 1980s and then a drastic decline in 1997-1998. In addition to a decrease in the extension of eelgrass beds, other factors of the Eeyou Istchee's environment could affect the abundance of geese.

One of the avenues of research to explain the decline in geese abundance is to better understand the natural habitat of these Geese. The purpose of this study is to map the land cover of the eastern coast of Eeyou Itschee to characterize the natural habitat of geese. The map was drawn by Armand LaRocque and was used by Sorais *et al.* (2022, in revision) for determining the use of the coastal habitat by geese. It only considers the terrestrial part of the geese' habitat, given that there is another study (Clyne et al. 2021) that addresses the current status of eelgrass beds in the eastern coast of James Bay.

3.3.2 METHOD

The study area for the coastal habitat map was the whole eastern coast of Eeyou Itschee (Figure 42). This study first used freely available imagery acquired by the Landsat-8 Operational Land Imager (OLI) obtained from the United States Geological Survey's (USGS) Earth Explorer website. The images were acquired in three seasons (Spring, Summer, and Fall) to take into consideration seasonal changes such as leaf on and leaf off, varying water levels, soil moisture, and the state of the vegetation. A total of nine cloud-free images were acquired, three for each season. A flowchart describing how the data were processed is given in Figure 43. We produced one mosaic for each season to cover the entire study area. Landsat imagery was atmospherically corrected using the

ATCOR program with PCI Geomatica Banff (PCI Geomatics, ON, Canada). This correction removes some atmospheric interferences and converts the image top of atmosphere (TOA) reflectance values into ground reflectance values. In addition, the optical imagery was reprojected to a 15-m pixel resolution, using the Pansharpening module of PCI Geomatica Banff. The images were then used to compute vegetation indices to bolster the potential separability between the classes (Table 16).

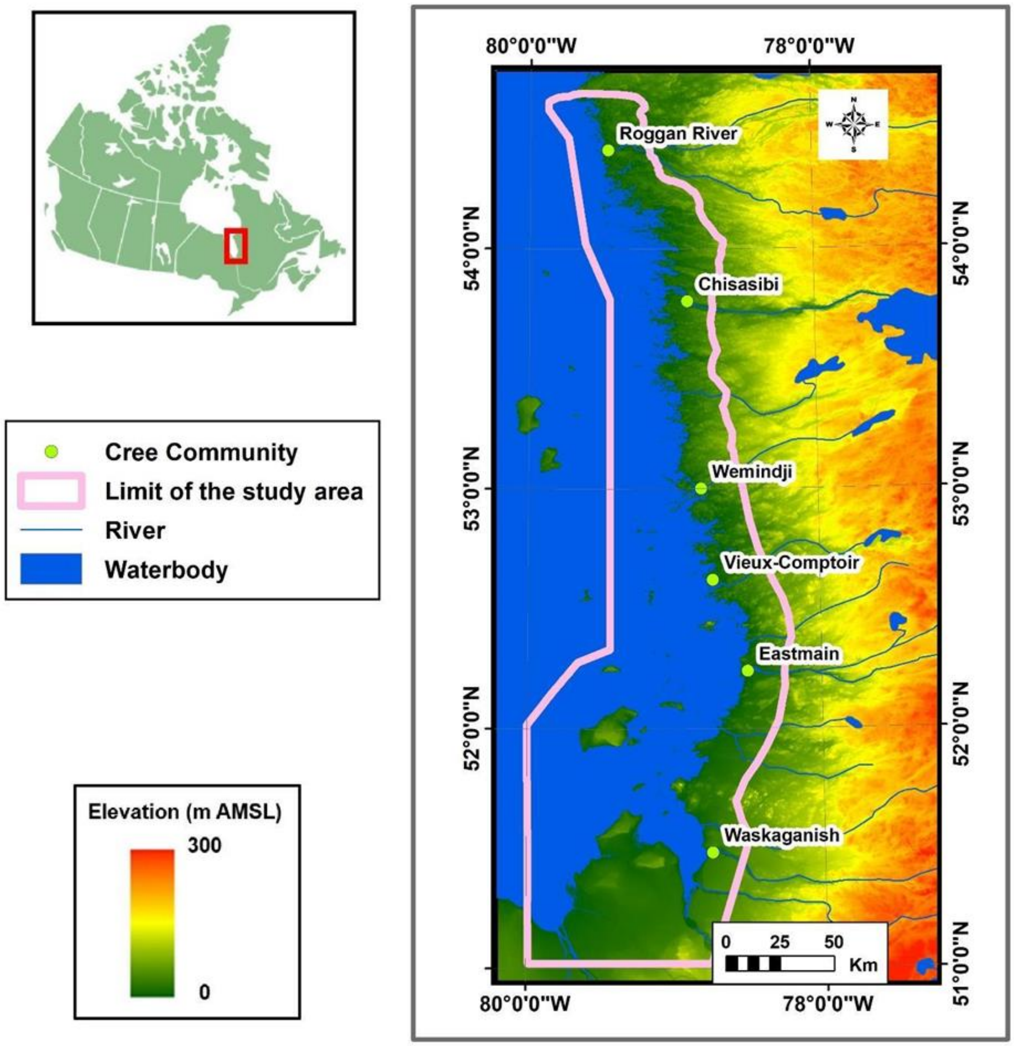

Figure 43 Location and extent of the study area.

Table 16 Vegetation indices computed from the Landsat images.

Variable	**Vegetation index**	**Formula (*)**	Reference
DVI	Difference vegetation index	NIR – R	Tucker (1979)
GDVI	Green difference vegetation index	NIR – G	Sripada et al. (2006)
GNDVI	Green normalized difference vegetation index	(NIR – G) / (NIR + G)	Buschmann and Nagel (1993)
NDVI	Normalized difference vegetation index	(NIR – R) / (NIR + R)	Rouse et al. (1974)
NG	Normalized green	G / (NIR + R + G)	Sripada et al. (2006)
NR	Normalized red	R / (NIR + R + G)	Sripada et al. (2006)
NNIR	Normalized near-infrared	NIR / (NIR + R + G)	Sripada et al. (2006)
RVI	Red simple ratio vegetation index	NIR / R	Birth and McVey (1968)
GRVI	Green ratio vegetation index	NIR / G	Sripada et al. (2006)
NDAVI	Normalized difference aquatic vegetation index	(NIR – B) / (NIR + B)	Villa et al. (2014)
WAVI	Water adjusted vegetation index	1.5 * (NIR – B) / (NIR + B + 0.5)	Villa et al. (2014)

(*) B = reflectance in the blue band; G = reflectance in the green band; NIR = reflectance in the near-infrared band; R = reflectance in the red band.

The SAR imagery includes Sentinel-1 C-band dual-polarized (HH and HV or VV and VH) images downloaded from the European Space Agency's Sentinels Scientific Data Hub website (https://scihub.copernicus.eu/) for the three seasons (Spring, Summer, and Fall). The SAR imagery was acquired during two different passes: ascending orbit with a northeast look direction and descending orbit with a northwest look direction. Pre-classification processing of Sentinel-1 data included updating orbit metadata, noise removal, and terrain correction and was performed with the SNAP toolbox.

The depth of penetration of SAR microwaves into vegetation canopy depends on the radar wavelength. For C-band, the wavelength is approximately 5.55 cm long. In a forested area, Solberg et al. (2007) showed that the C band radar beam can penetrate through the canopy to the ground surface, before being reflected towards the SAR sensor. C band imagery over forests was also shown elsewhere to be able to map flooded grounds or soils saturated with water under a dense temperate forest (Olatunji 2022).

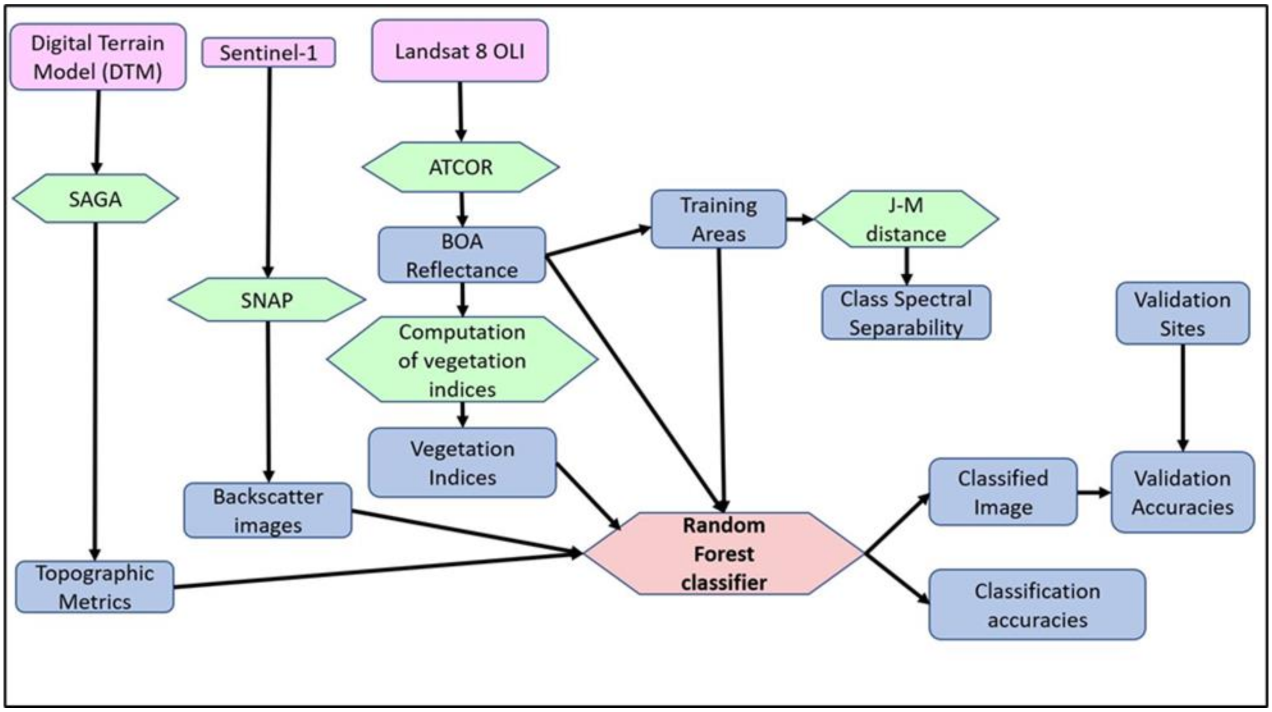

Figure 44 Flowchart presenting the methodology for processing the Landsat-8, Sentinel-1, and DTM data to produce the 2019-2020 classified images.

This study also uses a digital terrain model (DTM) to characterize the local topography. This DTM was extracted from the Shuttle Radar Topographic Mission (SRTM) data from the United States Geological Survey (https://earthexplorer.usgs.gov/). The SRTM-DTM was used for computing the following four topographic metrics: (1) the slope (SLP), (2) the Compound Topographic Index (CTI), (3) the Curvature (CRV), and (4) the Topographic Position Index (TPI). SLP shows where the surface water runoff is slower (or faster) and was derived using the maximum rate of change from one cell to its eight neighbors to show the steepest downhill descent. CTI shows wetter areas using slope combined with where flow is predicted to accumulate. CRV shows deceleration (or acceleration) of water runoff. TPI gives the relative position in the landscape (hilltop to valley bottom) for each pixel. All these topographic metrics are produced with the System for Automated Geoscientific Analyses (SAGA) GIS software.

The combination of the band reflectance images, the associated vegetation indices, the Sentinel-1 data, and the topography metrics were then inputted into a supervised classifier that requires delineation of training areas for each class. We considered in the classification the classes that are described in Table 17. Ground pictures of each class are given in Table 18. 23 habitat classes were determined after a field survey and a photointerpretation of satellite images with a high spatial resolution, from 32 to 65 cm.

The supervised image classification was performed over optical Landsat-8 and Sentinel-1 SAR imagery with Random Forests, a non-parametric decision tree type supervised classifier. We used the package randomForest in R software to classify habitats with 555 randomly distributed training polygons. The classified image was transformed into a map using the Banff version of PCI Geomatica and ArcGIS Pro (ESRI, CA, USA).

Table 17 Description of the habitat classes considered in the study.

Code	Class name	Description
A1	Deep water	Open water more than 2 m deep. Includes fresh water in rivers and salt water located some distance from the coast. Characterized by their black or very dark color on the image, showing no vegetation or floor bottom
A2	Shallow water	Open water, both fresh and salt water, which is less than 2 m deep. In the pre-littoral zone, between the coast and the islands, the bottom of the shallow water is visible in the image, while aquatic vegetation can appear on the surface in water bodies located on land
B1	Tidal flat	Land without vegetation, made of silt and/or sand and located between the lower and upper sea level limits
B2	Cobble beach	Land without vegetation made mainly of coarse elements (pebbles and boulders) and found in the upper part of the foreshore exposed to storm waves
B3	Salt marsh	Wetland dominated by low vegetation, without any trees, and periodically inundated by salt water during high tides. Shrubs may be present, but they cover less than 25% of the surface This habitat is found along the coast of James Bay or at the mouths of rivers influenced by tides and the influx of saltwater
C1	Freshwater marsh	Wetland dominated by low vegetation, bordering current rivers or old channels sometimes used during floods. This habitat is susceptible to seasonal flooding. Shrubs may be present, but they cover less than 25% of the surface
C2	Shrub swamp	Wetland dominated by shrub vegetation (trees less than 4 m high), deciduous, covering more than 25% of the surface. This habitat is found only on the banks of streams or old river channels periodically submerged by running water
C3	Open fen	Wetland dominated by low vegetation (mainly sedge, moss, and some shrubs) growing on organic soil still saturated with relatively stagnant water. This habitat is located at the edge of a meandering stream or body of water, often showing that the water table is near the ground surface
C4	Sting fen	Wetland dominated by low vegetation (mainly sedge, moss, and some shrubs) growing on organic soil still saturated with relatively stagnant water. This habitat is recognized by the alternation of raised strips, with the presence of Tamarack (*Larix laricina* (Du Roi) K. Koch) and narrow and parallel depressions filled with herbaceous vegetation. These depressions do not show apparent water, but this water is found at a minimal depth, giving them a dark brown color

Table 17 (Continued)

Code	**Class name**	**Description**
C5	Shrub fen	Wetland dominated by low vegetation (mainly sedge, moss), growing on organic soil still saturated with relatively stagnant water. Shrubs (trees less than 4 m high), mainly Tamarack (*Larix laricina* (Du Roi) K. Koch), cover between 25 and 50% of the surface. This habitat is located at the edge of a meandering stream or body of water, often showing signs that the water table is near the surface
C6	Open bog	Wetland dominated by low vegetation (mainly moss and some shrubs) growing on organic soil. This habitat is found in the bottom of basins, often without an apparent outlet and showing no indication that the water table is out to the surface. In the northern part of the region, the surface of some open peatlands can be affected by thufurs
C7	Shrub bog	wetland dominated by an understory, mainly composed of moss, with shrub vegetation (trees less than 4 m high) covering more than 25% of the surface, growing on organic soil. The shrubs are mainly made up of black spruce (*Picea mariana (P. Mill) B.S.P.*), dark green in color, or tamarack (*Larix laricina (Du Roi) K. Koch*), which is lighter green in color. This habitat is located on the edge or at the bottom of basins, often without an apparent outlet and showing no sign that the water table is near the surface.
C8	Treed bog	Wetland dominated by evergreen trees (trees over 4 m in height), covering more than 50% of the surface and growing on organic soil. The trees are mainly made up of black spruce (*Picea mariana* (P. Mill) B.S.P.*),* dark green in color. This habitat is located on the edge or at the bottom of basins, often without an apparent outlet and showing no sign that the water table is near the surface
C9	Muskeg	Complex wetland, consisting of a succession of shallow mounds, covered with low vegetation (mainly sedge and moss) and partially shrubby growing on organic soil, separated by ponds filled with stagnant water. The shrubs (trees less than 4 m tall) consist mainly of black spruce (*Picea mariana* (P. Mill) B.S.P.*)* and tamarack (Larix laricina (Du Roi) K. Koch). This habitat is found at the bottom of basins, often without an apparent outlet but showing the presence of shallow water in the often narrow and linear ponds
D1	Bedrock	Habitat consisting mainly of rock, and the surface of which is almost devoid of vegetation (less than 25% of the surface). This habitat can be found both along the coast and on inland writers. Rock deformation structures (fractures, joints, faults) are sometimes visible.
D2	Tundra	Tundra (sometimes referred to as Heath) = habitat covered by low plant formation (between 25 and 50% density), associated with a subarctic plant association (mixture of lichens, Ericaceae, shrubs, grasses, and mosses), growing on mineral soil. This habitat occupies land located on the coast, above the high tide line, or inland, in the northern part of the study area, beyond the forest line

Table 17 (Continued)

Code	Class name	Description
D3	Shrubland	Habitat consisting of relatively dense shrub vegetation (trees less than 4 m high) (more than 50% of the surface), mainly composed of deciduous species. This habitat is primarily installed on slopes made of inorganic soils, rarely saturated with water. It is often the result of plant recolonization occurring after a natural (especially forest fires) or artificial disturbance (forest cuts).
D4	Evergreen forest	Habitat dominated by coniferous trees (more than 50% of the area), mainly white spruce (*Picea glauca* (Moench) Voss) and black spruce (*Picea mariana* (P. Mill) B.S.P.), growing on mineral soils occupying land generally sloping or higher than flood-prone or water-saturated areas.
D5	Deciduous forest	Habitat dominated by deciduous trees (more than 50% of the surface), mainly White Birch (*Betula papyrifera Marsh*), Trembling Aspen (*Populus tremuloides Michx*), and Balsam Poplar (*Populus balsamifera L. ssp. balsamifera*). Conifers, such as white spruce (*Picea glauca* (Moench) Voss) and black spruce (*Picea mariana* (P. Mill) B.S.P.), may be present but do not account for more than 50% of the species present. This entity occupies mineral soils occupying terrain that is generally sloping or higher than the flood-prone or water-saturated areas, mainly in the southern part of the study region. The deciduous forest trees are more easily detected in the images acquired in autumn, while the yellowish leaves of the deciduous trees contrast with the dark green of the conifers.
D6	Burned area	Habitat corresponding to an area with less than 50% vegetation cover, with less than 25% trees, occurring because of a fairly recent fire, less than 50 years old. Snags (dead trees with many branches burned) can appear on the surface of most recent forest fires. This entity is only found on mineral soils, occupying land generally sloping or higher than flood-prone or water-saturated areas
D7	Bareland	Habitat corresponding to an area without vegetation or with dispersed vegetation covering not more than 10% of the area. The substrate is mainly composed of unconsolidated deposits, while rocky outcrops, when present, occupy less than 25% of the surface. This entity is often associated with very recent erosion or deposition phenomena

Table 18 Ground pictures of the land cover classes (Credits: Armand LaRocque 2019).

a) Deep Water  	b) Shallow water 
c) Tidal flat  	d) Cobble beach 
e) Salt marsh  	f) Freshwater marsh 
g) Shrub swamp  	h) Open fen 

Table 18 (Continued)

i) Structured fen 	j) Shrub fen 
k) Open bog 	l) Shrub bog 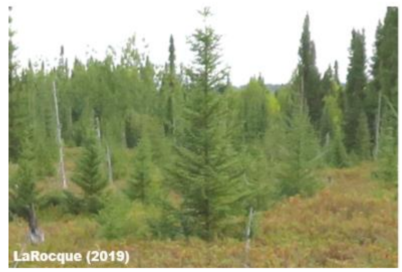
m) Treed bog 	n) Muskeg 
o) Bedrock 	p) Tundra 

Table 18 (Continued)

q) Shrubland 	r) Evergreen forest 
s) Deciduous forest 	t) Burned area 
u) Bareland 	

3.3.3 RESULTS

The classified image was assessed for accuracy using two metrics; the first metric was classification accuracy measured using a subset training of the training data within the RF classifier (referred to as “out-of-bag”, or OOB training data).

Table 19 shows the confusion matrix (and associated classification accuracies) comparing the training areas with the classified image for all the 21 landcover classes when RF was applied to the whole dataset. We achieved an overall accuracy (OA) of 97.88% and a kappa coefficient (Kappa) of 97.69%, indicating an excellent classification accuracy. As shown in this table, the highest User's (UA) and Producer's (PA) accuracies for all upland classes were obtained for the Deep Water (A1) class (100% and 99.9%), respectively. The highest error of commission (EC) was obtained with the Tundra (D2) class (6.0%), mainly because of confusion with other treed classes, such as Bedrock (D1), Treed bog (C8), and Salt marsh (B3). The highest error of omission (EO) occurred with the Deciduous forest (D5) class (7.5%).

The classified image was then compared to an independently created validation dataset, corresponding to 1088 sites different from the training areas. Table 20 shows the confusion matrix (and associated accuracies) obtained by comparing the field sites to the classified. With the validation sites, we obtained an overall accuracy of 82.20%. The highest UA and PA occurred with the Deep Water class (A1) (98.40%) and (95.90), respectively. Treed bog (D3) has the highest EC (59.1%) because of a confusion with the Burned area (D6), Shrub fen (C5), Open fen (C3), Shrub swamp (C2), Freshwater marsh (C1), and Salt marsh (B3) classes. Open fen (C3) class has the highest EO (46.7%), which is due to a confusion with the Open bog (C6), Muskeg (C9), Structured fen (C4), Freshwater marsh (C1), Burned area (D6), Evergreen forest (D4), Shrubland (D3), Salt marsh (B3) and Shallow water (A2). The highest errors found in this validation process is essentially related to the fact that most of the validation sites were identified by photointerpretation and the field survey was never performed because of the health restrictions associated with the fight against the Covid-19.

Table 19 Confusion matrix (in number of pixels) and associated accuracies when Random Forests is applied to all the 2019-2022 dataset.

Class	A1	A2	B1	B2	B3	C1	C2	C3	C4	C5	C6	C7	C8	C9	D1	D2	D3	D4	D5	D6	D7	Total	UA (%)	EO (%)
A1	**1599**	0	0	0	0	0	0	0	0	0	0	0	0	0	0	0	0	0	0	0	0	1599	100.0	0.0
A2	0	**337**	2	0	2	0	0	0	2	0	0	0	0	0	0	0	0	0	0	0	0	343	98.3	1.7
B1	1	0	**736**	0	0	0	0	0	0	0	0	0	0	0	0	0	0	0	0	0	3	740	99.5	0.5
B2	0	0	4	**162**	0	0	0	0	0	0	0	0	0	2	1	1	0	0	0	0	1	171	94.7	5.3
B3	0	1	3	0	**567**	1	0	0	0	0	0	0	0	0	0	3	0	0	0	4	4	583	97.3	2.7
C1	0	0	0	0	1	**209**	1	0	0	0	0	1	0	0	0	2	0	0	0	0	0	214	97.7	2.3
C2	0	1	0	0	0	2	**208**	0	0	7	0	0	0	0	0	0	0	1	0	0	0	219	95.0	5.0
C3	0	3	0	0	2	0	0	**403**	1	3	0	0	0	0	0	1	0	0	0	0	0	413	97.6	2.4
C4	0	1	0	0	0	0	0	0	**193**	0	0	0	0	0	0	0	0	0	0	0	0	194	99.5	0.5
C5	0	0	0	0	1	0	0	2	0	**258**	0	3	0	1	0	0	0	0	0	0	0	265	97.4	2.6
C6	0	0	0	0	1	0	0	0	0	1	**260**	0	0	0	0	1	0	0	0	0	0	263	98.9	1.1
C7	0	0	0	0	0	0	0	0	0	0	2	**382**	0	0	0	0	0	2	0	0	0	386	99.0	1.0
C8	0	0	0	0	0	0	0	0	0	0	0	5	**137**	0	0	3	0	1	0	0	0	146	93.8	6.2
C9	0	4	0	0	1	0	0	1	3	0	1	0	0	**140**	0	0	0	0	0	0	0	150	93.3	6.7
D1	1	0	3	0	0	0	0	3	0	0	0	0	1	0	**282**	12	0	0	0	0	0	302	93.4	6.6
D2	0	0	0	0	3	1	0	2	0	0	0	1	0	1	0	**471**	0	0	0	5	1	485	97.1	2.9
D3	0	0	0	0	3	0	0	0	0	1	1	0	0	0	0	1	**212**	0	0	0	0	218	97.2	2.8
D4	0	0	0	0	0	0	0	0	0	0	0	1	0	0	0	1	0	**201**	0	0	0	203	99.0	1.0
D5	0	2	2	0	1	0	0	3	0	1	0	0	0	0	0	2	0	0	**135**	0	0	146	92.5	7.5
D6	0	1	2	2	1	0	0	0	0	0	0	0	0	0	0	2	1	0	0	**257**	2	268	95.9	4.1
D7	0	0	0	0	0	0	0	0	0	0	0	0	0	0	0	1	0	0	0	0	**243**	244	99.6	0.4
Total	1601	350	752	164	583	213	209	414	199	271	264	393	138	144	283	501	213	205	135	266	254	7552		
PA (%)	99.9	96.3	97.9	98.8	97.3	98.1	99.5	97.3	97.0	95.2	98.5	97.2	99.3	97.2	99.6	94.0	99.5	98.0	100.0	96.6	95.7	OA (%) = 97.88		
EC (%)	0.1	3.7	2.1	1.2	2.7	1.9	0.5	2.7	3.0	4.8	1.5	2.8	0.7	2.8	0.4	6.0	0.5	2.0	0.0	3.4	4.3	Kappa (%) = 97.69		

(*) Bold figures indicated well-classified pixels; EC = Error of commission; EO = Error of omission; PA = Producer's accuracy; UA = User's

Table 20 Confusion matrix (in number of pixels) and associated accuracies from validation sites related to the 2019-2020 classified images.

Class	A1	A2	B1	B2	B3	C1	C2	C3	C4	C5	C6	C7	C8	C9	D1	D2	D3	D4	D5	D6	D7	Total	UA (%)	EO (%)
A1	**183**	0	3	0	0	0	0	0	0	0	0	0	0	0	0	0	0	0	0	0	0	186	98.4	1.6
A2	3	**45**	0	1	0	1	0	1	1	0	0	0	0	0	0	0	0	0	0	3	0	55	81.8	18.2
B1	5	1	**66**	1	1	0	0	1	0	0	0	0	0	0	1	0	0	0	0	1	0	77	85.7	14.3
B2	0	0	1	**59**	0	0	0	0	0	0	0	0	0	0	3	0	0	0	0	0	5	68	86.8	13.2
B3	0	0	0	0	**62**	4	2	1	0	1	1	0	0	0	0	0	4	0	0	3	0	78	79.5	20.5
C1	0	0	0	0	1	**46**	1	0	0	0	1	0	0	0	0	0	1	0	0	0	0	50	92.0	8.0
C2	0	0	0	0	0	3	**18**	1	0	1	0	2	0	0	0	0	2	0	1	0	0	28	64.3	35.7
C3	0	1	0	0	1	1	0	**16**	1	0	3	0	0	3	0	0	1	1	0	2	0	30	53.3	46.7
C4	0	0	0	0	0	0	0	0	**12**	0	1	0	0	0	0	0	0	0	0	0	0	13	92.3	7.7
C5	0	1	0	0	0	2	4	1	1	**28**	1	1	0	0	0	1	2	1	1	0	0	44	63.6	36.4
C6	0	0	0	0	0	0	0	0	0	1	**22**	0	0	0	0	0	0	0	0	0	0	23	95.7	4.3
C7	0	0	0	0	0	0	0	0	0	4	1	**17**	0	0	0	0	0	0	0	0	0	22	77.3	22.7
C8	0	0	0	0	0	0	1	0	0	0	0	0	**15**	0	0	0	0	1	1	0	0	18	83.3	16.7
C9	0	3	0	0	0	2	0	0	1	0	0	0	0	**36**	0	0	0	1	0	0	0	43	83.7	16.3
D1	0	0	2	1	0	0	0	2	0	0	1	0	0	0	**59**	2	0	0	0	4	3	74	79.7	20.3
D2	0	0	0	0	0	0	0	6	0	0	1	1	0	3	1	**57**	0	0	1	1	2	73	78.1	21.9
D3	0	0	0	0	0	0	1	1	0	0	0	0	0	0	0	0	**9**	0	2	2	0	15	60.0	40.0
D4	0	0	0	0	0	0	0	0	0	0	0	1	4	0	0	0	0	**45**	1	0	0	51	88.2	11.8
D5	0	0	0	0	0	0	6	0	0	3	0	2	0	0	0	0	0	4	**24**	0	0	39	61.5	38.5
D6	0	0	0	0	5	2	1	0	0	1	2	0	0	0	0	1	3	1	1	**53**	4	74	71.6	28.4
D7	0	0	1	1	0	0	0	0	0	0	0	0	0	0	3	0	0	0	0	0	**22**	27	81.5	18.5
Total	191	51	73	63	70	61	34	30	16	39	34	24	19	42	67	61	22	54	32	69	36	1088		
PA (%)	95.8	88.2	90.4	93.7	88.6	75.4	52.9	53.3	75.0	71.8	64.7	70.8	78.9	85.7	88.1	93.4	40.9	83.3	75.0	76.8	61.1	OA (%) = 82.2		
EC (%)	4.2	11.8	9.6	6.3	11.4	24.6	47.1	46.7	25.0	28.2	35.3	29.2	21.1	14.3	11.9	6.6	59.1	16.7	25.0	23.2	38.9	Kappa (%) = 80.8		

(*) Bold figures indicated well-classified pixels; EC = Error of commission; EO = Error of omission; PA = Producer's accuracy; UA = User's accuracy

3.4 OBJECTIVE 4

Evaluating the capability of Landsat-5 TM, Landsat-8 OLI, and Sentinel-1 SAR imagery to map the changes in the coastal habitats along the coast of Eeyou Itschee between 1984-1985 and 2019-2020

3.4.1 INTRODUCTION

In Eeyou Istchee, the Cree inhabitants who are living there for time immemorial consistently rely on geese hunting as a form of subsistence. The Cree Land Users have observed a decline in geese abundance, explained by a steady decline in eelgrass coverage along the coast in the late 1980s and then a drastic decline in 1997-1998. In addition to a decrease in the extension of eelgrass beds, other factors of the Eeyou Istchee's environment could affect the abundance of geese. Among these factors are the change in the natural habitat of the geese. The purpose of this study is to map the land cover of the eastern coast of Eeyou Itschee to characterize the natural habitat of geese.

The fourth objective for the coastal mapping project aims to assess the use of Landsat and SAR imagery to map the change in geese' habitat in Eeyou Istchee between 1984-1985 and 2019-2020. This study only considers the terrestrial part of the geese' habitat, given that there is a complementary study (Clyne 2022) that addresses the change in eelgrass beds in Eeyou Istchee over the same period. A. LaRocque already established a geese habitat map for 2019-2022 using Landsat-8 OLI and Sentinel-1 C-band imagery (Sorais et al. 2022; in revision) but it is necessary to have a similar map done for the 1980s period, based on the earliest available Landsat-5 TM imagery. This study is the subject of a Master report (Olatunji 2022).

3.4.2 METHOD

The study area was the same as for Objective 3 and extent along the whole eastern coast of Eeyou Itschee (Figure 40). The study used freely available imagery acquired by the Landsat-5 Thematic Mapper (TM) in 1984 and 1985 and the Landsat 8 Operational Land Imager (OLI) in 2019-2022. These images were obtained from the United States Geological Survey's (USGS) Earth Explorer website. The images were acquired in three seasons (Spring, Summer, and Fall) to take into consideration seasonal changes such as leaf on and leaf off, varying water levels, soil moisture, and the state of the vegetation. A total of nine cloud-free images were acquired for each satellite, three for each season. We produced one mosaic for each season to cover the entire study area. A flowchart describing how the 1984-1985 data were processed is given in Figure 43, while the flowchart related to the processing of the 2019-2022 data is shown in Figure 44.

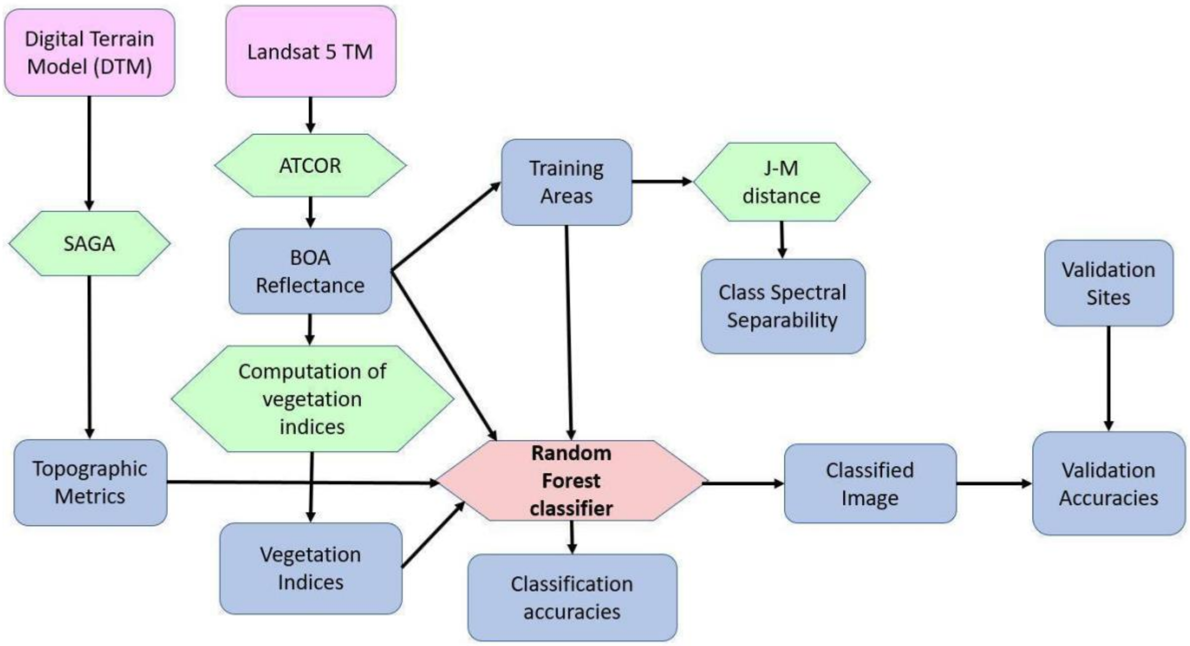

Figure 45 Flowchart presenting the methodology for processing the Landsat-5 TM and DTM data to produce the 1984-1985 classified image.

Landsat imagery was atmospherically corrected using the ATCOR program with PCI Geomatica Banff (PCI Geomatics, ON, Canada). This correction removes some atmospheric interference and converts the image top of atmosphere (TOA) reflectance values into ground reflectance values. In addition, the 2019-2022 optical imagery was reprojected to a 30-m pixel resolution, using the Pansharpening module of PCI Geomatica Banff. The imagery for each satellite and each season were then used to compute vegetation indices to bolster the potential separability between the classes (Table 15).

The SAR imagery includes Sentinel-1 C-band dual-polarized (HH and HV or VV and VH) images downloaded from the European Space Agency's Sentinels Scientific Data Hub website (https://scihub.copernicus.eu/) for the three seasons (Spring, Summer, and Fall). The SAR imagery was acquired during two different passes: ascending orbit with a northeast look direction and descending orbit with a northwest look direction. Pre-classification processing of Sentinel-1 data included updating orbit metadata, noise removal, and terrain correction and was performed with the SNAP toolbox. The depth of penetration of SAR microwaves into vegetation canopy depends on the radar wavelength. For C-band, this wavelength is approximately 5.55 cm long. In a forested setting, Solberg et al. (2007) showed that C band can penetrate through the canopy to the ground surface, before being reflected towards the SAR sensor. C band imagery over forests was also shown elsewhere to be able to map flooded grounds or soils saturated with water under a dense temperate forest (LaRocque et al. 2020).

This study also used a digital terrain model (DTM) to characterize the local topography. This DTM was extracted from the Shuttle Radar Topographic Mission (SRTM) data from the United States Geological Survey (https://earthexplorer.usgs.gov/). The SRTM-DTM was used for computing the following four topographic metrics: (1) the slope (SLP), (2) the Compound Topographic Index (CTI), (3) the Curvature (CRV), and (4) the Topographic Position Index (TPI). SLP shows where the surface water runoff is slower (or faster) and was derived using the maximum rate of change from one cell to its eight neighbours to show the steepest downhill descent. CTI shows wetter areas using slope combined with where flow is predicted to accumulate. CRV shows deceleration (or acceleration) of water runoff. TPI gives the relative position in the landscape (hilltop to valley bottom) for each pixel. All these topographic metrics are produced with the System for Automated Geoscientific Analyses (SAGA) GIS software.

All the data related to each time period were then inputted into a supervised classifier that requires delineation of training areas for each class. We considered in the classification the habitat classes that are described in Table 16. Ground pictures of each class are given in Table 17. The habitat classes were determined from field surveys and photo interpretation of satellite images having a high spatial resolution between 32 and 65 cm.

The supervised image classification was performed with Random Forests, a non-parametric decision tree type supervised classifier. We used the package randomForest in R software to classify habitats with 555 randomly distributed training polygons. The classified image was transformed into a map using the Banff version of PCI Geomatica and ArcGIS Pro (ESRI, CA, USA). The resulting habitat map for each time period has a 30-m resolution.

3.4.3 RESULTS

Each classified image was assessed for accuracy using two metrics; the first metric was classification accuracy measured using a subset training of the training data within the RF classifier (referred to as “out-of-bag”, or OOB training data).

Table 21 shows the confusion matrix (and associated classification accuracies) comparing the training areas with the classified image for all the landcover classes when RF was applied to the whole 1984-1985 dataset. We achieved an overall accuracy (OA) of 93.69% and a kappa coefficient (Kappa) of 93.25%, both indicating an excellent classification accuracy. The highest User's (UA) and Producer's (PA) accuracies for all upland classes were obtained for the Deep Water (A1) class (100% and 99.58%), respectively. The highest error of commission (EC) was obtained with the Cobble beach (B2) class (13.27%), mainly because of confusion with other unvegetated soil types, such as Bedrock (D1), Bareland (D7), and Tidal flat (B1). The highest error of omission (EO) occurred with the Shrub swamp (C2) class (16.67%).

Table 21 Confusion matrix (in number of pixels) and associated accuracies when Random Forests is applied to all the 1984-1985 dataset.

Class	A1	A2	B1	B2	B3	C1	C2	C3	C4	C5	C6	C7	C8	C9	D1	D2	D3	D4	D5	D6	D7	Total	UA (%)	EO (%)
A1	**708**	0	0	0	0	0	0	0	0	0	0	0	0	0	0	0	0	0	0	0	0	708	100.00	0.00
A2	3	**173**	1	1	1	1	0	1	5	0	0	0	0	7	0	1	2	2	0	0	0	198	87.37	12.63
B1	0	2	**365**	5	1	0	0	0	0	0	0	0	0	0	1	0	0	0	0	0	4	378	96.56	3.44
B2	0	1	5	**170**	0	0	0	0	0	0	0	0	0	0	0	0	0	0	0	0	4	180	94.44	5.56
B3	0	0	1	1	**266**	0	0	3	0	0	0	0	0	0	1	0	4	0	0	0	3	279	95.34	4.66
C1	0	0	4	0	3	**152**	2	1	0	2	0	0	0	0	0	2	4	0	1	0	0	171	88.89	11.11
C2	0	2	0	0	0	0	**105**	2	1	2	0	5	3	0	0	0	1	0	5	0	0	126	83.33	16.67
C3	0	1	0	0	7	0	1	**196**	2	3	6	0	0	1	0	7	0	1	0	0	0	225	87.11	12.89
C4	0	1	0	0	0	0	0	1	**105**	0	0	0	0	7	0	0	0	3	0	0	0	117	89.74	10.26
C5	0	2	0	0	0	5	0	1	0	**163**	0	2	3	0	0	2	0	2	0	0	0	180	90.56	9.44
C6	0	0	0	0	0	0	0	0	0	0	**191**	3	0	0	0	4	0	0	0	0	0	198	96.46	3.54
C7	0	0	0	0	0	0	0	0	0	0	0	**214**	0	1	0	0	0	1	0	0	0	216	99.07	0.93
C8	0	0	0	0	0	0	0	0	0	0	0	2	**113**	0	0	0	0	2	0	0	0	117	96.58	3.42
C9	0	6	0	0	0	0	0	2	0	0	1	0	0	**124**	0	2	0	0	0	0	0	135	91.85	8.15
D1	0	0	4	11	1	0	0	1	0	0	0	0	0	0	**140**	5	0	0	0	0	0	162	86.42	13.58
D2	0	1	0	3	3	0	0	1	0	0	2	1	0	0	4	**435**	2	1	0	4	2	459	94.77	5.23
D3	0	0	0	0	6	0	2	0	0	0	1	1	0	0	0	12	**166**	1	0	0	0	189	87.83	12.17
D4	0	0	0	0	0	0	0	1	0	0	0	3	1	0	0	0	0	**175**	0	0	0	180	97.22	2.78
D5	0	0	0	0	0	1	6	0	0	1	1	0	2	0	0	0	0	0	**133**	0	0	144	92.36	7.64
D6	0	0	0	0	0	0	0	1	0	0	0	0	0	0	0	10	0	0	0	**123**	1	135	91.11	8.89
D7	0	0	0	5	5	0	0	0	0	0	0	0	0	0	1	4	0	0	0	0	**165**	180	91.67	8.33
Total	711	189	380	196	293	159	116	211	113	171	202	231	122	140	147	484	179	188	139	127	179	4677		
PA (%)	99.58	91.53	96.05	86.73	90.78	95.60	90.52	92.89	92.92	95.32	94.55	92.64	92.62	88.57	95.24	89.88	92.74	93.09	95.68	96.85	92.18	OA (%) = 93.69		
EC (%)	0.42	8.47	3.95	13.27	9.22	4.40	9.48	7.11	7.08	4.68	5.45	7.36	7.38	11.43	4.76	10.12	7.26	6.91	4.32	3.15	7.82	Kappa (%) = 93.25		

(*) Bold figures indicated well-classified pixels; EC = Error of commission; EO = Error of omission; PA = Producer's accuracy; UA = User's

The classified image was then compared to an independently created validation dataset, corresponding to 544 sites different from the training areas. Table 22 shows the confusion matrix (and associated accuracies) obtained by comparing the field sites to the 1984-1985 classified image. With the validation sites, we obtained an overall accuracy of 61.20%. The highest UA and PA occurred with the Deep water class (A1) (62.13%) and (95.90), respectively. Open fen (C3) has the highest error of commission (100.00%) because of a confusion with Deep water (A1), Salt marsh (B3), Shrub fen (C5), Open bog (C6), Shrub bog (C7), Treed bog (C8), Muskeg (C9), Tundra (D2), Evergreen forest (D4) and Deciduous forest (D5). The Open fen (C3) class has the highest EO of 100.00%, which is due to a confusion with Shallow water (A2), Salt marsh (B3), Freshwater marsh (C1), Shrub swamp (C2), String fen (C4), Shrub fen (C5), Open bog (C6), Shrub bog (C7), and Muskeg (C9). Two factors explain the highest errors found in this validation process: 1) no SAR image was available for this period, and 2) all the validation sites were identified by photointerpretation and no field survey was performed.

Figure 45 presents a comparison between the two time periods for each landcover class. The two water classes (A1 and A2) experienced a decline over the study period with the Deep water class showing a greater percentage decline than the Shallow water class. Shrub fen and Muskeg (C5 and C9) wetland classes experienced the most increase over the study period, while Tidal flat and Structured fen (B1 and C4) wetland classes declined the most over the study period. Burned area and Deciduous Forest (D6 & D5) upland classes experienced the most increase over the study period, while Bareland and Tundra (D7 & D2) upland classes declined the most over the study period. Some interpretations could be used to explain the land cover change between the periods of 1984-1985 and 2019-2020.

1) The decline in the area occupied by Deep water (A1), Shallow water (A2), and Tidal flat (B1) could be linked to the isostatic rebound, but also to the difference in the tide height. The isostatic rebound could also explain the expansion of the Salt marsh (B3) and the Freshwater marsh (C1).

2) The increase in the extent of treed surfaces, particularly the Deciduous forest (D5), the Shrub fen (C5), the Shrub swamp (C2) and the Evergreen forest (D4), as well as the decline of the Bareland (D7), Shrubland (D3), String fen (C4), Open fen (C3) and Tundra (D2) could be related to the global warming, favoring an migration of the tree line towards the north.

3) There are more Burned areas (D6) in 2020 than in 1985 because of a greater number of forest fires and drier weather due to global warming.

Table 22 Confusion matrix (in number of pixels) and associated accuracies from validation sites related to the 1984-1985 classified images.

Class	A1	A2	B1	B2	B3	C1	C2	C3	C4	C5	C6	C7	C8	C9	D1	D2	D3	D4	D5	D6	D7	Total	UA (%)	EO (%)
A1	**187**	6	6	1	0	12	5	6	4	4	11	5	3	10	13	14	0	6	6	1	1	301	62.13	37.87
A2	3	**28**	1	4	2	3	1	0	3	0	0	0	0	3	0	0	0	1	1	0	0	50	56.00	44.00
B1	4	3	**59**	13	5	2	1	0	0	0	0	0	0	0	2	0	0	0	0	4	1	94	62.77	37.23
B2	0	0	4	**37**	1	0	0	0	0	0	0	0	0	0	10	0	0	0	0	2	3	57	64.91	35.09
B3	0	0	0	1	**44**	8	1	2	0	0	2	0	0	0	0	3	3	0	0	6	0	70	62.86	37.14
C1	0	1	1	0	1	**14**	4	0	0	0	0	0	0	0	0	0	0	0	1	0	0	22	63.64	36.36
C2	0	1	0	0	0	4	**10**	0	0	0	0	0	0	0	0	0	1	0	3	1	0	20	50.00	50.00
C3	0	1	0	0	1	2	1	**0**	3	1	2	1	0	1	0	0	0	0	0	0	0	13	0.00	100.00
C4	0	4	0	0	0	1	1	0	**4**	0	1	1	0	7	0	0	0	0	0	0	0	19	21.05	78.95
C5	0	1	0	0	0	9	5	5	0	**19**	1	0	2	0	0	0	2	0	1	0	0	45	42.22	57.78
C6	0	0	0	0	0	0	0	2	1	0	**3**	2	0	2	0	3	0	0	1	2	0	16	18.75	81.25
C7	0	1	0	0	0	1	0	2	2	4	1	**11**	0	2	0	0	1	1	2	0	0	28	39.29	60.71
C8	0	0	0	0	0	0	3	1	0	0	1	0	**7**	0	0	0	0	4	1	0	0	17	41.18	58.82
C9	0	3	0	0	0	0	0	1	1	0	0	0	0	**5**	0	0	0	1	0	0	0	11	45.45	54.55
D1	0	0	0	4	0	2	0	0	0	0	0	0	0	0	**18**	5	0	0	0	1	3	33	54.55	45.45
D2	0	0	0	0	8	2	0	2	0	3	7	2	1	3	7	**22**	5	2	3	33	10	110	20.00	80.00
D3	0	0	0	0	2	1	3	0	0	0	0	1	0	0	0	1	**10**	1	0	5	0	24	41.67	58.33
D4	1	0	0	0	0	1	1	2	0	0	0	1	7	0	0	0	3	**33**	1	4	0	54	61.11	38.89
D5	0	3	0	0	0	2	8	3	1	1	1	0	0	1	0	0	0	1	**14**	0	0	35	40.00	60.00
D6	0	0	0	0	0	0	0	0	0	0	0	0	0	0	15	5	0	0	0	**0**	3	23	0.00	100.00
D7	0	0	2	0	3	2	0	0	0	0	0	0	0	0	2	9	0	0	0	9	**19**	46	41.30	58.70
Total	195	52	73	60	67	66	44	26	19	32	30	24	20	34	67	62	25	50	34	68	40	544		
PA (%)	95.90	53.85	80.82	61.67	65.67	21.21	22.73	0.00	21.05	59.38	10.00	45.83	35.00	14.71	26.87	35.48	40.00	66.00	41.18	0.00	47.50	OA (%) = 61.20 Kappa (%) = 57.67		
EC (%)	4.10	46.15	19.18	38.33	34.33	78.79	77.27	100.00	78.95	40.62	90.00	54.17	65.00	85.29	73.13	64.52	60.00	34.00	58.82	100.00	52.50			

(*) Bold figures indicated well-classified pixels; EC = Error of commission; EO = Error of omission; PA = Producer's accuracy; UA = User's accuracy

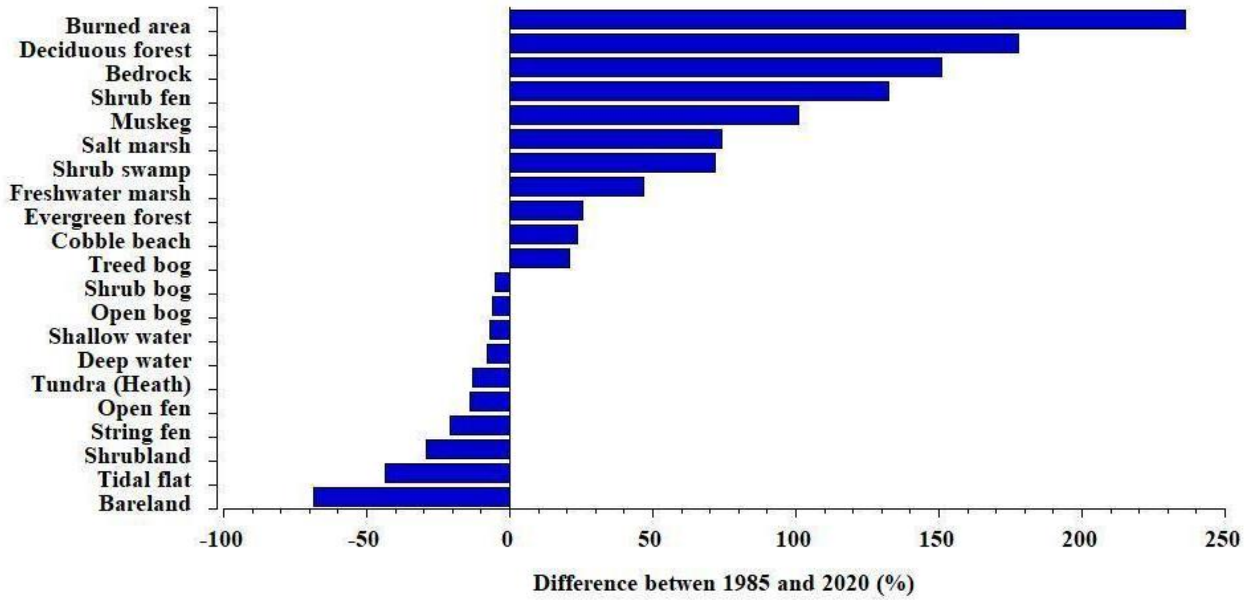

Figure 46 Land cover changes over the study area between 1985 and 2020.

3.4.3 CONCLUSIONS

In this study, we used Landsat and Sentinel images acquired between 1984-1985 and 2019-2020 to ascertain if there were changes in the terrestrial part of Canada and brant geese habitats in Eeyou Itschee (James Bay) between both periods. The study is complementary to Clyne's (2022) thesis which deals with the eelgrass bed changes over the same period. Changes in the terrestrial part of the habitat were assessed by comparing the 1984-1985 and 2019-2020 land cover maps that were established by applying the RF classifier to a combination of Landsat, Sentinel-1, and DTM data. Classification overall accuracies of 93.7% and 97.9% were achieved for the 1984-1985 and 2019 images, respectively.

Our study was able to show that, there have been changes in the terrestrial part of the Canada and brant geese habitats. The most significant changes were an increase in the burned area (+236.24%), in the deciduous forests (+177.91%), and the shrub fen (+132.39%). We also observed a decrease in the bareland area (-68.6%), in the tidal flat area (-43.52%), and in the shrubland area (-29.19%). The exact causes of these changes were not analyzed in this study, so further work is needed to determine if the changes were caused by natural (climate change, wildfire occurrences) or anthropogenic phenomena (damming, deforestation). There is also a need to infer whether these changes have an impact on the geese population.

3.4 PEER-REVIEWED RESEARCH PAPERS

PAPER 1:

Title	Use of Landsat-8 OLI imagery and local indigenous knowledge for eelgrass mapping in Eeyou Istchee
Authors	Kevin Clyne, Brigitte Leblon, Armand LaRocque, Maycira Costa, Mélanie Leblanc, Ernie Rabbitskin, and Marc Dunn.
Data	Imagery = Landsat-8 OLI images (2019/08/22; 2019/09/16) Field data = Coastal Habitat Comprehensive Research Program (CHCRP) dataset, Hydro-Québec dataset
Status	Reviewed by the Steering Committee and published in ISPRS Annals of the Photogrammetry, Remote Sensing and Spatial Information Sciences, 3-2021, 15–22. https://doi.org/10.5194/isprs-annals-V-3-2021-15-2021
Abstract	The eastern coastline of James Bay (Eeyou Istchee) is known to be home to beds of subarctic eelgrass (Zostera marina L.). These eelgrass beds provide valuable habitat and food source for coastal and marine animals and contribute valuable ecosystem services such as sediment stabilization all along the coast. Despite reports from Cree communities that eelgrass bed health has declined, limited research has been performed to assess and map the spatial distribution of eelgrass within the bay. This study aims to address that issue by evaluating the capability of Landsat-8 Operational Land Imager (OLI) imagery to establish a baseline map of eelgrass distribution in 2019 in the relatively turbid waters of Eeyou Istchee. Three images acquired in September 2019 were merged and classified using Random Forests into the following classes: Eelgrass, Turbid Water, Highly Turbid Water, and Optically Deep Water. The resulting classified image was validated against 108 ground truth data that were obtained from both the eelgrass health and Hydro-Quebec research team. The resulting overall accuracy was 78.7%, indicating the potential of the Random Forests classifier to estimate baseline eelgrass coverage in James Bay using Landsat-8 imagery. This project is part of a Cree driven project, the Coastal Habitat Comprehensive Research Program (CHCRP). The CHCRP aims to combine Cree's traditional knowledge with Western science to better understand environmental changes in the coastal ecosystems and ecosystem services of eastern James Bay. The study is funded by a MITACS grant sponsored by Niskamoon Corporation, an indigenous non-profit organization.

PAPER 2:

Title	Migration patterns and habitat use by molt migrant temperate-breeding Canada geese in James Bay, Canada
Authors	Manon Sorais, Martin Patenaude-Monette, Christopher Sharp, Ryan Askren, Armand LaRocque, Brigitte Leblon, and Jean-François Giroux.
Data	Imagery = Landsat-8 OLI and Sentinel-1 images Ancilary data = SRTM- DTM (Digital terrain model) Field data = Armand LaRocque
Status	Reviewed by the Steering Committee and published in Wildlife Biology, e1062 https://onlinelibrary.wiley.com/doi/full/10.1002/wlb3.01062
Abstract	The number of temperate-breeding Canada geese has greatly increased in the Atlantic and Mississippi Flyways since the 1980s. Consequently, the number of yearlings, subadults, and failed breeders that undertake a pre-molt migration to northern latitudes has also increased, potentially providing additional hunting opportunities for Cree hunters living near James Bay, Canada. Our objective was to describe the movement patterns of molt migrant Canada geese and their habitat use along the east coast of James Bay. We tracked nine geese fitted with GSM-GPS devices during 11 northward and eight southward migrations. Geese arrived in the James Bay region during the first week of June when moving north and during the first week of September when returning south. The time spent by molt migrants in eastern James Bay was relatively short, averaging 2.8 ± 0.6 (mean ± SEM) and 3.8 ± 1.8 days in spring and fall, respectively. In spring, geese used an average of 3.2 ± 0.6 staging sites in areas dominated by tidal flats and salt marshes. In fall, geese used 2.0 ± 0.5 staging sites characterized by inland freshwater wetlands, peatlands, and tidal flats. Shallow and deep water habitats were also used as resting sites during the pre- and post-molt migrations. Molt migrant temperate-breeding geese can increase harvest opportunities and represent supplement wildlife food for Cree communities.

PAPER 3:

Title	Distribution of Canada geese during their spring and fall migrations along the east coast of James Bay
Authors	Manon Sorais, Martin Patenaude-Monette, Armand LaRocque, Brigitte Leblon, and Jean-François Giroux.
Data	Imagery = Landsat-8 OLI and Sentinel-1 images Ancilary data = SRTM- DTM (Digital terrain model) Field data = Armand LaRocque
Status	Reviewed by Steering Committee and Submitted to Arctic Science
Abstract	Canada geese (*Branta canadensis*) are the main waterfowl species harvested by Cree hunters in James Bay. However, many environmental changes that can affect the number, distribution, and migration patterns of Canada geese have occurred along the east coast of James Bay in the last 50 years. Aerial surveys had been conducted in the early 1970s before the development of hydro-electric projects in northern Quebec and in the early 1990s after the completion of a portion of these projects. The objective of our study was to determine the current distribution of Canada geese along the east coast of James Bay and to determine the habitats that explained the density of geese with an emphasis on eelgrass (*Zostera marina*) beds. Two helicopter surveys were conducted during each of the spring and fall seasons of 2018 between Waskaganish and Chisasibi. The main concentrations of geese were observed between Eastmain and Wemindji during both seasons. In spring, goose density increased with the percentage of salt marshes whereas in fall, the highest densities were found in sections with the greatest proportion of tidal flats and turbid water. Eelgrass beds did not explain Canada goose distribution contrary to what was expected based on the 1970s surveys. However, it agrees with the current Traditional Ecological Knowledge that shows that the eelgrass habitat has become unsuitable for Canada geese. It is suspected that the decline of this submerged vegetation and the increase of molt-migrant temperate-breeding Canada geese (*B. c. maxima*) have resulted in the general expansion of habitat use by Canada goose flocks along the east coast of James Bay.

PAPER 4:

Title	Temporal Monitoring of *Zostera marina* Along the Eastern Coast of James Bay Utilizing Multispectral Landsat Imagery and Random Forests Classifier
Authors	Kevin Clyne, Armand LaRocque, Brigitte Leblon, Maycira Costa

Data	Imagery = Landsat-8 OLI and Landsat-5 TM Hydro-Québec aerial photographs Hydro-Québec maps Field data = Eelgrass team
Status	Submitted to the Steering Committee in February 2023 and will be submitted to Remote Sensing
Abstract	The eastern coastline of James Bay is known to be home to sizeable beds of eelgrass (*Zostera marina* L.), which thrive in the bay's shallow, subarctic waters. The region was subjected to substantial hydroelectric dams, large fires, and other human activities in the past half-century. To assess the impact of these factors on eelgrass beds, a historical reconstruction of eelgrass bed distribution was performed from images acquired by Landsat-5 Multispectral Scanner (MSS) in 1988, 1991, and 1996, and images of the Landsat-8 Operational Land Imager (OLI) in 2019. All the images were classified using the Random Forests classifier and assessed for accuracy each year on a bay-wide scale using an independent field validation dataset. The validation data were extracted from eelgrass bed maps that were established from aerial photos and field surveys in 1986-1987, 1991-1992, and 1995-1996 and from a field survey in 2019. The overall validation accuracy of the classified images (between 72% and 85%) showed good agreement with the other datasets for most locations, making it possible to use satellite imagery for detecting past changes to eelgrass distribution within a bay. The classified images of 1988 and 1996 were also compared to aerial photos taken at close years at ten sites to determine their capability to assess the shape and presence of small eelgrass beds. Such a comparison revealed that the classified images accurately portrayed eelgrass distribution even at finer scales.

THESE:

Title	Use of Satellite Imagery for Monitoring Canadian and Brant Geese Habitat Changes in Eeyou Itschee (James Bay, Québec)
Authors	Abraham Olatunji
Data	Imagery = Landsat-5 TM, Landsat-8 OLI and Sentinel-1 images Ancilary data = SRTM- DTM (Digital terrain model) Field data = Armand LaRocque
Status	Defended
Reference	Olatunji, A. 2022. Use of Satellite Imagery for Monitoring Canada and Brant Geese Habitat Changes in Eeyou Itschee (James Bay, Québec), Master of

	Forestry Report, Faculty of Forestry and Environmental Management, University of New Brunswick, June 2022, 97 pages
Abstract	This thesis aims to assess the use of Landsat imagery to map the change in geese' habitat in Eeyou Istchee between 1984-1985 and 2019-2020. This thesis will only consider the terrestrial part of the geese' habitat, given that there is a complementary thesis (Clyne 2022) that addresses the change in eelgrass beds in Eeyou Istchee over the same period of time. Dr. LaRocque has established a geese habitat map for 2019 using Landsat-8 OLI and Sentinel-1 imagery (Sorais et al. 2022), but it is needed to have a similar map done for the 1980s time period before the river damming to assess whether the river damming has influenced the geese habitat in Eastern James Bay. This study is part of the James Bay Coastal Habitat Comprehensive Research Program (JBCHCRP), a Cree-driven project aiming to combine Cree's traditional knowledge with Western science to understand better environmental changes in the coastal ecosystems and ecosystem services of Eeyou Istchee.

THESE:

Title	Temporal Monitoring of *Zostera marina* Along the Eastern Coast of James Bay Utilizing Multispectral Landsat Imagery and Random Forests Classifier
Authors	Kevin Clyne
Data	Imagery = Landsat-5 TM, Landsat-8 OLI Ancilary data = SRTM- DTM (Digital terrain model)
Status	Defended
Reference	Clyne, K. 2022. Temporal Monitoring of Zostera marina Along the Eastern Coast of James Bay Utilizing Multispectral Landsat Imagery and Random Forests Classifier. M. Sc. Environmental Management, University of New Brunswick, Forestry and Environmental Management. October 2022, 86 pages
Abstract	Along the eastern coastline of James Bay, also known to the local Cree as Eeyou Istchee, exist large subtidal eelgrass meadows. This study assessed the feasibility of evaluating the distribution of eelgrass beds along the entire eastern coastline of James Bay using imagery from the Landsat-8 Operational Land Imager and supervised classification using random forests machine learning algorithm. The methodology was then applied to historical imagery from the Landsat archive (Landsat-5 Multispectral

Instrument), and image classifications were evaluated for accuracy using a randomly generated subset of digitized eelgrass distribution maps from Hydro-Quebec. Our classified images from 1988, 1991, 1996, and 2019 achieved overall accuracies ranging from 74.6 – 84.6% when evaluated using our ground-truth datasets. Our supervised classification approach showed the ability to detect eelgrass along the entire coast where turbid water was not present. The total area classified as eelgrass appeared to decrease over the study period (1988 – 2019).

SECTION 4 COMMUNITY COMMUNICATIONS AND ENGAGEMENT

In section 4, we described the outreach activities, meetings and consultations organized in different communities from 2019 to 2022.

In 2019, we organized several informal meetings to get feedback from land users in Chisasibi, Wemindji, Eastmain and Waskaganish. In June, Mary O'Connor, Melanie Leblanc and Zou Zou Kuzyc met land users to plan fieldwork activities in Chisasibi. From July to August, Mary O'Connor, Fanny Noisette, Kaleigh Davis and Melanie Leblanc organized various outreach activities in Chisasibi, Wemindji, and Eastmain to provide information about the project and get feedback from land users.

Figure 47 Mary O'Connor, Fanny Noisette and Julián Idrobo at workshop, July 2019, Wemindji. Photo credit: Geraldine Mark

Figure 48 First day of fieldwork July 2019, Wemindji. Photo credit: Geraldine Mark.

In September 2019, Melanie Leblanc, Manuelle Landry-Cuerrier (McGill) and Julián Idrobo conducted Canada Geese surveys in two traplines (CH33 and CH34).

Figure 49 Canada Geese surveys near John Sam's camp, CH33 trapline, Chisasibi, September 2019. Photo credit: Melanie Leblanc and Julián Idrobo

In November 2019, Marie-Hélène Carignan, Fanny Noisette, Brigitte Leblon and Armand LaRocque prepared and presented youth outreach activities at Chisasibi's James Bay Eeyou School. Melanie Leblanc participated in youth outreach activities in Waskaganish.

Figure 50 Marie-Hélène Carignan, youth outreach activity, Waskaganish, November 2019.

In 2020, fieldwork activities for the eelgrass team for the summer were suspended due to the COVID-19 pandemic. To maintain community engagement, Fanny Noisette and Mélanie Leblanc prepared an eelgrass sampling protocol for Ernie Rabbitskin and Laura-Lee Sam (protocol included in progress report of 2020).

Figure 51 Cree team monitoring eelgrass during the summer of 2020. Photo credit: Laura-Lee Sam

During the summer of 2020, Mélanie Leblanc and Kaleigh Davis prepared a research pamphlet and posters. The pamphlet and poster are available on the CHCRP website. To keep communities informed, Mélanie Leblanc created a Facebook Page for the CHCRP project (https://www.facebook.com/EeyouCoastalHabitats). The eelgrass team used the CHCRP's Facebook page to share information about the project, including the research findings from the other teams, information about up-coming fieldwork and research progress. Mélanie Leblanc also created content for the CHCRP webpage.

During fieldwork in 2021, Kaleigh Davis, Fanny Noisette and Mélanie Leblanc worked at the Niskamoon office to facilitate conversations with the land users and participated in formal and informal meetings.

Figure 52 Kaleigh Davis, Fanny Noisette, Caroline Fink-Mercier and Mélanie Leblanc installed a stall outside the Niskamoon office and provided information about the project during the Chisasibi Pow Wow.

April 2022, Zou Zou Kuzyk, Fanny Noisette, Mary O'Connor, Melanie Leblanc and Caroline Fink-Mercier attended a workshop in Chisasibi to discuss early CHCRP results with land users.

Figure 53 Mary O’Connor presenting preliminary results to land users in Chisasibi, April 2022.

In preparation of the symposium, a writing retreat was held in Montréal from June 8 and 9 to enhance communication among the research teams.

In August of 2022, Mary O’Connor, Zou Zou Kuzyk and Manon Sorais presented preliminary results in Chisasibi, Wemindji, Eastmain - Kaleigh Davis and Melanie Leblanc attended the meetings.

Figure 51 Manon Sorais presenting preliminary results to land users in Wemindji, August 2022.

In September of 2022, the eelgrass team (Mary O'Connor, Fanny Noisette, Brigitte Leblon, Armand LaRocque, Melanie Leblanc, Kaleigh Davis) attended the CHCRP Symposium in Chisasibi September 2022. Mary O'Connor presented the major findings on behalf of the team. Mélanie Leblanc, Fanny Noisette, Mary O'Connor, Zou Zou Kuzyk and Caroline Fink-Mercier prepared several posters for the symposium.

Figure 54 Workshop at CHCRP symposium, Chisasibi, September 2022.

In December of 2022, Melanie Leblanc, along with Ernie Rabbitskin, Robbie Tapiatic and ZouZou Kuzyk, presented the project at the Hudson Bay Summit in Montréal. Mélanie, Zou Zou and Ernie also presented several project posters during the summit.

On March 8th and 9th of 2023, Zou Zou Kuzyk, Mary O'Connor, Fanny Noisette and Melanie Leblanc attended a steering committee meeting to discuss the first draft of the integration report and attended a workshop to discuss recommendations for future coastal monitoring efforts.

Finally, from 2019 to 2023, Mary O’Connor, Brigitte Leblon, Armand LaRocque, Fanny Noisette and the associated graduate students presented their research at various national and international conferences (ArcticNet 2019, ArcticNet 2022, ISPRS 2021, CEES, to name a few conferences). Information presented at these conferences was reviewed by the Steering Committee.

References

Bertelli and Unsworth. 2018. Light stress responses by the eelgrass, *Zostera marina* (L) Front. Environ. Sci. 6, 39.

Bulthuis 1987. Effects of temperature on photosynthesis and growth of seagrasses. Aquatic Botany, 27, 27-40.

Clyne et al. 2021. Use of LANDSAT-8 OLI Imagery and Local Indigenous Knowledge for Eelgrass Mapping in Eeyou Istchee. *ISPRS Annals of Photogrammetry, Remote Sensing and Spatial Information Sciences* 53: 15-22. doi:10.5194/isprs-annals-V-3-2021-15-2021.

Clyne. 2022. Temporal Monitoring of Zostera marina Along the Eastern Coast of James Bay Utilizing Multispectral Landsat Imagery and Random Forests Classifier. M. Sc. Environmental Management, University of New Brunswick, Forestry and Environmental Management. October 2022, 86 pages

Clyne et al. in revision Temporal Monitoring of Zostera marina Along the Eastern Coast of James Bay Utilizing Multispectral Landsat Imagery and Random Forests Classifier. Remote Sensing (*submitted to the Steering committee for late submission to Remote Sensing*)

Curtis, S.C. 1974-1975. Distribution of eelgrass: east coast, James Bay. Map at a scale of 1:125, 000. Canadian Wildlife Service, Ottawa, ON.

DFO. 2009. Does eelgrass (*Zostera marina*) meet the criteria as an ecologically significant species? DFO Can. Sci. Advis. Sci. Advis. Rep. Rep.2009/018.

Duarte et al. 1990. Assessing the capacity of seagrass meadows for carbon burial: current limitation and future strategies. Ocean and Coastal Management, 83, 32-38.

Duarte et al. 2005. Major role of marine vegetation on the oceanic carbon cycle. Biogeosciences, 2, 1-8.

Duffy 2006. Biodiversity and the functioning of seagrass ecosystems. Marine Ecology Progress Series, 311, 233-250.

Duffy et al. 2015. Biodiversity mediates top-down control in eelgrass ecosystems: a global comparative-experimental approach. Ecology Letter 18, 696-705.

Fonseca et al. 1983. The role of current velocity in structuring eelgrass (*Zostera marina* L.) meadows. Estuarine, Coastal and Shelf Science, 17, 367-380.

Groupe Environnement Littoral. 1992. Complexe NBR. La zostère marine. Rapport présenté à Hydro-Québec, Vice-présidence Environnement. Montréal, Québec, Groupe Environnement Littoral, 9 p., 1 figure et 2 pl

Gross et al. 2022. The biogeography of community assembly: latitude and predation drive variation in community trait distribution in a guild of epifaunal crustaceans. Proc. R. Soc. B. 289: 20211762.

Keddy. 1982. Quantifying within-lake gradients of wave energy: interrelationship of wave energy, substrate particle size and shoreline plants in axe lake, Ontario. Aquatic Botany 14:41-58.

Kollars et al. 2018. Meta-analysis of reciprocal linkage between temperate seagrass and waterfowl with implication for conservation. Frontiers in Plant Science, 8, 2119.

Krause-Jensen et al. 2020. Imprint of climate change of pan-arctic marine vegetation. Frontiers in Marine Science, 7, 617324.

Lalumière et al. 1996. Répartition de la zostère marine (*Zostera marina*) sur la côte nord-est de la baie James – Éte 1996. Rapport du Groupe-conseil Génivar présenté au Service écologie, Direction Ingénierie et Environnement, Société d’énergie de la Baie James. 44 p. et 4 annexes.

Lalumière et al. 1994. Eelgrass meadows in a low arctic environment, the northeast coast of James Bay, Québec. Aquatic Botany 47 (3-4), 303-315.

LaRocque et al. 2020. Wetland mapping with Landsat 8 OLI, Sentinel-1, ALOS-1 PALSAR, and LiDAR data in Southern New Brunswick, Canada. Remote Sensing, *12*(13), 2095

LaZerte and Albers 2018. weathercan: Download and format weather data from Environment and Climate Change Canada. Journal of Open Source Software, 3:571.

Leblanc et al. 2022. Limited recovery following a massive seagrass decline in subarctic eastern Canada. Global Change Biology. 29, 432-450.

Leblanc et al. 2023a. Hunting and seagrass affect fall stopover Canada goose distribution in eastern Canada. Journal in Wildlife Management (*accepted*).

Leblanc et al. 2023b. The Tabusintac Bay (New Brunswick, Canada): an important spring migratory stopover site for Atlantic Brant (*Branta bernicla hrota*). Canadian Field-Naturalist 136 (3), 213-216.

Lepoint et al. 2004. Applications of C and N stable isotopes to ecological and environmental studies in seagrass ecosystems. Marine Pollution Bulletin, 49, 887-891.

Marsh et al. 1986. Effects of temperature on photosynthesis and respiration in eelgrass (*Zostera marina* L.). Journal of Experimental Marine Biology and Ecology, 101, 257-267.

Murphey and Fonseca 1995. Role of high and low energy seagrass beds as nursery areas for *Penaeus duorarum* in North Carolina. MEPS 121:91-98.

Olatunji 2022. Use of Satellite Imagery for Monitoring Canada and Brant Geese Habitat Changes in Eeyou Itschee (James Bay, Québec), Master of Forestry Report, Faculty of Forestry and Environmental Management, University of New Brunswick, June 2022, 97 pages

Orth et al. 2006. A global crisis for seagrass ecosystems. Bioscience, 56, 987-996.

Richer 2022. Condition physiologique des herbiers de zostères (*Zostera marina*) selon la distribution des nutriments sur la côte oriental de la Baie James (Québec, Canada). M. Sc., ISMER, Université de Rimouski. August 2022, 72 pages

Roca et al. 2016. Response of seagrass indicators to shifts in environmental stressors: a global review and management synthesis. Ecological Indicators, 63, 310-323.

Roche ltée. 1982. Études océanographiques de la côte est de la baie James. Tome III. La végétation littorale. Rapport réalisé pour le compte de la SEBJ. 105 pages + annexes.

Roche ltée. 1985. Études de la végétation aquatique de l’estuaire de la Grande Rivière et de la côte est de la Baie James. Rapport réalisé pour le compte de la SEBJ. 105 pages + annexes.

Ruesink et al. 2015. Variability in carbon availability and eelgrass (*Zostera marina*) biometrics along an estuarine gradient in Willapa Bay, WA, USA. Estuaries and Coasts, 38, 1908-1917.

Schubert et al. 2018. Photoacclimation strategies in northeastern Atlantic seagrasses: integrating responses across plant organization levels. Scientific Report, 8, 14825.

U.S. Army, Corps of Engineers, Coastal Engineering Research Center. 1977. Shore Protection Manual. Third edition, Vol. 1,2,3. U.S. Army Corps of Engineers, Coastal Engineering Research Center, Port Belvoir, VA pp. 1,262.

Short and McRoy 1984. Nitrogen Uptake by Leaves and Roots of the Seagrass *Zostera marina* L. 27, 547-55.

Short and Duarte. 2001. Methods for the measurement of seagrass growth and production. In: Global Seagrass Research Methods, ed. F.T. Short & R.G. Coles, pp: 155-182. Amsterdam, the Netherlands: Elsevier.

Sorais et al. 2022. Migration patterns and habitat use by molt migrant Canada Geese in James Bay, Canada, Wildlife Biology, e1062

Sorais et al. in revision. Distribution of Canada geese during their spring and fall migrations along the east coast of James Bay. Submission to Arctic Science.

Valentine et al. 2006. Food web interactions along seagrass-coral reef boundaries: effects of piscivore reductions on cross-habitat energy exchange. Marine Ecology Progress Series, 333, 37-50.

Warren et al. 2010. Increasing density of juvenile Atlantic (*Gadus morhua*) and Greenland cod (*G. ogac*) in association with spatial expansion and recovery of eelgrass (*Zostera marina*) in a coastal nursery habitat. Journal of Experimental Marine Biology and Ecology, 394, 154-160.

Waycott et al. 2009. Accelerating loss of seagrass across the globe threatens coastal ecosystems. PNAS, 106, 12377-12381.


arctus.ca
Arctus
Télédétection des environnements aquatiques
& veille environnementale

Arctus

Monday, February 26, 2024

A satellite-based monitoring system and services for Eeyou Istchee coastal habitats

SmartEarth: Accelerating Earth Observation Application Innovations

Applications Challenge:
Climate Change Action and Resilience - Monitoring Change in the Arctic Climate and Northern Ecosystem

CANADIAN SPACE AGENCY
AGENCE SPATIALE CANADIENNE

MISKAMOON CORPORATION

Context and Project presentation

CSA's SmartEarth accelerator program time line

Sept. 2023:
Request for proposal (RFP)

CSA' RFP

Oct. 2023
Proposal submitted by Arctus and Niskamoon

Feb 2024:
20 projects selected

Phase 1

19 April 2024:
« Concept Design » delivrable

Later 2024:
CSA will issue an RFP

Phase 2

Arctus will build a consortium to answer the CSA RFP

Knowledge dissemination

“Concept Design” and how to improve it?

*This project aims to create a **satellite-based monitoring system** and **data processing services** specifically designed to meet to the needs of the Eeyou Istchee stakeholders and land users .*

Arctus

Simon Bélanger, PhD
Scientific director

Thomas Jaegler, Msc
Project Manager

Carlos Araújo, PhD
Remote sensing specialist

Raphael Mabit, , Msc
Remote sensing specialist

ISKAMOON CORPORATION

Mélanie Leblanc, PhD
Research Wildlife Biologist

Sammy Blackned
Cree consultant

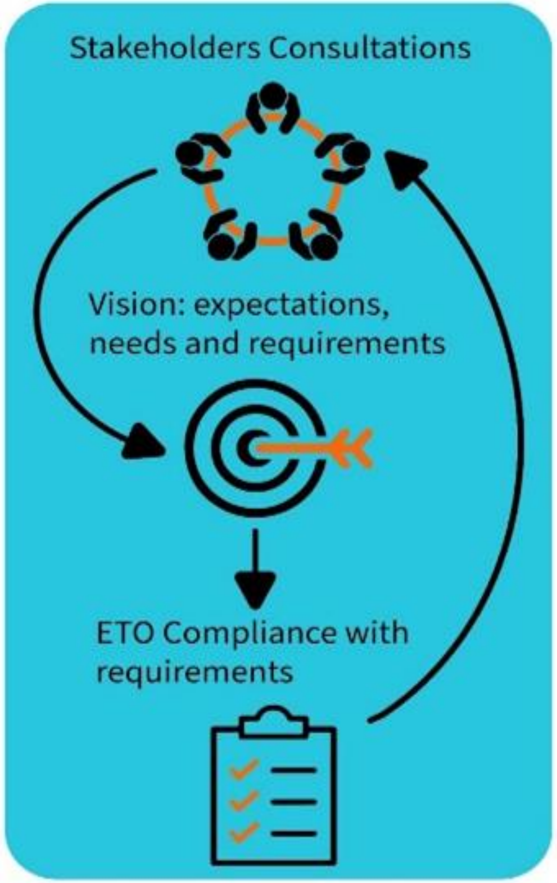

Stage 1: System and Service design

Goals of the consultation

1. To assess the needs and perspective of stakeholders with interest in environmental assessment or monitoring of the Eeyou Istchee region.

2. To inform stakeholders about the potential of Earth Observation Satellite Technology for environmental monitoring.

3. To inform stakeholders about the opportunity offered by the Canadian Space Agency to implement a system tailored to fit their needs.

What is remote sensing for environmental applications?

Remote sensing can include multiple platforms…

- Unmanned Aerial Vehicles (UAV)
- Aerial Remote Sensing (ARS)
- Unmanned Surface Vessels (USV)
- Unmanned Underwater Vehicles (UUV)
- Static Sensors (SS) with telemetry
- Satellite Remote Sensing (SRS)

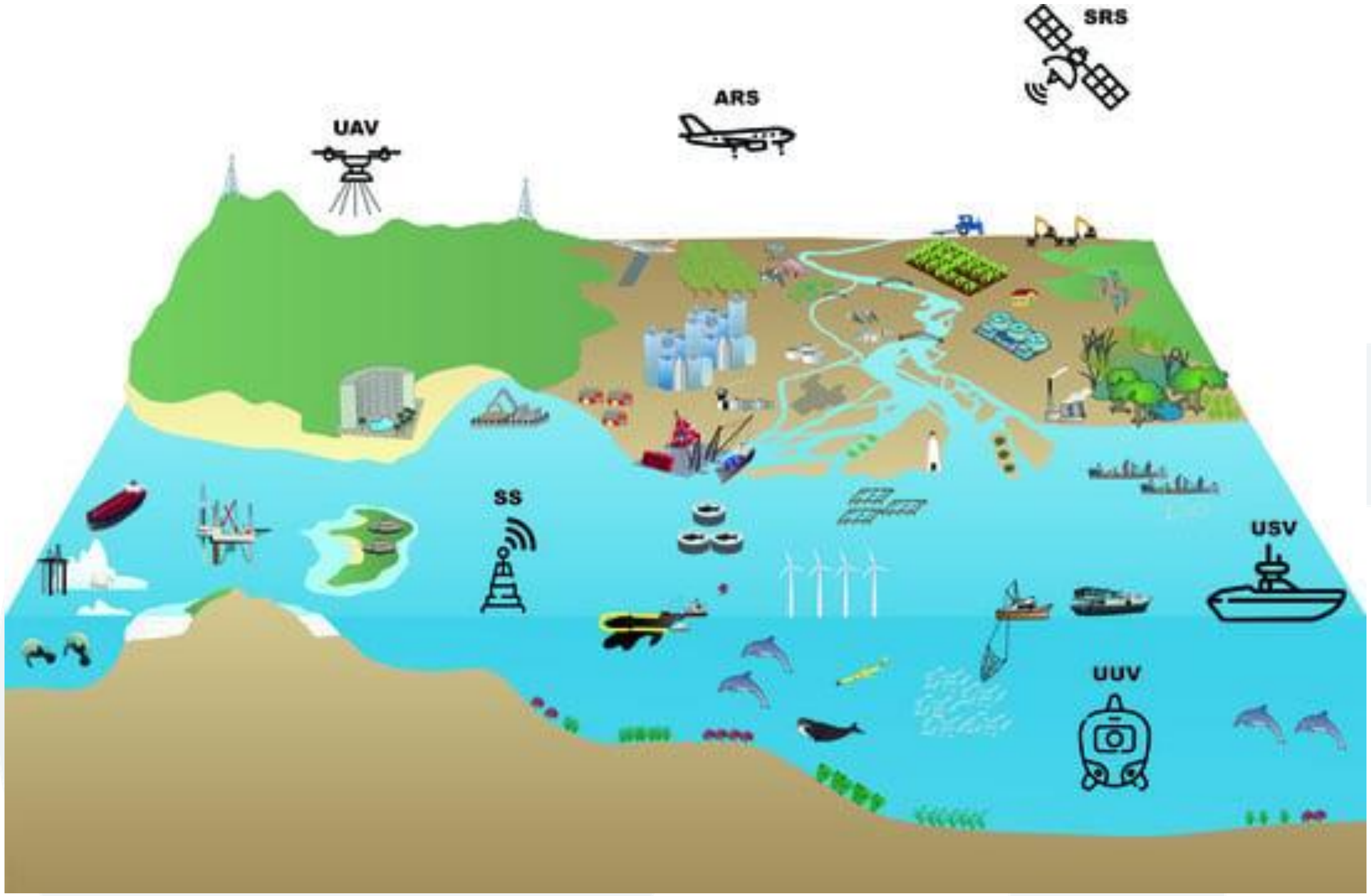

El Mahrad et al. 2020

→ **Earth Observation Technologies**

Earth Observation Technologies (satellites)

(Mainly) developed and maintained by governmental space agencies (example: NASA, ESA, CSA, …)

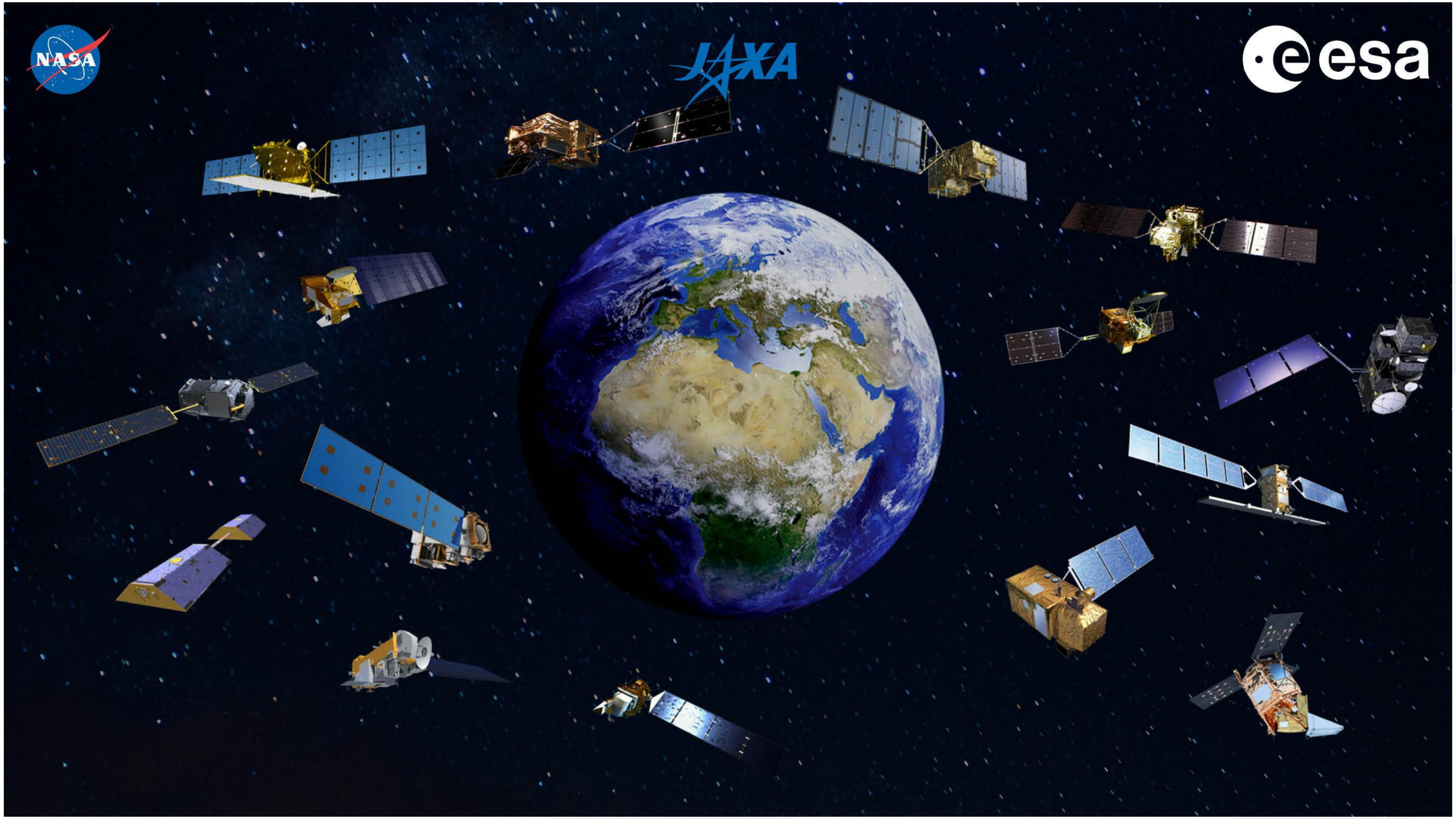

Earth Observation Technologies (satellites)

Earth Observation Technologies (satellites)

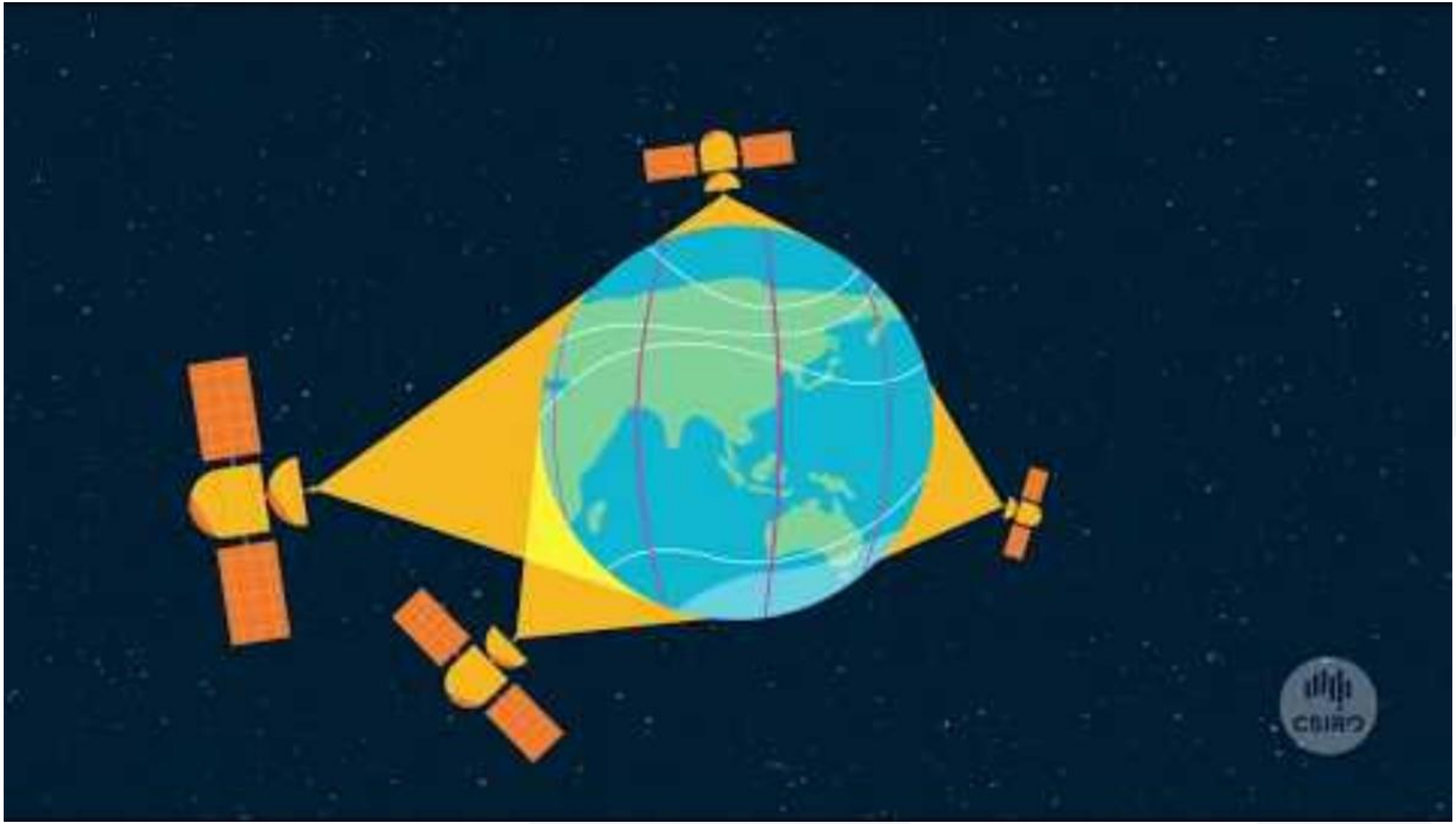

https://youtu.be/Q4WK_J9HtDE

The Commonwealth Scientific and Industrial Research Organisation

EOT application examples
Water: Arctus expertise

Sea Surface Temperature

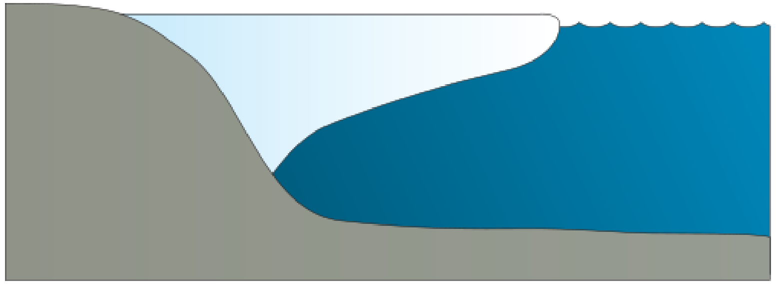

Coastal sea-ice

Shallow water bathymetry

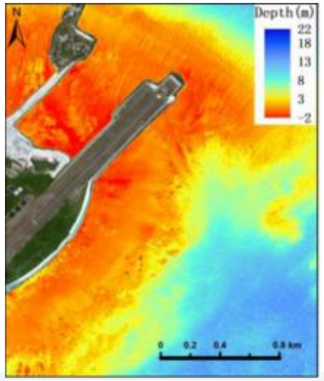

Water quality (e.g., suspended sediments and plumes, phytoplankton, water transparency)

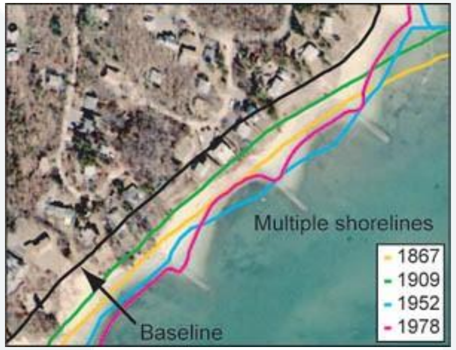

Shoreline detection and trends

Coastal habitat mapping (e.g., seagrass, saltmarsh)

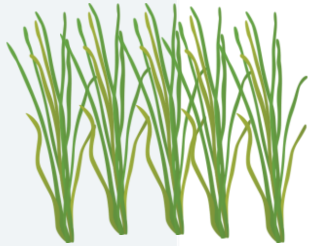

Water quality parameters
(monthly composites) :

Colored Dissolved Organic Matter (CDOM)

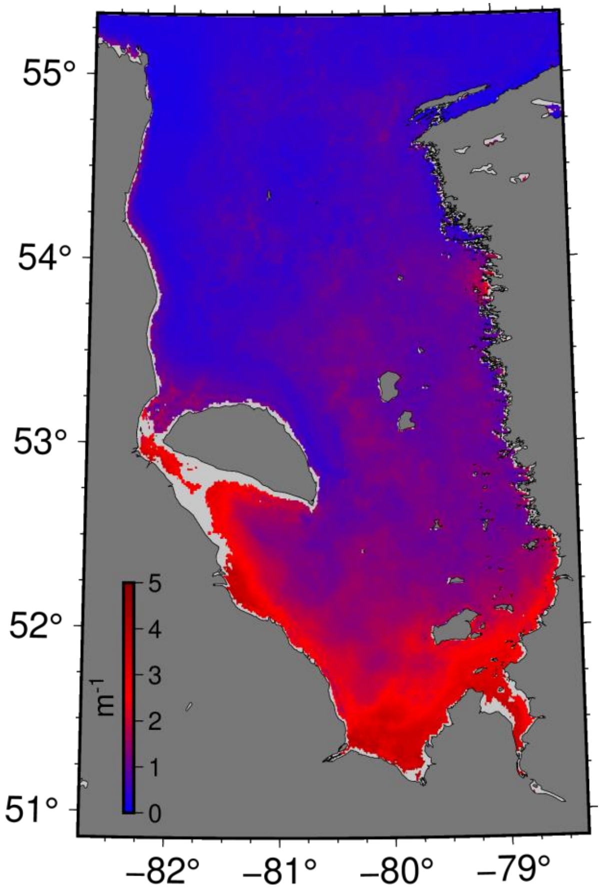

Phytoplankton Chlorophyll-*a* concentration

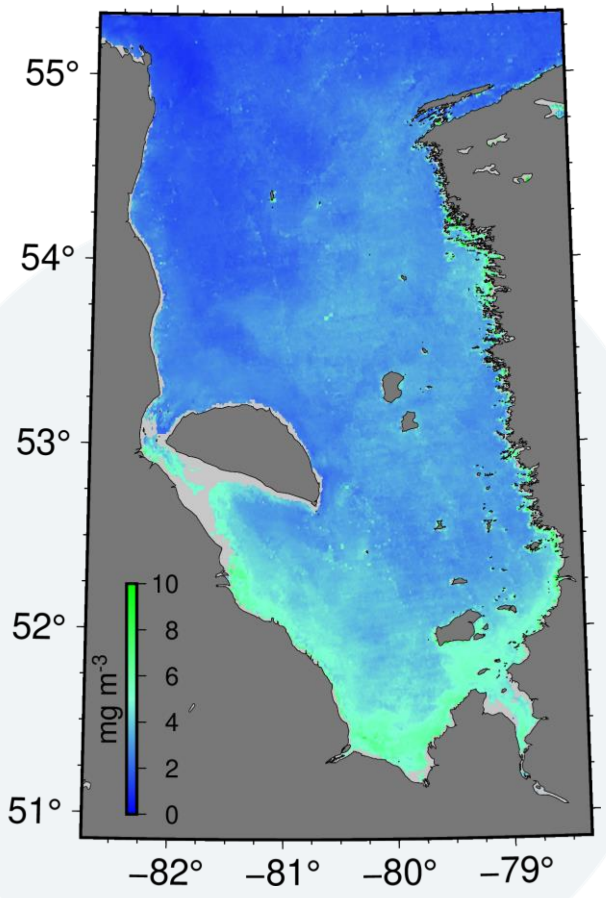

Suspended Sediment or Turbidity

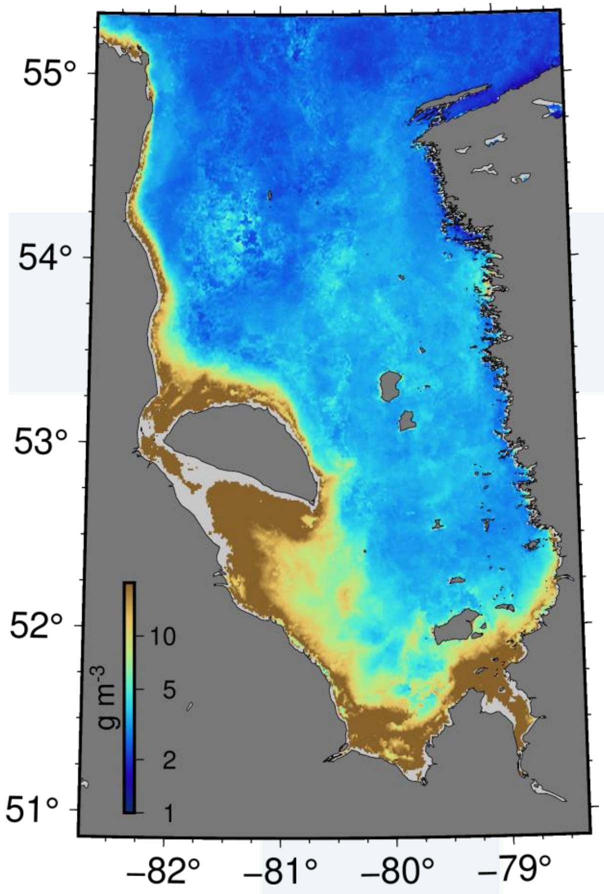

Credit: Singh and Bélanger, CHCRP phase 1

Sediment plumes:

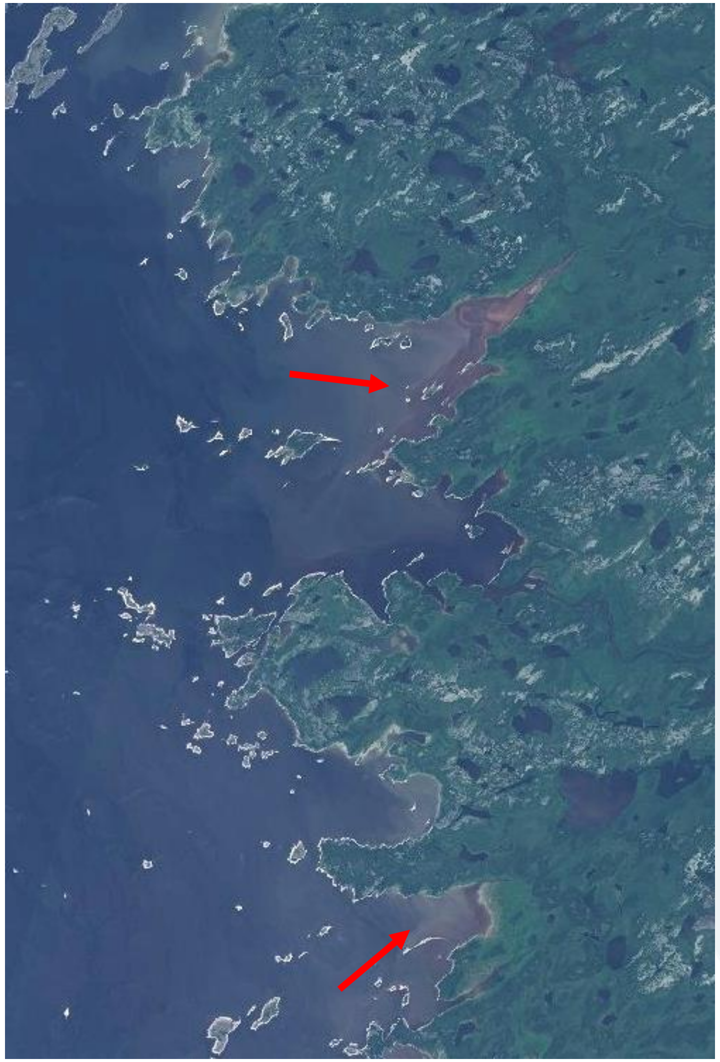

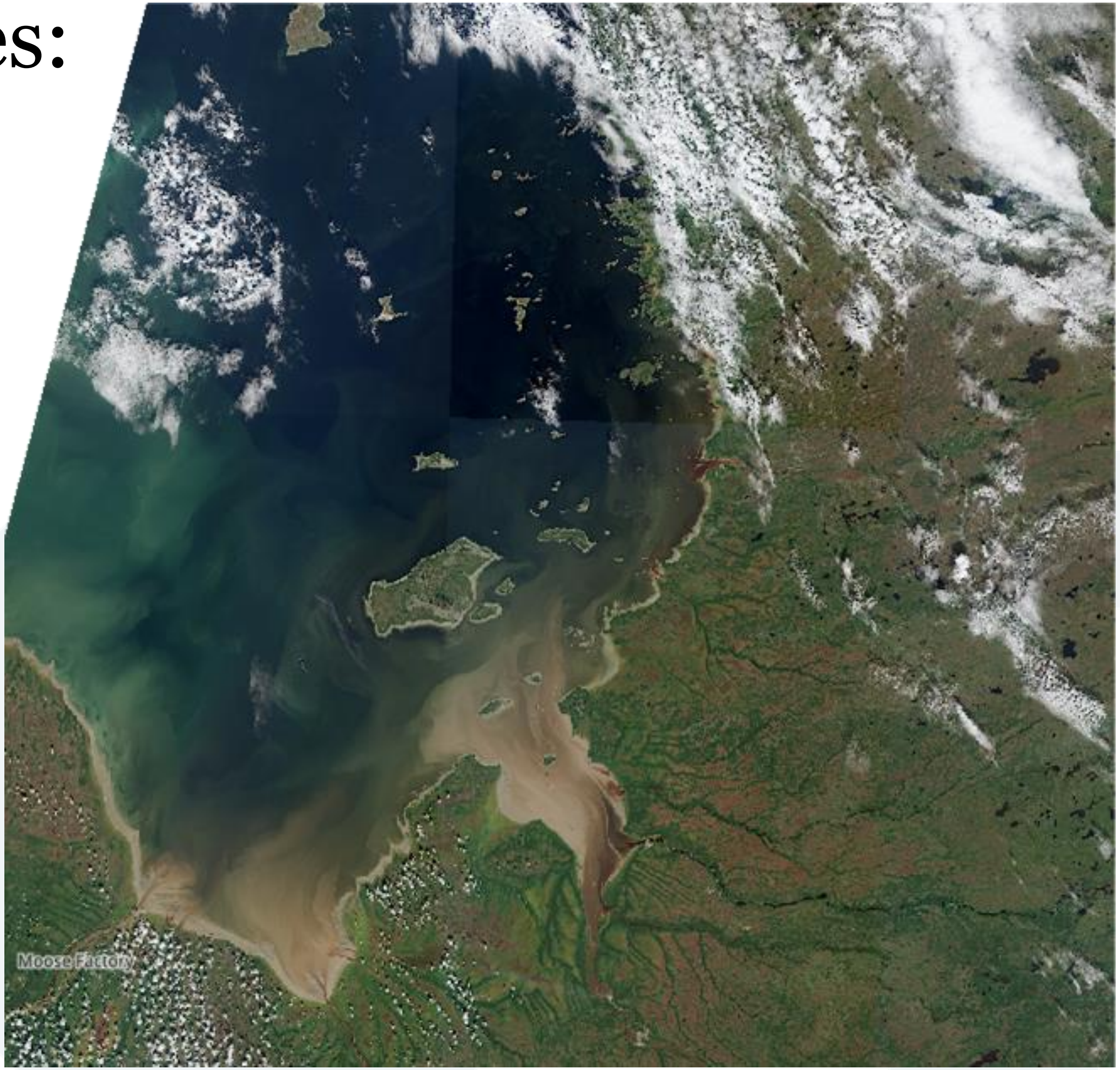

Sea Surface Temperature :

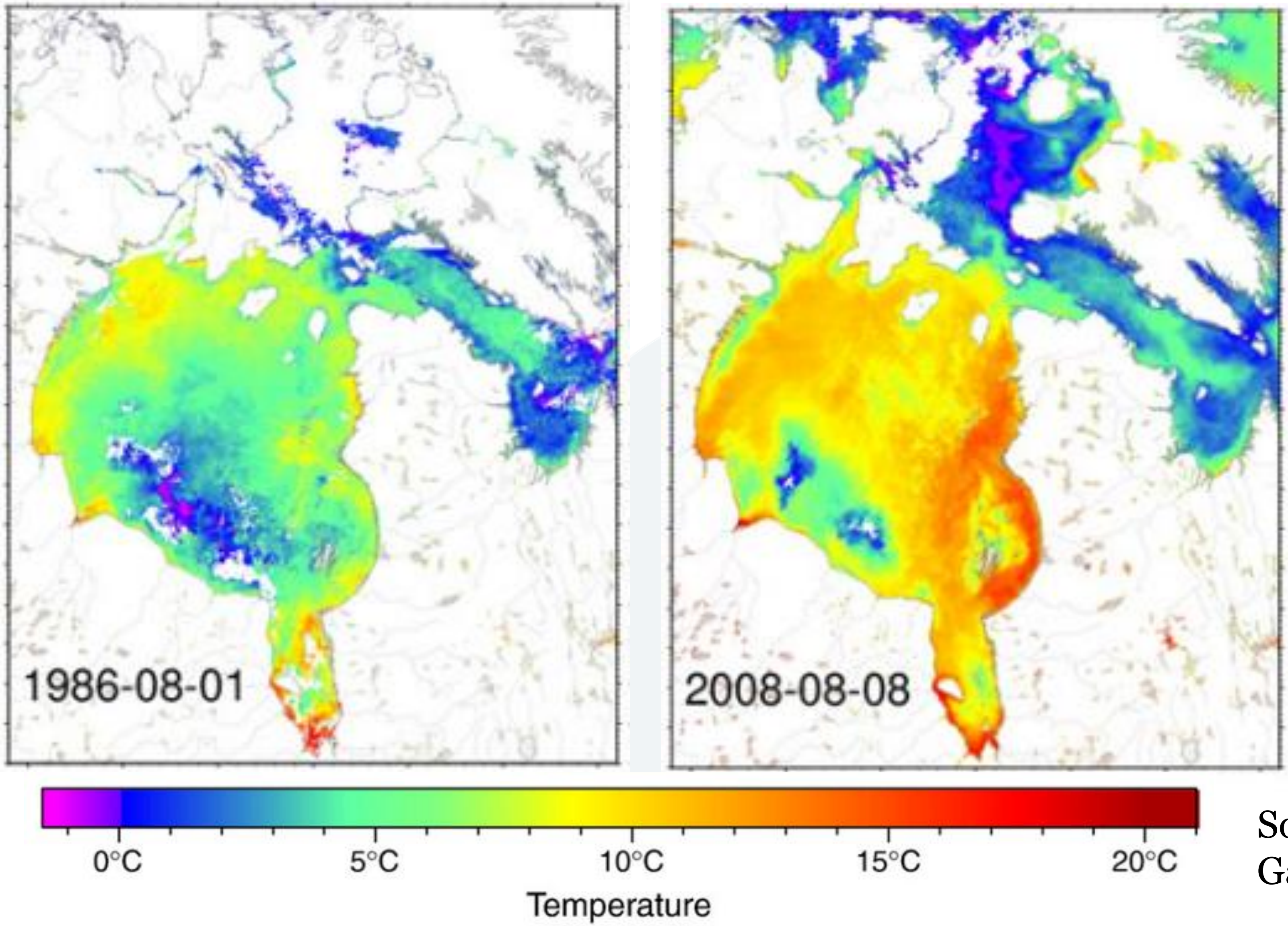

Source:
Galbraith and Larouche (2011)

Sea ice monitoring:

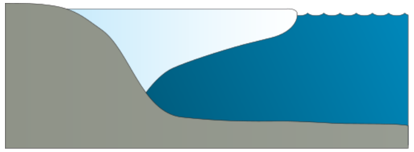

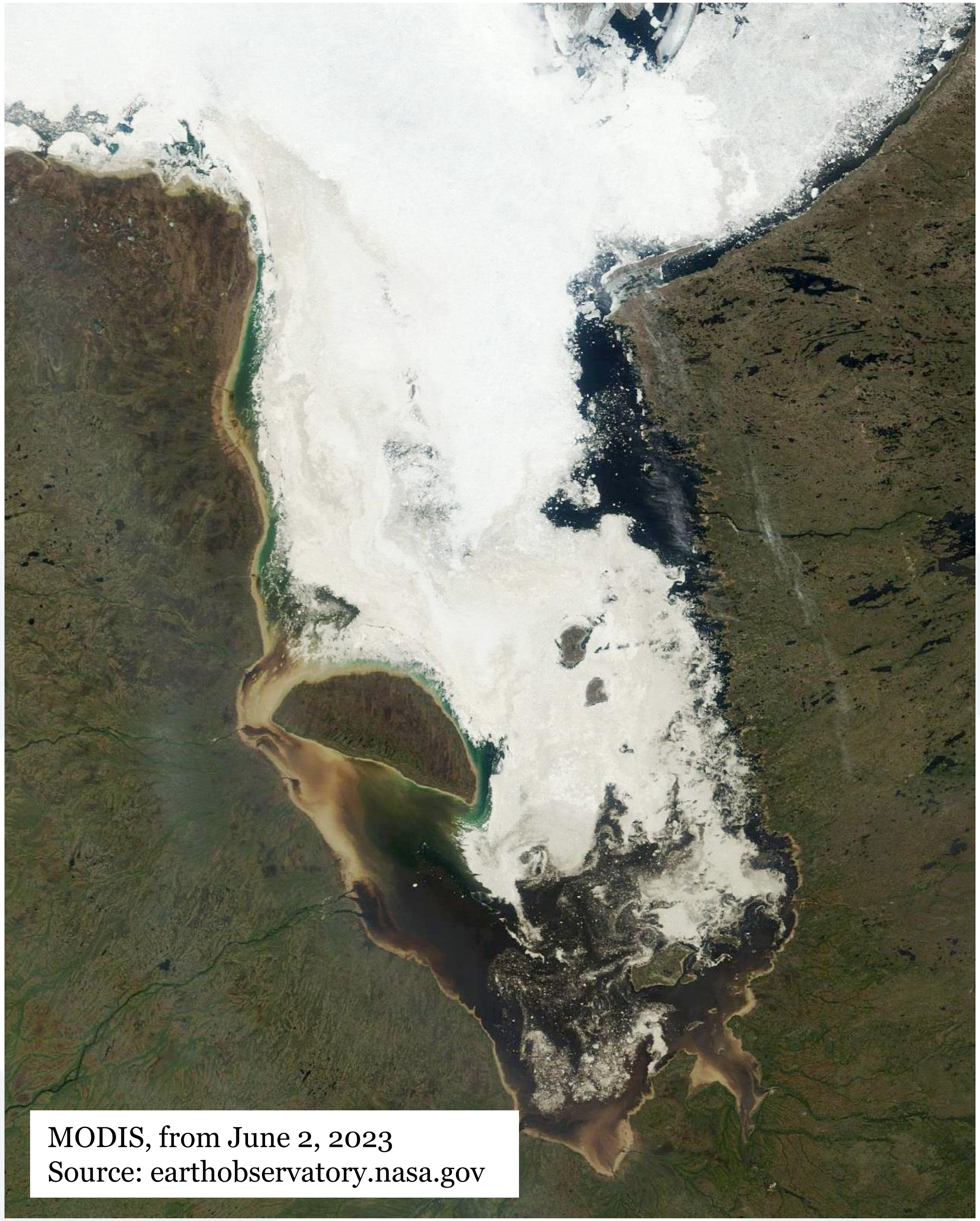

MODIS, from June 2, 2023
Source: earthobservatory.nasa.gov

Shallow water bathymetry:

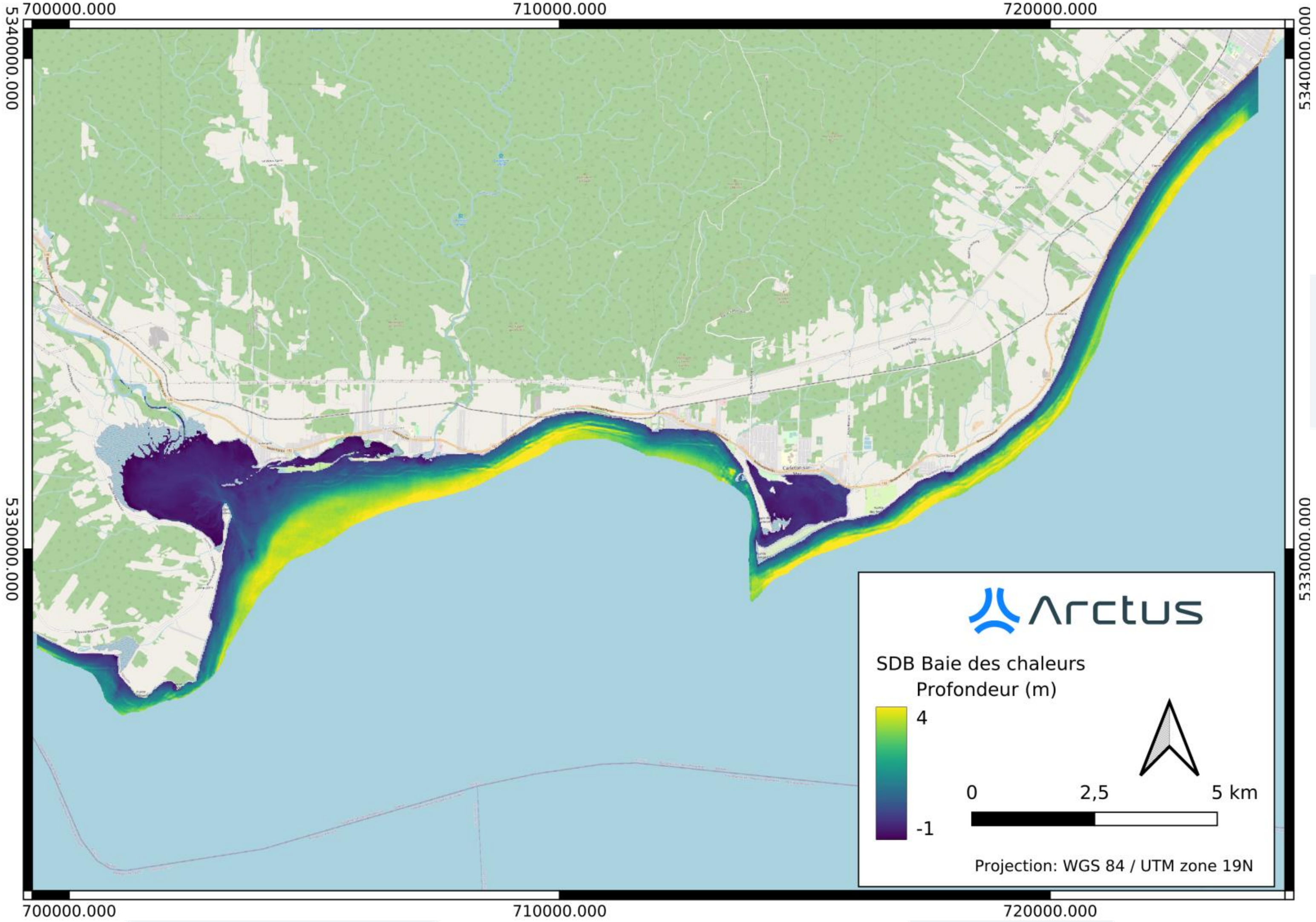

Coastline detection and trend:

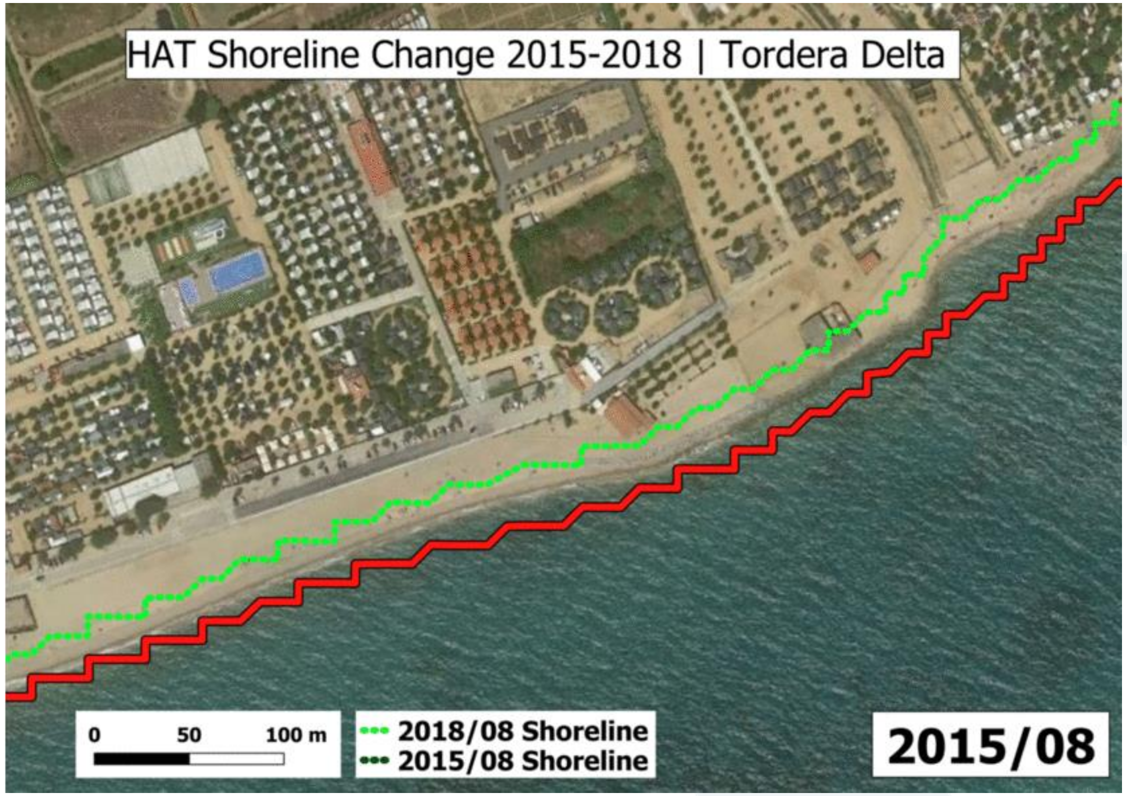

Coastal habitat mapping:

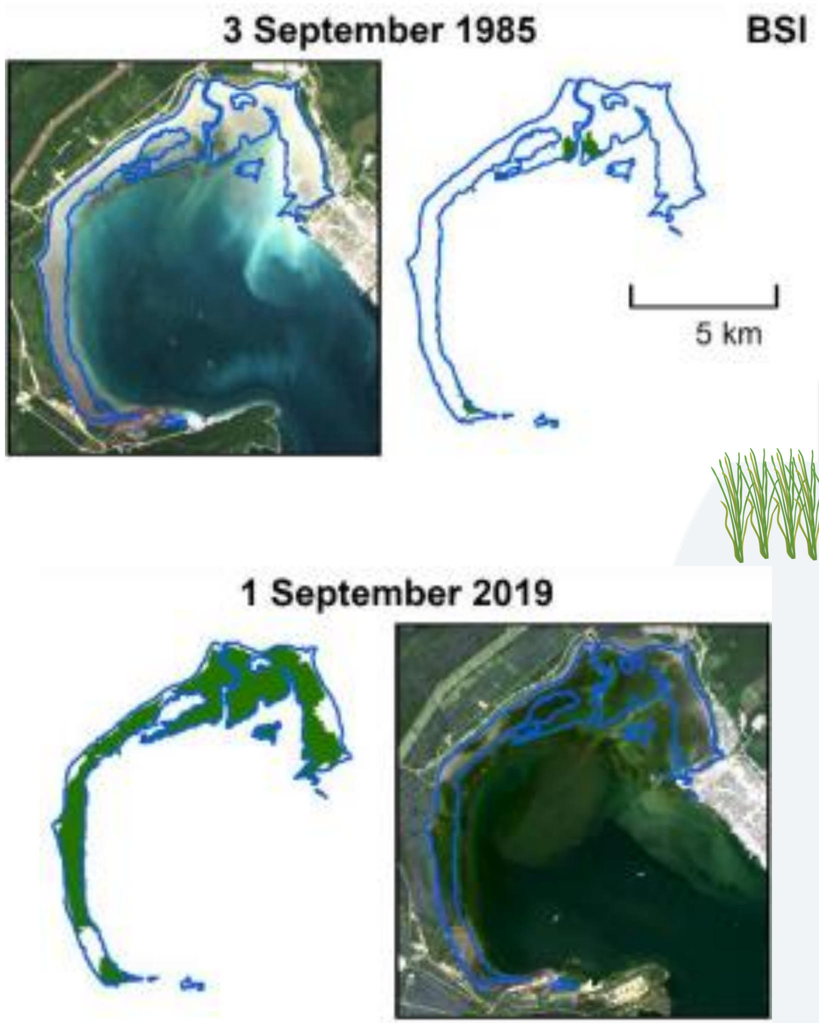

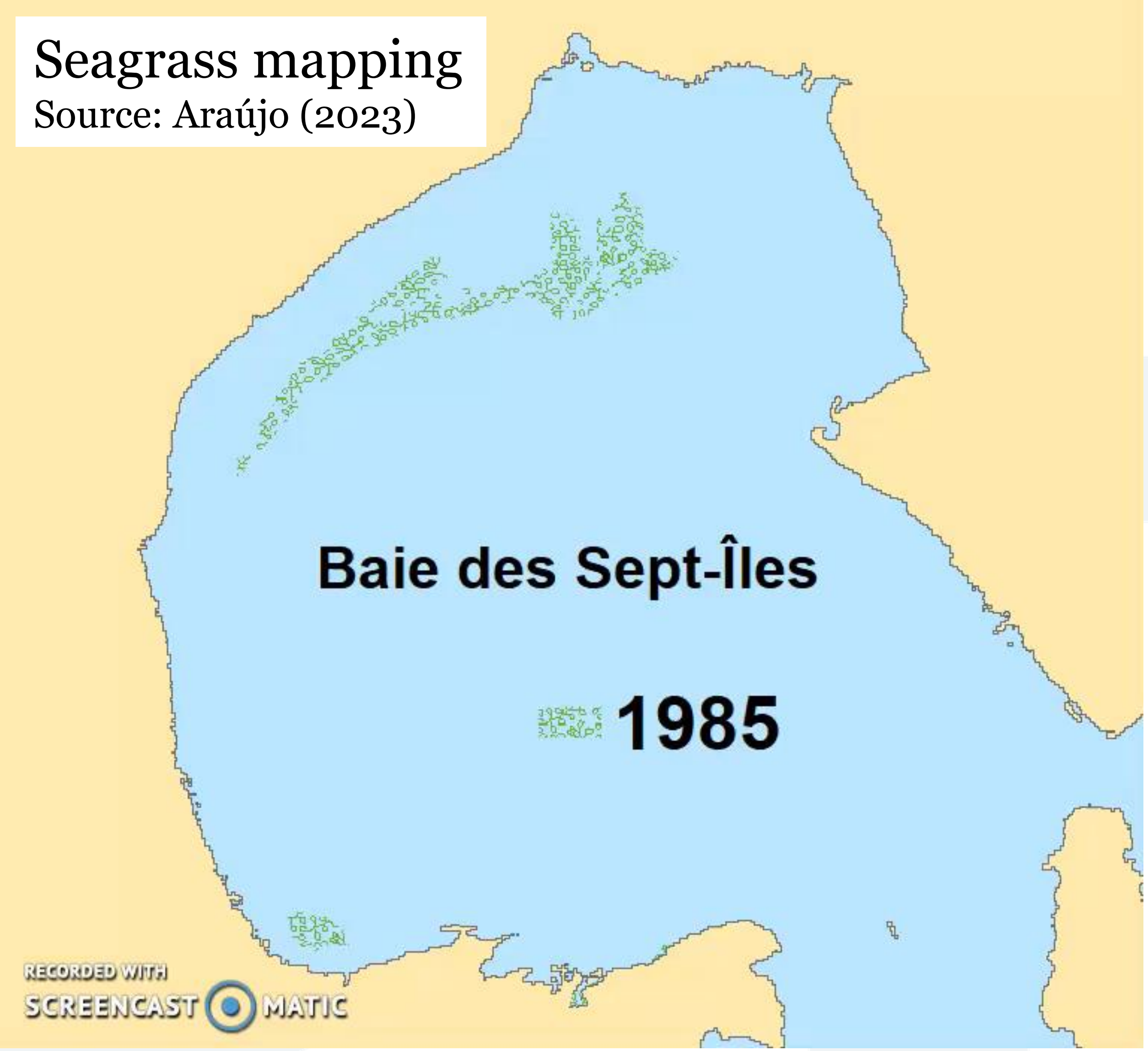

Wetlands mapping
Peatlands:

Source:
Marc Doucette / Global News

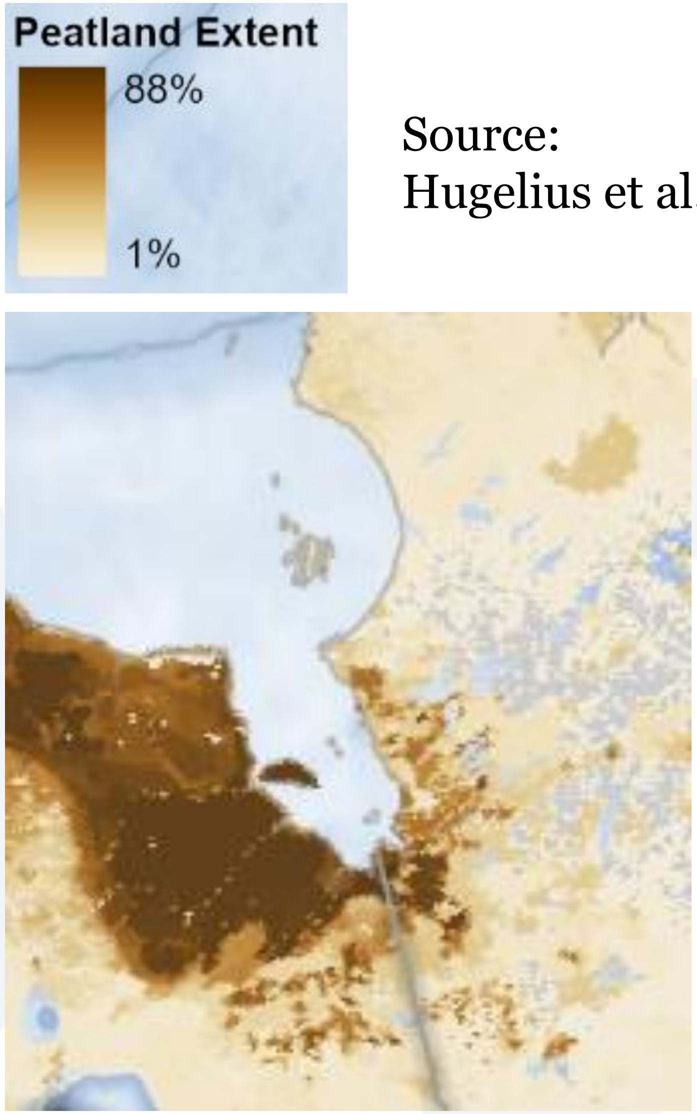

Source:
Hugelius et al. (2020)

EOT - other application examples

Forests

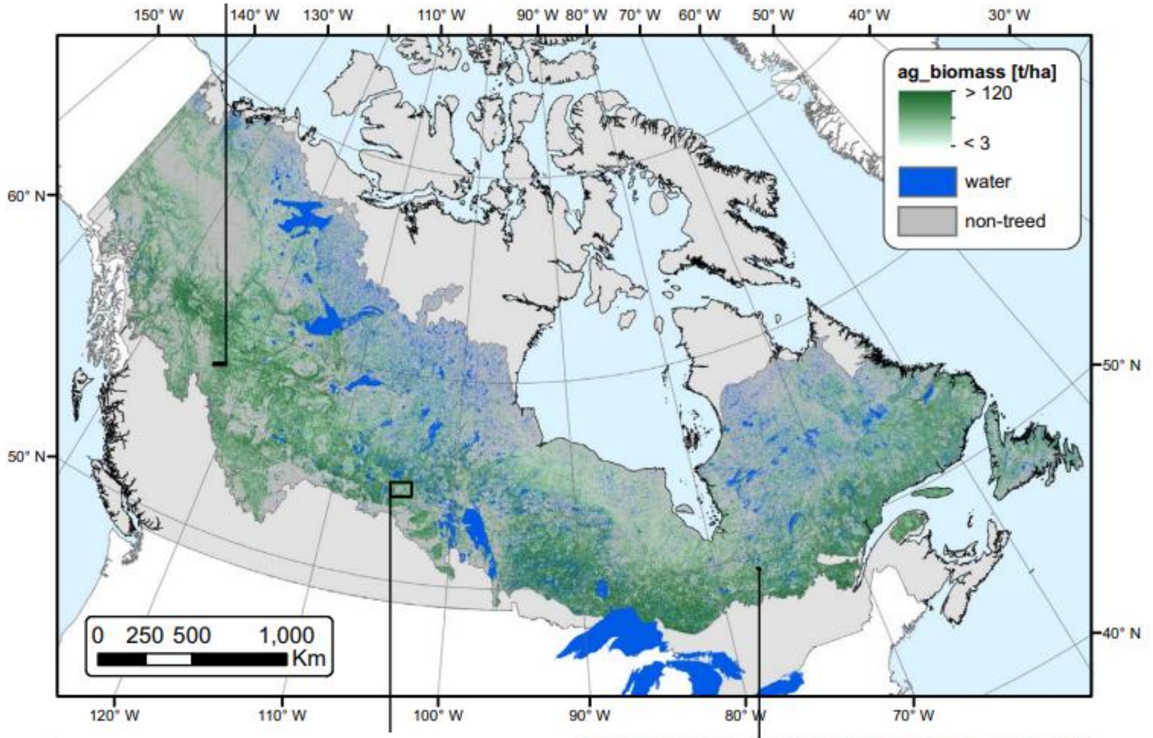

Forest monitoring

Source:
Matasci et al. (2018)

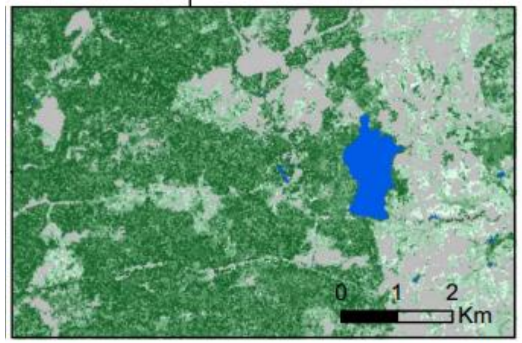

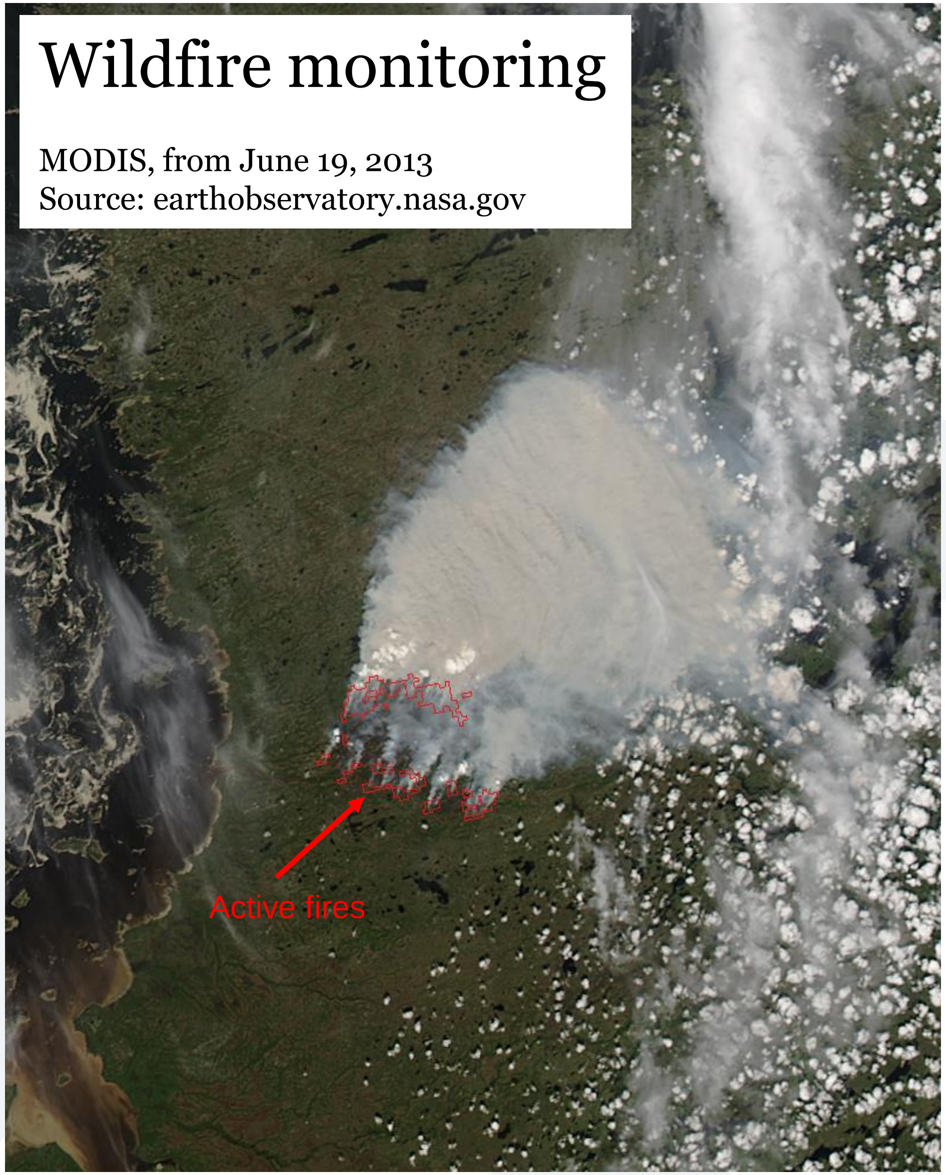

Wildfire monitoring

MODIS, from June 19, 2013
Source: earthobservatory.nasa.gov

EOT - other application examples

Meteorological variables (near-real time and predictions) uses several types of satellite data

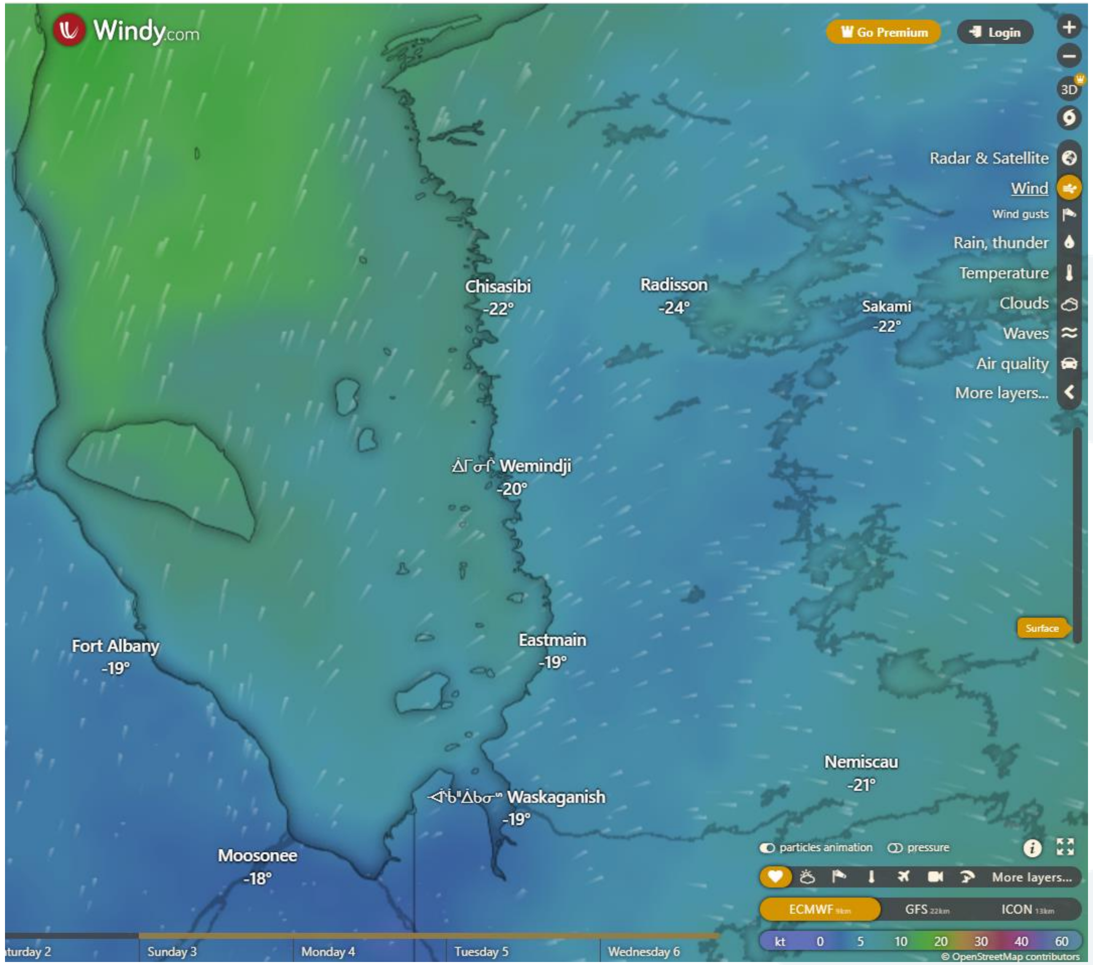

Examples: wind, precipitation

Source:
https://gpm.nasa.gov/data/imerg

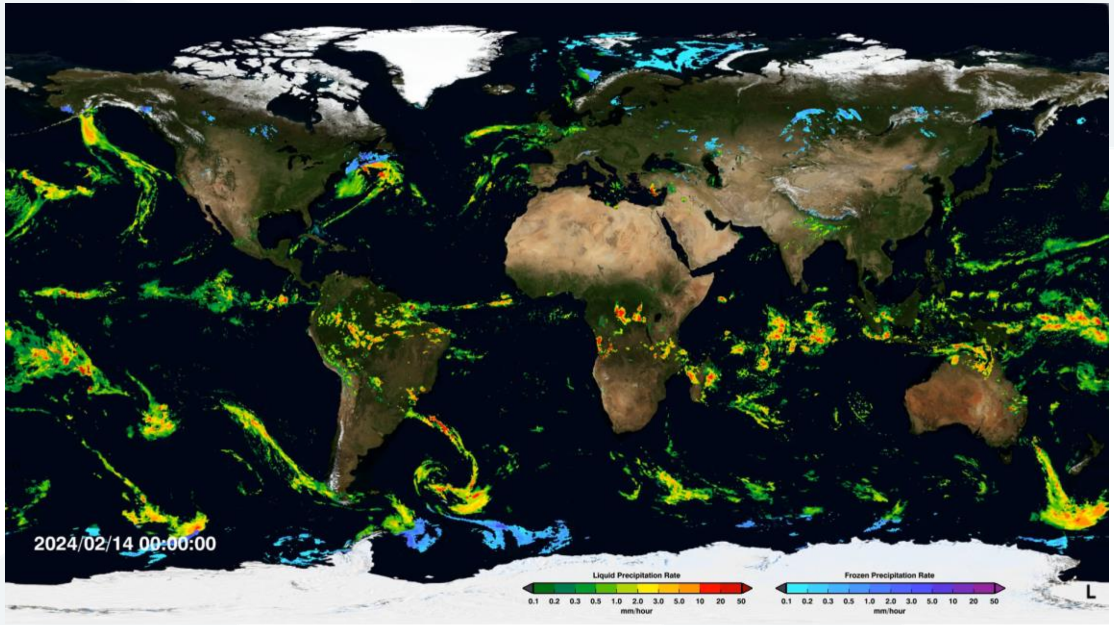

Remote sensing:
Basic concepts

Temporal resolution:

= Revisit time

The frequency a determined satellite sensor image the same region

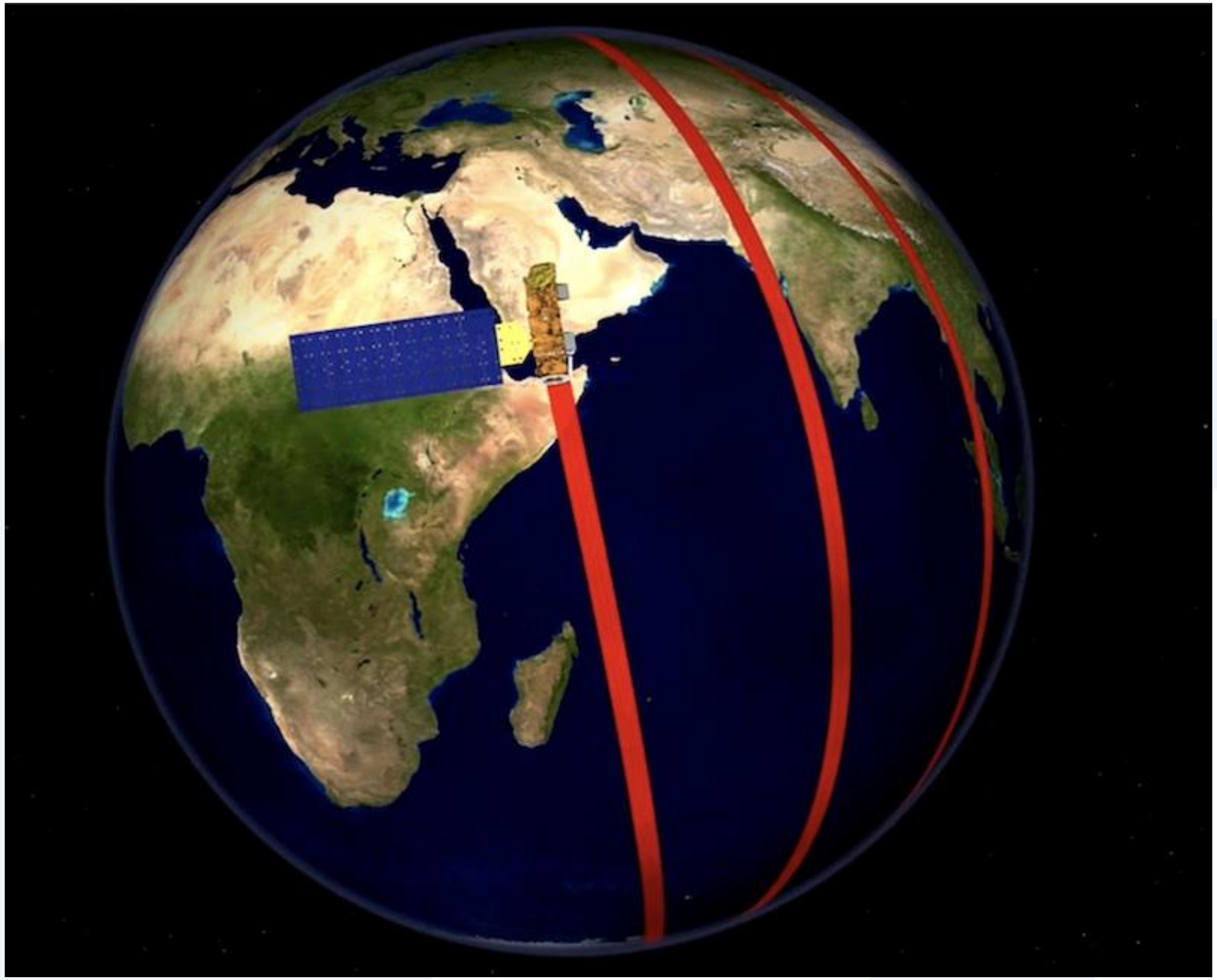

Remote sensing:
Basic concepts

Spatial resolution:

Spatial resolution is a measurement of how detailed objects are in an image based on pixels

Source: GISGeography

Remote sensing:
LIMITATIONS

Inherent limitations for some applications:

- Optical remote sensing is limited by cloud cover
- Coastal and nearshore habitat mapping may be limited in turbid conditions
- Image acquisition geometry constraints for water quality parameters (example: glint)
- Choice between better spatial resolution or higher temporal coverage
- Data with spatial resolution better than 10 meters are not free (commercial)

Remote sensing:
Example of product visualization and interactive platforms

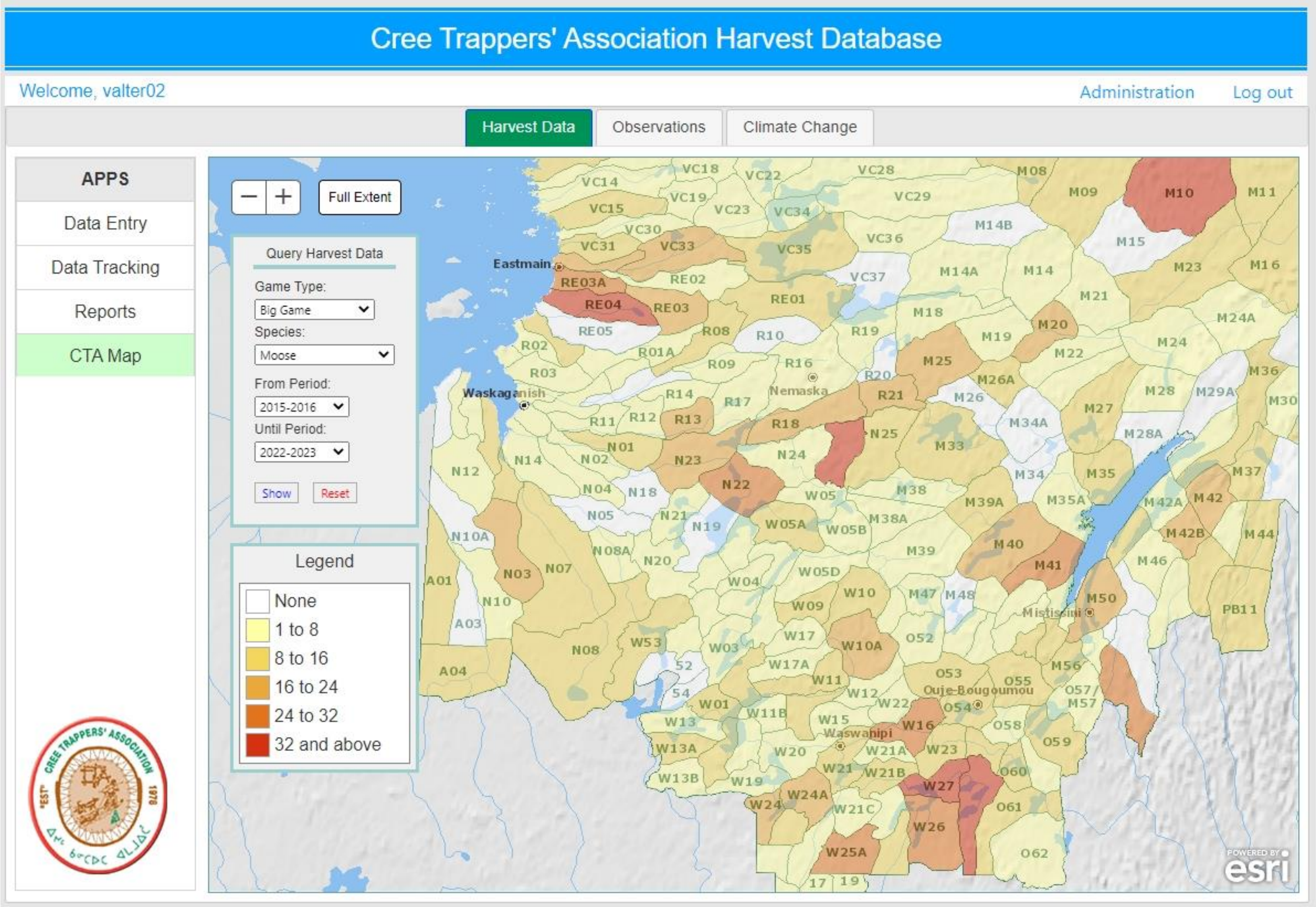

Source: CTA Wildlife Harvest and Monitoring Mobile Application

Remote sensing:
Product visualization and interactive platforms

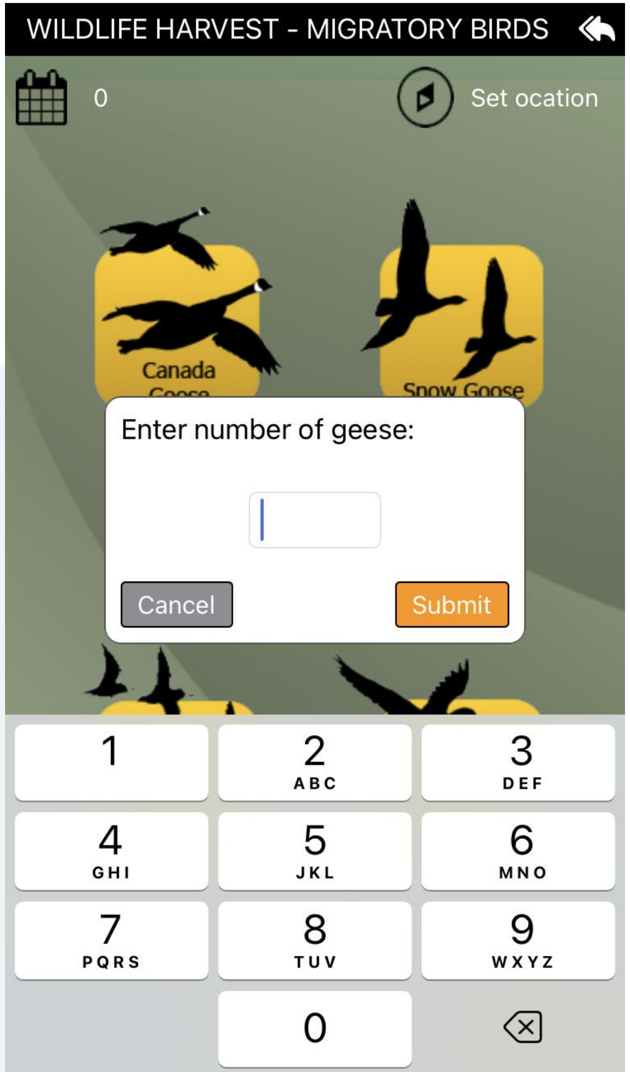

Source:

CTA Wildlife Harvest and Monitoring Mobile Application

Please answer the online questionnaire to help us to improve the "concept design"

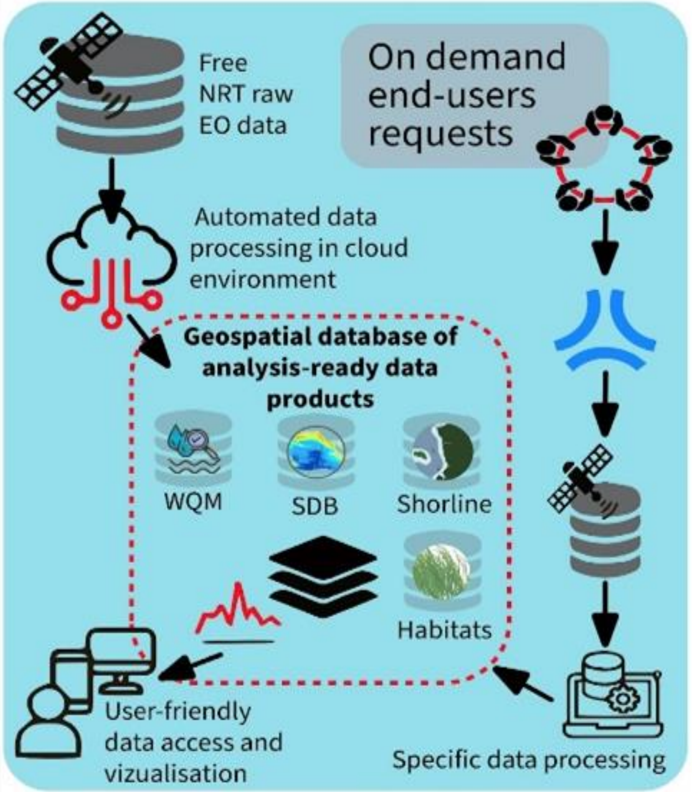

Stage 2: System development on-demand services

https://forms.gle/jrw8vjZLVeyeSyd38